8-2020

Design and Implementation of Rotational Print Heads to Control Fiber Orientation in Material Extrusion Additive Manufacturing

Michael David Roberts
University of Tennessee

To the Graduate Council:

I am submitting herewith a thesis written by Michael David Roberts entitled "Design and Implementation of Rotational Print Heads to Control Fiber Orientation in Material Extrusion Additive Manufacturing." I have examined the final electronic copy of this thesis for form and content and recommend that it be accepted in partial fulfillment of the requirements for the degree of Master of Science, with a major in Mechanical Engineering.

<div align="right">Brett G. Compton, Major Professor</div>

We have read this thesis and recommend its acceptance:

Caleb Rucker, Subhadeep Chakraborty

<div align="right">Accepted for the Council:
Dixie L. Thompson</div>

<div align="right">Vice Provost and Dean of the Graduate School</div>

(Original signatures are on file with official student records.)

Design and Implementation of Rotational Print Heads to Control Fiber Orientation in Material Extrusion Additive Manufacturing

A Thesis Presented for the
Master of Science
Degree
The University of Tennessee, Knoxville

Michael David Roberts
August 2020

Acknowledgements

Abstract

Short fibers are being incorporated into 3D printable polymers to modify the properties of the printed composite. These fibers are, however, highly aligned in the print direction limiting the range of programmable site-specific characteristics. Recent work has demonstrated a novel approach of adding an additional shear field, through rotation, during the direct ink writing process, enabling control over the fiber orientation. This work endeavors to reproduce those results and demonstrate the same novel concept in fused filament fabrication, and outlines the challenges using these two systems.

Table of Contents

List of Figures

List of Tables

Nomenclature

ABS	Acrylonitrile Butadiene Styrene
AM	Additive Manufacturing
CAD	Computer-aided design
CF	Carbon Fibers
DIW	Direct Ink Writing
Extruder	Deposition mechanism for material extrusion AM
FFF	Fused Filament Fabrication
Fiber loading	Percentage of the fibers in the composite.
Filament	Thermoplastic feedstock materials for FFF processes
GF	Glass Fibers
Hotend	The portion of the extruder that melts the filament
Inks	Thermoset feedstock materials for DIW processes
PC	Polycarbonate
PEEK	Polyether Ether Ketone
PEI	Polyetherimide
PETG	Polyethylene Terephthalate Glycol
PLA	Polylactic Acid
PMC	Polymer Matrix Composite
PWM	Pulse Width Modulation
Ratio	Rotational ratio. Dimensionless ratio described in work done by Raney, Compton et al.
STL/SLA	Stereolithography
Tg	Glass transition temperature

Chapter 1 Introduction

1.1 Overview

AM can manufacture truly remarkable parts. Currently, on the large scale, AM can manufacture small buildings [1], short bridges [2], large scaffolding [3], components for aircraft [4], rocket engines [5] and nozzles [6], and even off-earth habitats [7]. While on the small scales, AM can manufacture intricate art pieces [8], sneakers [9], passive electronic components [10], circuit board vias [11], bearings [12], heat exchangers [13], prosthetics [14, 15], and even with living tissue [16, 17]. All with technology introduced merely 40 years ago. More manufacturing possibilities open as more feedstock materials become available, and manufacturing technologies advance to fully utilizes the materials' characteristics. Polymer composites have been a key area of research for both large and small-scale AM. These polymers are often reinforced by fibers, nanotubes, and other nanoparticles. These filler materials give some additional control over the properties of the composites. They can increase tensile and impact strength [18, 19] while decreasing density [20, 21]. These composites could have an electrically conductive path, or be dielectric [22]. These fibers help resist warping by lowering the coefficient of thermal expansion [23]. However, during extrusion-based AM of fiber reinforced composites, the embedded fibers are aligned in the print direction by the velocity gradient in the melt being deposited on the build platform [21], and this alignment increases as the print speed increases [24]. This alignment leads to anisotropic behavior in the composite since the fibers themselves are anisotropic [25]. Previous work has shown these fibers can be reoriented during the 3D printing process using standing pressure waves via piezoelectric actuators coupled with direct-write deposition, requiring no specific material properties other than density or matrix compressibility [26]. Another method used 3D magnetic printing which utilized an external magnetic field to reorient the fibers in a direct-write deposited layer before consolidation via light [27]. This method required the fibers to be sensitive to a magnetic field or coated with a sensitive material. Recent work has demonstrated an alternative approach to reorienting fibers during DIW printing by introducing an additional shear field by rotating the nozzle [28]. This method is effective without the need for an external field and at high fiber loading. This thesis will endeavor to reproduce these results and extend this idea to thermoplastic 3D printing.

1.2 Background

Traditional manufacturing takes a large source material and selectively removes material until only the desired part remains, similar to how a sculptor removes marble until only the sculpture remains. This can be referred to as subtractive manufacturing since material must be removed to get the desired part. Conversely, in AM, material is selectively added until the part is produced. The process of AM, often referred to as 3D printing, takes a CAD model, slices the part into discrete sections called layers, then selectively deposits material layer-by-layer to generate the desired model's geometry. The seven categories for 3D printing are: material extrusion, powder bed fusion, vat photopolymerization, material jetting, binder jetting, directed energy deposition, and sheet lamination [29]. These methods vary in how the material is deposited, what materials can be deposited, layer resolution, and processing time. Some methods require additional steps such as curing (solidifying through heat or photopolymerization) or washing to remove any residue from the manufacturing process. Table 1 summarizes the differences of these methods. The first AM process to be demonstrated was SLA, which falls

under the Vat photopolymerization category. In SLA, a laser is used to selectively solidify a liquid photopolymer, layer by layer. This technique was first demonstrated by Hideo Kodama in 1981 [30]; Charles Hull, however, is considered to be the father of SLA because he submitted a patent for the technology in 1984 [31]. Though it is worth noting that two other patents were filed for an AM process around the same time as Hull's. Jean Claude André, Alain Le Méhauté, and Olivier de Witte submitted a patent for the SLA technology a few weeks before Hull, but their pursuit was abandoned as a result of the financial considerations of the inventors' company [32]. Additionally, Bill Masters patented a computer automated manufacture process and system—which was later named ballistic particle manufacturing—which is classified under the material jetting category since, as Bill Masters described the system, it is like building with spit wads [33, 34]. This thesis will focus on the material extrusion category.

1.2.1 Material Extrusion Additive Manufacturing

Material extrusion additive manufacturing (MEAM) is the process of selectively depositing a feedstock material through an orifice onto a substrate. The material should flow and retain its shape when placed on the substrate or previous layer. Since the part is free standing, certain geometries would require an additional support material to assist in holding the shape. MEAM was first demonstrated by S. Scott Crump when he developed and patented the process of Fused Deposition Modeling (FDM) in 1989 [35]. Crump later co-founded Stratasys. FDM uses a thermoplastic polymer as a feedstock material which is drawn into a heated extruder that can translate up and down, depositing material onto a build platform that can translate on a plane orthogonal to the extruder. This allows the extruder to selectively deposit the material layer by layer, throughout three dimensions. Several years later, a similar process called Robocasting was submitted to be patented by Joseph Cesarano, III and Paul D. Calvert in 1997 [36]. This process used a thermoset slurry as the feedstock material, which removed the need for a heated extruder, but still allowed the deposited part to hold it shape until it could be cured.

In 2004 Andrew Bowyer started the replicating rapid prototyper (RepRap) project [37]. The objective of the RepRap project is to generate an open-source design for a machine that can reproduce most of its own parts—a self-replicating machine—using the 3D printing process of FFF. FFF is the same process as FDM, but even when the patent for the technology expires, Stratasys would still maintain a trademark over the term. It is with the expiration of the FDM patent in 2009 and the work of the RepRap community, that a wave of commercial FFF printers came to market. These printers did not have the same resolution or accuracy as Stratasys's FDM printers; however, they were a fraction of the price, which lead to a lot of hobbyists participating in the RepRap community. De Bruijn estimated there were 3872-4840 participants in the RepRap project in 2010 [38] and the field has only grown as the technology gets refined, with FDM being the most common 3D printing technology companies were using in 2017 [39]. FFF and DIW comprise the vast majority of MEAM processes.

Table 1-1: Additive manufacturing processes and technology technologies
Source: [40]
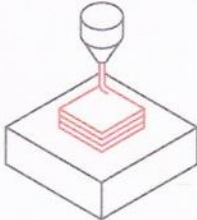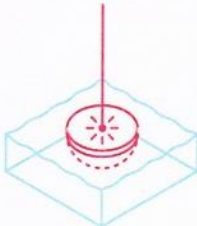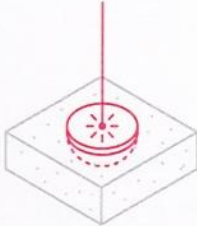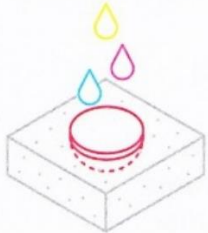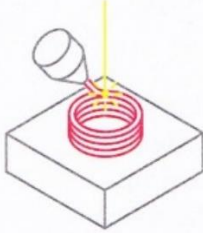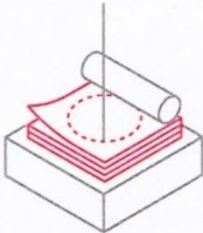
Process	Description	Technologies
Material Extrusion	Additive manufacturing process in which material is selectively dispensed through a nozzle or orifice.	Fused Filament Fabrication (FFF), more commonly referred to as Fused Deposition Modeling (FDM)
Vat Polymerization	Additive manufacturing process in which a liquid photopolymer in a vat is selectively cured by light-activated polymerization.	Stereolithography (SLA), Direct Light Processing (DLP)
Powder Bed Fusion	Additive manufacturing process in which thermal energy selectively fuses regions of a powder bed.	Selective Laser Sintering (SLS), Direct Metal Laser Sintering (DMLS), Selective Laser Melting (SLM), Electron Beam Melting (EBM)
Material Jetting	Additive manufacturing process in which droplets of material are selectively deposited and cured on a build plate.	Material Jetting (MJ), Drop On Demand (DOD)

Table 1-1: Continued

Process	Description	Technologies
Binder Jetting	Additive manufacturing process in which a liquid bonding agent selectively binds regions of a powder bed.	Binder Jetting (BJ)
Direct Energy Deposition	Additive manufacturing process in which focused thermal energy is used to fuse materials by melting as they are being deposited.	Laser Engineering Net Shaping (LENS), Laser-Based Metal Deposition (LBMD)
Sheet Lamination	Additive manufacturing process in which sheets of material are bonded to form a part.	Ultrasonic Additive Manufacturing (UAM), Laminated Object Manufacturing (LOM)

1.2.2 DIW & FFF Methods

The key differences between the processes of DIW and FFF are the feedstock material and the mechanisms to extrude the material. A generic DIW system can be seen in figure 1.1, while figure 1.2 depicts a generic FFF system. These systems can be broken up into four major components: feedstock material, deposition mechanism (often referred to as the head or extruder), build platform, and translational control.

Both DIW and FFF deposits a shear-thinning (pseudoplastic) fluid that can hold its shape until solidification. DIW feedstock materials—referred to as inks—are liquid thermosets that requires curing in order to solidify. FFF feedstock materials—referred to as filaments—are solid thermoplastics that needs to be melted in order to be deposited, these filaments then solidify as they cool. Inside their respective extruders, each feedstock material exhibits shear-thinning. This behavior is unlike Newtonians fluids because the viscosity decreases under shear stress, as depicted in figure 1.3, which allows these extruders to selectively start and stop depositing on a surface without the need for an iris or some other blockage.

With FFF, filaments must be heated in order to be selectively deposited through a nozzle. These filaments are either semi-crystalline polymers—PLA, PETG, and PEEK—or amorphous polymers—PC, ABS, and PEI, as seen in figure 1.4. Since these polymers are not fully crystalline, they have no true melting point, but rather a range where the material transitions from a brittle, rigid state to a more ductile state. This transition happens because the amorphous and semi-crystalline materials have disordered polymer chains, and as the temperature increases, these chains can maneuver past each other. This transition is called the glass transition temperature referred to as T_g [41]. The T_g for the polymer previously listed can be seen in Table 1-1. This value is not a discrete transition, but rather signifies a region where the ductility of the material significantly increases. To achieve the glass transition temperature a heated liquefier is used. The liquefier heats up the filament in the narrow channel of the heating block, creating a polymer melt. The solid filament being drawn into the extruder acts like a plunger to force the polymer melt out of the nozzle. As the polymer melt is laid down, the ambient temperature will cool the liquid filament. The subsequent layer is quickly deposited on top, allowing the layers to interact through polymer reptation—thermal motion of the polymer chains—to re-entangle the polymer chains (Figure 1.5) [42, 43]. If there is insufficient time for the layers to weld together, there will be a weak interaction between the two layers, causing the layers to separate under low shear stress, known as layer delamination. Thermoplastic materials with significant coefficient of thermal expansion (ABS for instance) can also experience warping, which is when the part curls up and inward due to the thermal gradient in the part as the layers cools. One means to counteract this is by using a heated
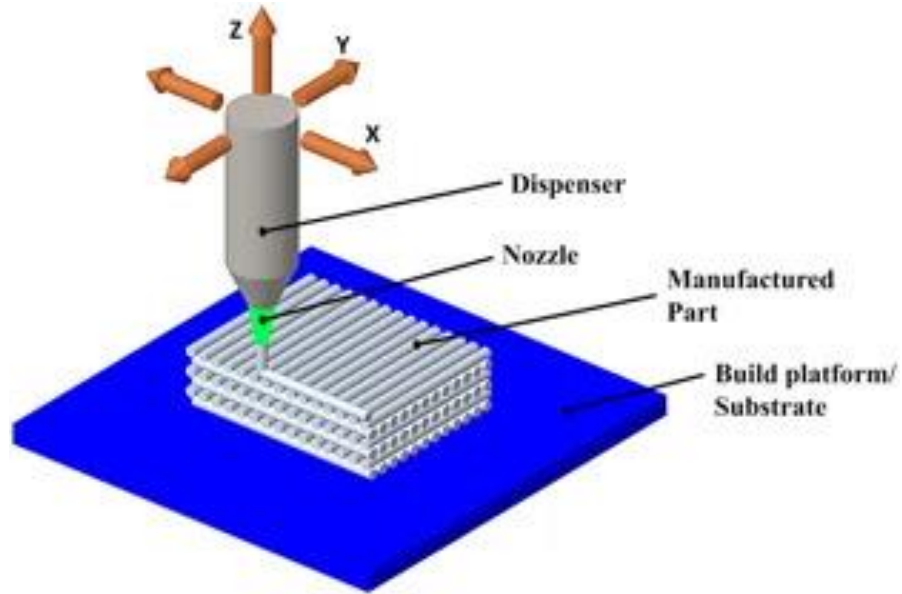
Figure 1.1: Generic DIW system
Source: [44]
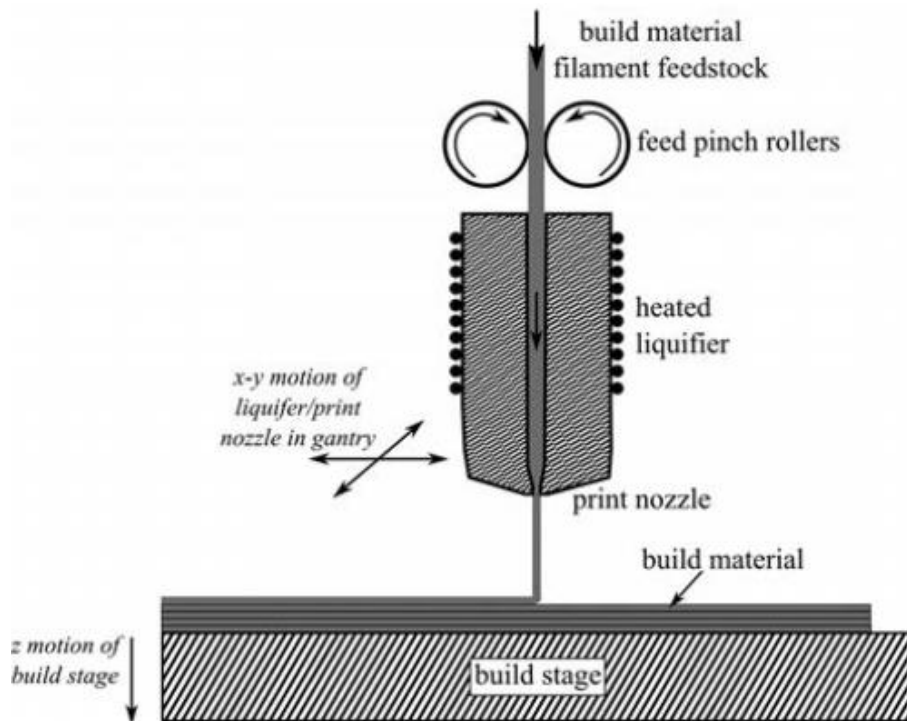
Figure 1.2: Generic FFF system
Source: [45]
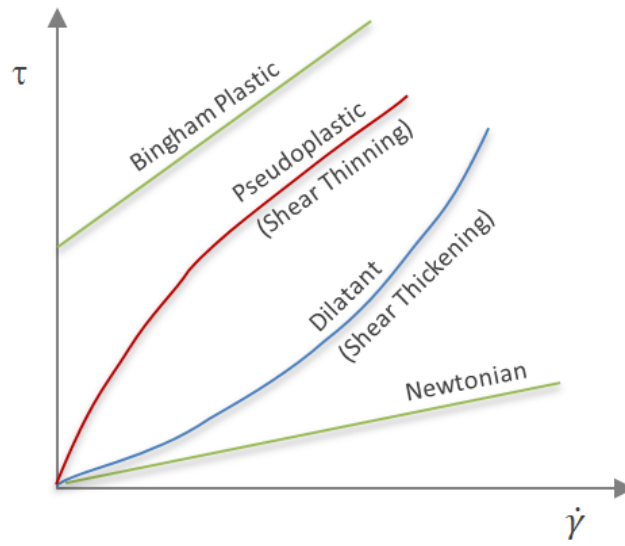
Figure 1.3: Shear rate vs shear stress curves for different types of materials
Source: [46]
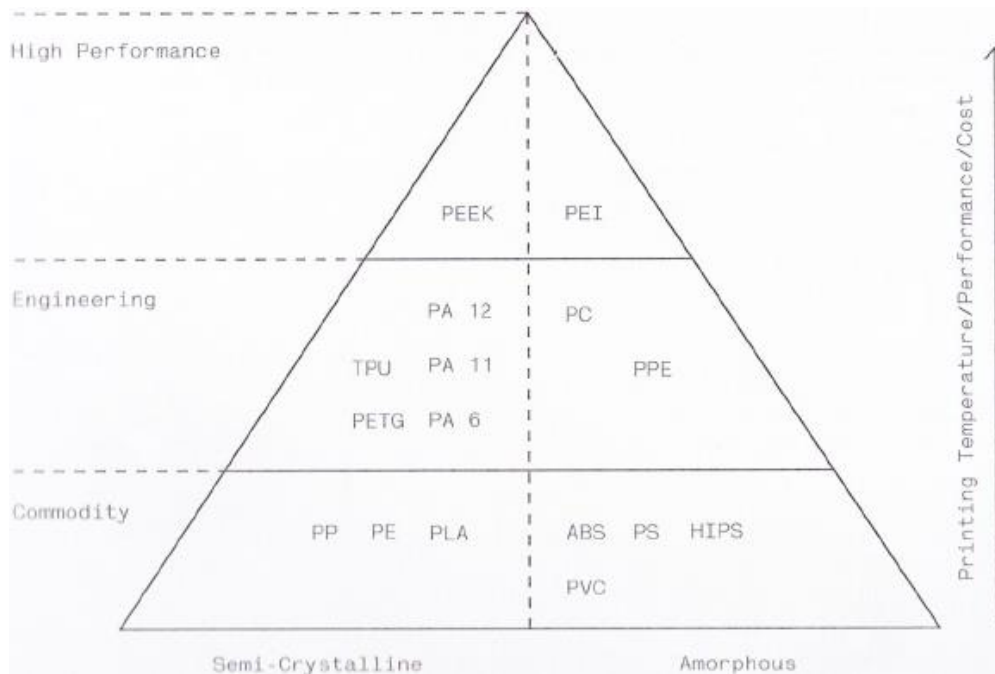
Figure 1.4: Thermoplastic materials pyramid
Source: [40]

Table 1-2: Glass transition temperatures of common thermoplastic filaments

Thermoplastic	Glass Transition Temperature [°C]
PLA	65
ABS	105
PETG	88
PC	147
PEEK	143
PEI	217
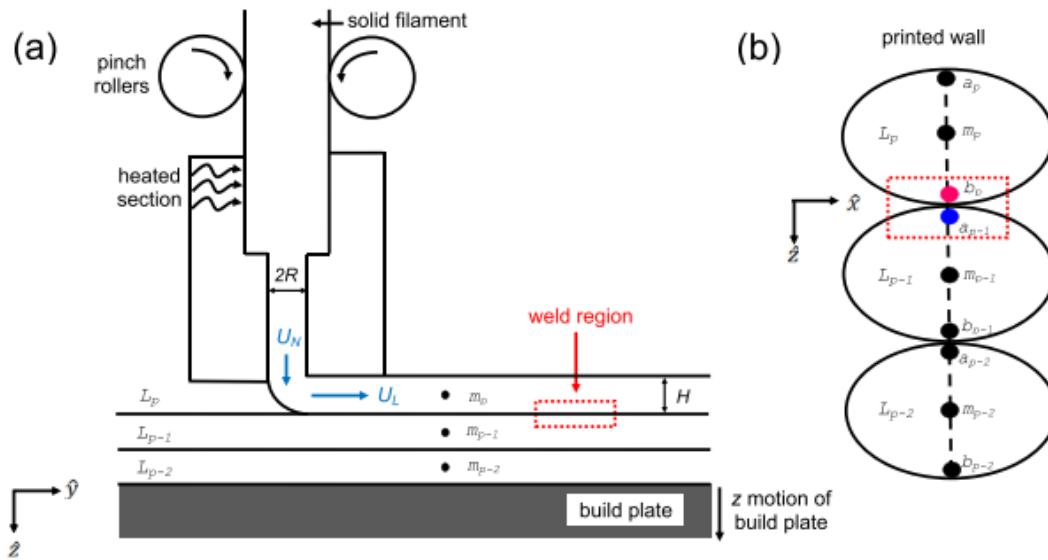
Figure 1.5: Weld formation of deposited material during FFF 3D printing
Source: [43]

build plate. This allows the lowest layers to maintain a minimum temperature that prevents them from contracting significantly. This is effective only for shorter parts, since as the part grows taller more layers can contract that the heated bed cannot interact with. The build surface also needs to be a material the thermoplastic can temporary bond to, however, still removable without damaging the part or peeling up during printing. This bonding can also be used to prevent small amount of warping of the part.

With DIW inks, like filaments, are deposited through a nozzle and maintain the structure even with additional loading from subsequent layers. However, these inks do not need heated to be deposited. These inks can be colloidal gels [47], geopolymers [48], epoxy resins [49], or other colloidal suspensions. These inks are typically selectively extruded using a plunger in a syringe, as depicted in figure 1.6, The pressure behind the plunger can come from pneumatics [36, 37] or a screw extending the plunger towards the material [50] . Each of these inks require curing to solidify. This curing can be accomplished either thermally [47-49] or using photopolymerization, if the material is a photopolymer [51, 52]. This curing step occurs after the printing process, meaning that as the part cures it has no memory where the layer boundaries were, therefore significant cross-linking—the entanglement of polymer chains—occurs between layers during the curing process [53]. Like thermoplastic the build surface can temporarily bond to the part to ensure warping doesn't distort the part.

MEAM is comparable to the same process computer numerical control (CNC) machines use in traditional manufacturing. There is a duality between these two systems; one adds material and avoids where it has already been—additive, the other removes material and avoids where it has not been—subtractive. It is because of this similarity that many 3D printing machines use stepper motors and function on a simple version of G-code, the programming language that operates CNC and other industrial machines. Stepper motors are DC motors that move in discrete steps, giving a greater degree of positional accuracy than traditional DC motors. However, CNC machines are typically built to handle strong forces and operate at slow speeds required during the milling processes. Therefore, though 3D printers may use a similar framework and similar stepper motors, they use a different translational system. While some 3D printers use a cartesian system—where each motor dictates movement along a specific axis, common with CNC machine—there are 3D printers that use alternative schemes like the Sculpto PRO2, where the extruder moves in an arc around a point and can be raised, while the print bed rotates in a circle (Figure 1.7). With this scheme any straight line would require coordination between the extruder movement and bed rotation. Another scheme would be a delta printer, where three arms, attached to the extruder, move on independent rails to pull or push the extruder away from that specific rail. With this scheme any straight line on the build surface would require coordination with all three axes (Figure 1.8). There are other schemes that could be used as a transitional control, however, cartesian systems are predominately used due to the simplicity of position orientation and control.

Figure 1.6: Plunger in a syringe used in direct ink writing 3D printing
Source: [54]
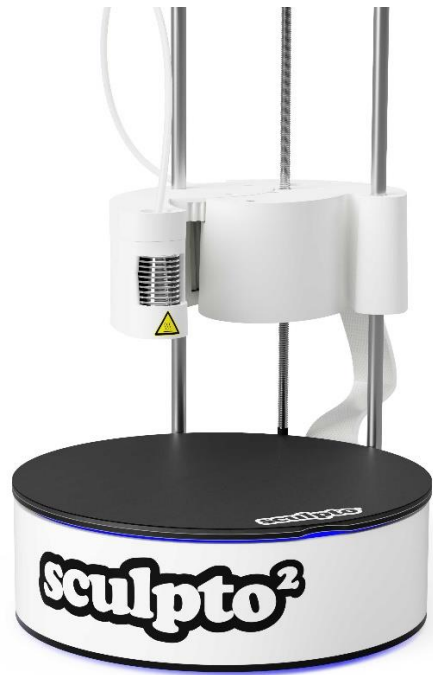
Figure 1.7: Sculpto Pro2 3D Printer
Source: [55]

Figure 1.8: Delta 3D printer
Source: [56]

1.2.3 Fiber Reinforced Polymer Composites

Nature has consistently inspired engineers with new ideas and processes. Among these is the method of combining multiple materials to be greater than the sum of its parts. This idea can be observed in the way rebar is used to reinforced concrete, cellulose fibers reinforce the lignin in wood, or how hydroxyapatite reinforces collagen in bones. These heterogenous mixtures, known as composites, achieve greater performance at a reduced cost or weight than using purely a single material. The classification of composites is based on the materials being suspended, and the material holding the other constituencies. Figure 1.9 depict a simplified version of a composite with a dispersed phase and matrix phase. Using reinforced concrete as an example, the dispersed phase is the rebar, while the matrix phase is the concrete. This is an example of a ceramic matrix with a metallic reinforcement, since the concrete is a ceramic, making this a ceramic matrix composite (CMC). However, the matrix material could also be a polymer—like PLA—resulting in a polymer matrix composite (PMC), or even metallic resulting in a metallic matrix composite (MMC). The dispersed phase could also vary in the same way such as polymer, ceramic, or metallic reinforcement. These reinforcements are typically of micro-nanoparticles size. They can be of the form of fibers, nanotubes, whiskers, or other types of nanoparticles. Fibers are rod-shaped with large aspect ratio—fiber length divided by fiber diameter, longest dimension divided by shortest dimension of the fiber— of 10 or greater and a diameter of 70um down to 100nm, these fibers can also be long continuous strands spanning on the order of centimeters to meters. Nanotubes are typically even smaller fibers consisting of single or multiple walled tubular structures with a diameter of 1 nm to 40 nm while the length can be over 50cm long [57] while whiskers are single crystal structure with a diameter of 1 um and length of 3-5 mm [58]. Some common materials used for reinforcement are CF, carbon nanotubes, GF, fumed silica, and nanoclay.

11
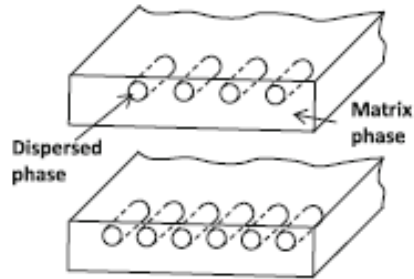
Figure 1.9: Schematic of a composite composition
Source: [59]

Others might classify the reinforcement (the dispersed phase) into alternative categories such as authors Ho and Erden classifies synthetic reinforcement material into three categories: organic, inorganic, and metallic [60]. Using this classifications CF, carbon nanotubes, and GF would be inorganic synthetics reinforcements, while other might classify these as ceramic reinforcements. In this thesis, the focus will be on PMC with ceramic reinforcement, particularly short fiber reinforced PMCs. These PMCs can be classified into three categories: thermoplastic, thermoset, and elastomers. Thermosets and thermoplastics have already been discussed in previous sections and are the focus of this work. Elastomers are highly elastic polymers due to having glass transition temperatures below room temperatures. The resulting material's properties are not only dependent on the properties of the constituent materials, but also on the concentration, shape, distribution, and orientation of the reinforcing material. The concentration of the fibers in the PMC is called the fiber loading, and it is the percentage of the composite that are fibers. Some percentages are by the weight (wt% or w%) others is by volume (vol%). While increasing the fiber loading increases the mechanical properties of the composite there is a limit to where additional loading will sharply reduce the mechanical properties, often referred to the critical fiber loading. It is believed this is due to insufficient stress transfer between matrix and fiber. As fiber concentration increases, the spacing between fibers decreases away from the optimal spacing. This reduced spacing causes the structure to disintegrate before the fiber tensile failure [61, 62]. S. Houshyar et al found a reduction in tensile modulus and flexural modulus after 50 wt% fiber loading with polypropylene fibers [63]. Y. J. Phua and Z. A. Mohd Ishak found CF in PC performed poorly at 40 wt% fiber loading while GF performed well at 40 wt% fiber loading. They observed that the CF did not bond as well to the PC compared to the GF, and that the mean CF length was less than anticipated as possible reasons for the reduced performance [64]. Orientation of the dispersed fibers can play a pivotal role in the overall material behavior. Since these fibers, whiskers, or nanotubes have a significant aspect ratio, the fibers' mechanical response can be anisotropic. This can result with fibers contributing more strength if the force transferred through the polymer matrix is transverse to the fiber. Moreover, if the fibers are thermally or electrically more conductive than the polymer matrix, then the fiber orientation will define pathways the heat or electricity can pass through. Therefore, how the fibers are arranged throughout the matrix will affect the part's overall strength and possibly thermal or electrical response. Prescribing how the structure should respond to outside stimulus by means of tuning the underlying fiber orientation is the process of optimized fiber orientation. Three possible

methods to define the desired fiber orientations to enhance mechanical properties are principal stress trajectories, load path trajectories, and genetic algorithms trajectories. With the principal stress trajectories method two patterns occur, the first is for compressive principal stress trajectories, and the second is for tensile principal stress trajectories [61]. This method works well if the composite component is loaded primarily in compression or tension. Another method using load path trajectories, which consist of following contour lines defined by total stress vectors throughout the part and yields only one pattern as compared to the principal stresses method [62]. The final method is using genetic algorithms, which use an evolution process to tweak fiber orientation towards some fit criteria. This iterative process yields a family of possible solutions close to the desired criteria vs a single solution [63]. Alternative trajectories could be used if fibers were used for electrical conductivity [17], or thermal conductively [18] instead of mechanical reinforcement. These genetic algorithms could assist in these cases, or if the desired design requires a tradeoff of mechanical improvement and thermal conductivity. Traditional manufacturing methods give little control of modifying the resulting fiber orientation. In injection and compression molding, the fibers are aligned along the flow paths that filled the mold. It is possible to reorient fibers during these processes by flow-induced alignment, where shear fields occur as the polymer composite fills the cavity [65], however this requires significant computation and modeling to determine the necessary flow path to achieve the desired fibers trajectories [66] and unique molds for different fiber trajectories. As an alternative, advance manufacturing techniques have been developed in order to lay fiber filled meshes in prescribed orientation in order to accomplish the optimized fiber orientation. Some such processes of fiber placement, called fiber steering, for large-scale parts consist of automated tape laying (ATL), automated fiber placement (AFP), tailored fiber placement (TFP), and fiber path preforming/placement (FPP). In ATL, wide unidirectional pre-impregnated composite tapes with continuous fibers are laid in straight lines on a relatively flat mold in successive layers using a roller system. This system is excellent for large parts that do not have complex geometries. In AFP several smaller pre-impregnated composite tapes (called tows) are independently laid down during a single run using a single roller head that travels in a straight line but follows the curvature of the mold's surface. Aircraft fuselage are a prominent application of this technique [64]. TFP is like the process of sewing, a fibrous material is laid down on a base material and then stitched together to create the composite behavior. This approach can handle complex fiber orientations. Finally, with FPP several patches of thin unidirectional pre-impregnated composite tapes are placed along designed trajectories on mold using a robotic system, allowing for the fabrication of highly complex parts. While these processes work well to align fibers in large structures, not all composites are designed to be incorporated into an aircraft. While these systems are being scaled down to smaller applications, small scale fiber alignment requires alternative strategies, especially to be utilized in material extrusion methods of fabrication. The most common technique is that of dictating the tool path due to fibers being highly aligned in the direction of print path by the velocity gradient in the deposited material [21].

1.2.4 Tool Path Consideration

During the slicing process of MEAM, tool paths are defined based on the nozzle diameter and the part's geometry. These tool paths fill out the volume of the specific layer of the part via lines—referred to as beads—that are directly related to the nozzle diameter. Different tool paths can fill out the same geometry.

Figure 1.10 depicts three common approaches with varied nozzle sizes. As the nozzle size increases the processing time decreases, regardless of these chosen tool path. Notice how portions of the part are consistent through the different tool paths, such as the beads around the perimeter, and around the holes in the part. These common paths are to help ensure a consistent perimeter finish to maintain part consistency. While not required, this approach is often utilized at least partially. In order to increase the part's strength successive layers are printed at different angles. A common approach is to use $\pm 45°$ alignment as depicted in figure 1.11. This strategy ensures that any force acting on the part will interface equally with beads that are parallel and orthogonal to the force vector. This is important when dealing with composite materials that have anisotropic behavior. This stacking sequence produces quasi-isotropic behavior. This $\pm 45°$ sequence is similar to the optimum stacking sequence of (0, 90, 45, -45) found by Song et al. [61]. However, there are some structures that cannot readily utilized this stacking method. Figure 1.12 depicts one such structure—the honeycomb. These thin walls limit the possible tool paths to fill out the layer. These paths do not readily allow the orthogonal stacking sequence. While the honeycomb structure might seem like an isolated structure, these thin walls are prevalent in non-fully infilled structures. Infill is the section of the part completely covered by perimeter walls, and top and bottom layers. This can reduce the total material used and processing time at the cost of strength [62, 63]. This infill method is common in AM with some possible infill patterns depicted in figure 1.13. Additionally, some parts themselves limit the size of the bead. Consider the leading edge of a wing, flow channels in a support structure—like the grill of a car—or a heat sink. Some of these structures benefit by the small minimum features or large surface area. All of this is considered in the design process of a part being manufactured by MEAM. A fully infilled structure has the greatest strength and allows for the most varied stacking sequences to accomplish quasi-isotropic behavior; however, the function or cost of the material might prohibit a solid part. Fortunately, AM can accomplish complex internal geometries to reduce the total material usage, or direct flow. One possible technique to modify the behavior of composites with high-aspect ratio fibers with limited tool paths is to decouple the fiber orientation from the print path. If fibers could be reoriented in such a way to resist the expected loading, more strength could be recovered. Even quasi-isotropic behavior could be accomplished if for any force an equal number of beads with reoriented fibers are orthogonal and parallel to the applied force. Heat sinks could utilize this if the embedded fibers were highly thermally conductive. Reorienting the fibers out of the plane of the print layer would allow for the heat to be transferred more efficiently away from the heat source. Additionally, heat exchangers could benefit from fibers orthogonal to the print path, allowing the walls to be very thin, but still transfer heat effectively. This alignment could be used to selectively specify how the heat is transferred through the wall if the polymer matrix was an insulator.
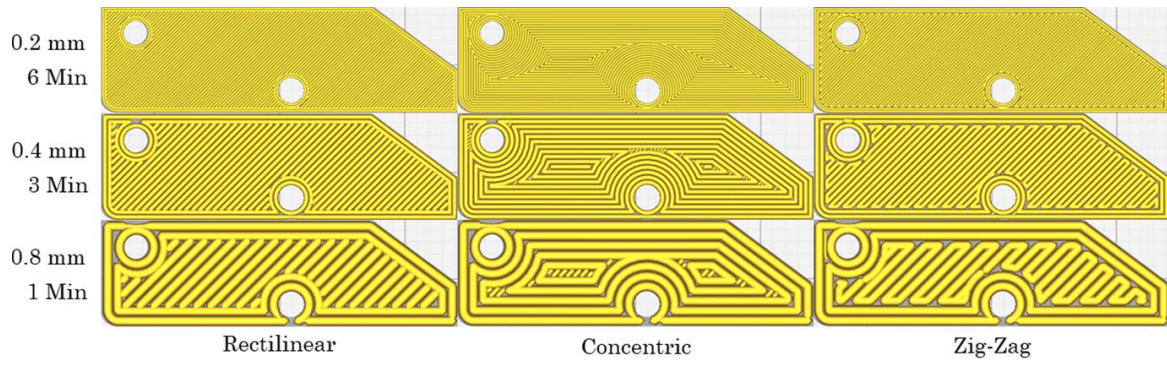
Figure 1.10: Various tool paths types at different nozzle diameter, and the resulting print time
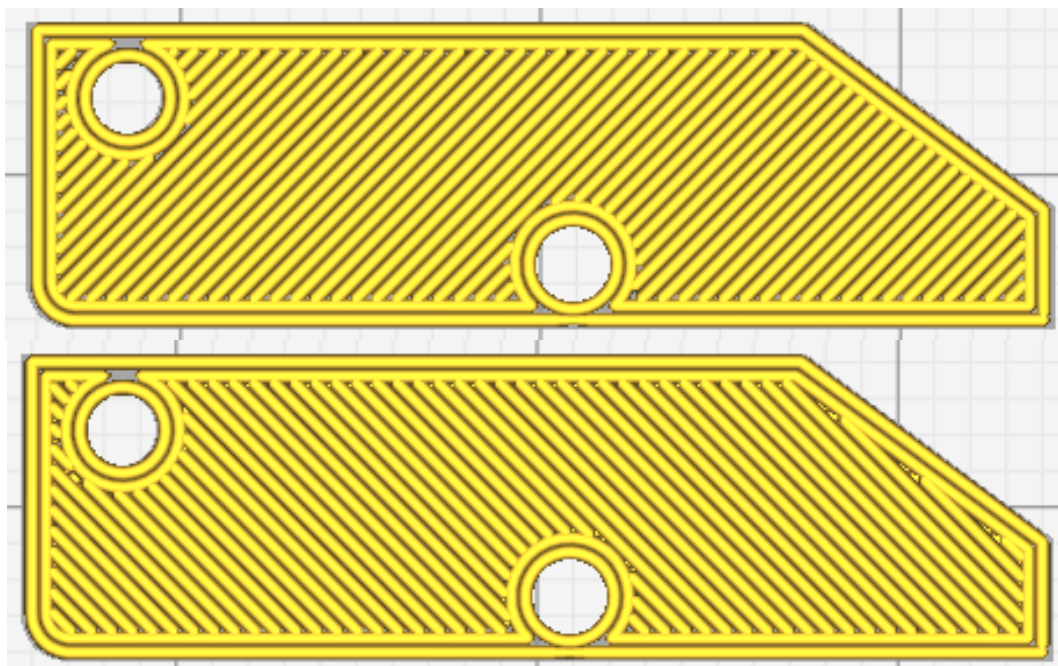
Figure 1.11: Successive layers are printed orthogonal to the previous layers
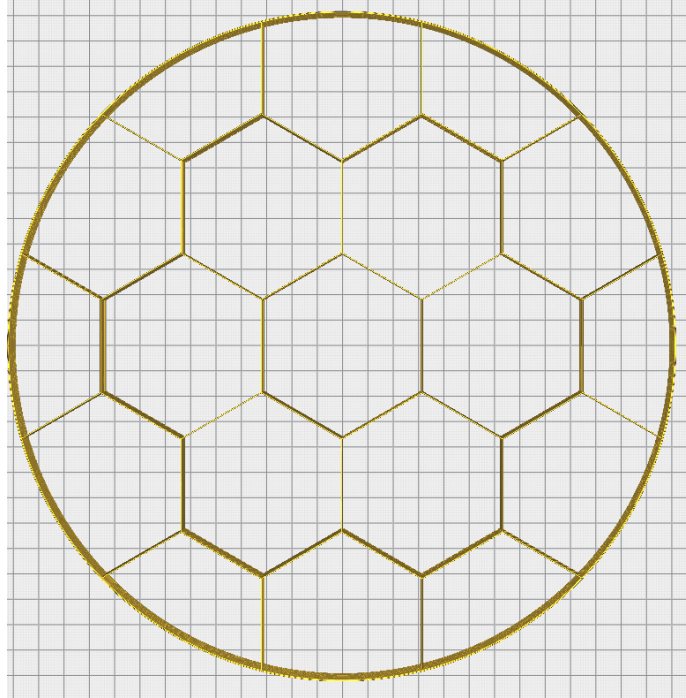
Figure 1.12: Honeycomb structure with thin connecting lines
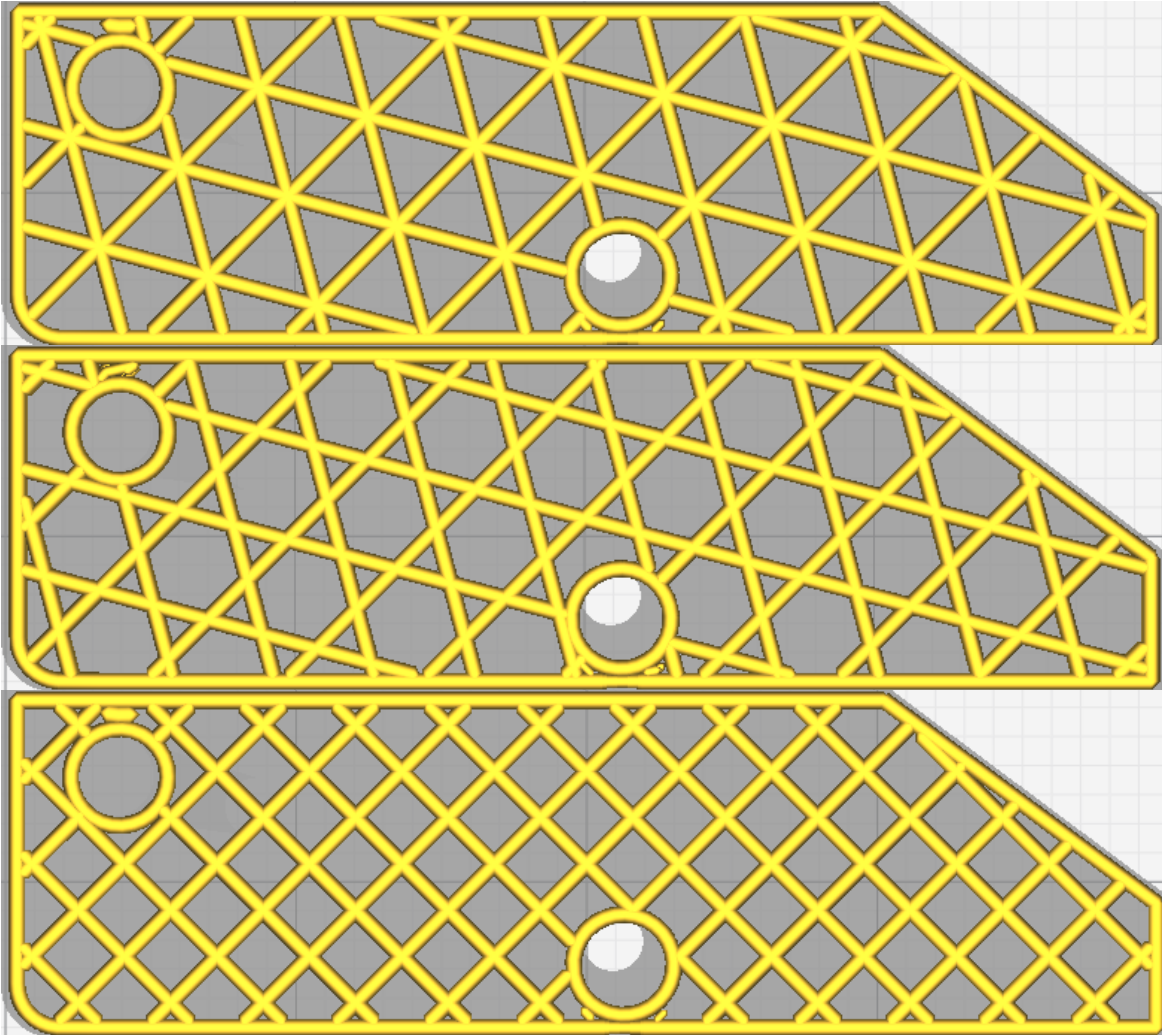
Figure 1.13: Three infill patterns. From top: Triangle infill, Tri-hexagonal infill, and Grid/Line infill

1.2.5 Small Scale Fiber Orientation Strategies

Fibers in a PMC could also be oriented by physical modifications such as stretching the thermoplastic polymer matrix during the fabrication process [64], however this method is less effective at higher fiber loading. Alternatively, these fibers could be oriented in an epoxy polymer through compressive loading [65], however this is limited on the amount it could reorient the fiber. Fibers in a PMC can also be reoriented by applying an external field to the composite. One such field could be an electric field by using aluminum plates on either side of the polymer composites as the material solidifies [66]. This method is ineffective with fibers that are not reactive to electric fields, and less effective with fiber loading greater than 10 v% with fibers diameters larger than 17μm since the external field is unable to overcome the internal forces of the matrix, or when the fibers are perpendicular to the applied fields where the force from the field is parallel to fiber orientation resulting in no torque on the fibers. The maximum size of the part is limited by the size of the electric field. Magnetic fields are another field that can reorient fibers by using two plates on either side of the deposited composite to generate a magnetic before it solidifies [67]. This is also limited to magnetically responsive fibers, fibers loading of less than 6 v%, and the maximum size of the magnetic field. Though this process can use a mask to orient fibers locally in the composite. Finally, acoustic field of standing waves could be used to orient fibers. This process uses a piezoelectric element either attached to the deposition mechanism or passing over the deposited material and through half-wave excitation fibers can be clustered and aligned [26, 68]. This method doesn't require specific materials, or a maximum size, however it requires low fiber concentration. Finally, a recent method demonstrated that adding an additional shear field during the deposition process of an epoxy-resin composite, fibers could be locally orient in the deposited bead [28]. This method accomplished this by rotating the nozzle during deposition which was able to locally reorient most fibers to a designed angle. It seems reasonable that this could extend to thermoplastic using the same rotational method, which is the inspiration for this body of work. Using the formulas defined by Raney, Compton et al. the rotational ratio, feedrate, or rotation rate can be found using (1-1,1-2,1-3) where ω is equal to the rotational speed of the nozzle, R is the desired dimensional ratio, F is the linear speed of the extruder, and r is the radius of the nozzle

$$R = \frac{\omega r}{v} \qquad\qquad (1\text{-}1)$$

$$F = \frac{2\pi r \omega}{60R} \qquad\qquad (1\text{-}2)$$

$$\omega = \frac{60RF}{2\pi r} \qquad\qquad (1\text{-}3)$$

Chapter 2 Rotational Direct Ink Writing (RDIW) Extruder

2.1 Introduction

Four major components were identified as necessary to emulate the work done by Raney, Compton et al [28]. First is a short fiber reinforced thermoset composite. Second is a DIW extruder compatible with the chosen composite and with a nozzle that can be rotated. Third is a means to rotate the nozzle. Finally, is a means to sync the rotation of the nozzle to the desired local reorientation during deposition. The following few sections will cover some background information pertaining to these specific requirements not previously discussed, then discuss the existing hardware for the RDIW extruder.

2.1.1 DIW Extruder Design

As discussed in section 1.2.2 DIW & FFF Methods, a DIW system deposits a thermoset material. Figure 1.6 depicts a typical mechanism to dispense the feedstock material. The syringe is loaded and primed with the desired material, while the displacement of the plunger controls the flow of the material. This displacement can either be controlled directly, by attaching the plunger to a lead screw system—such as a ball screw or ACME screw—or indirectly, through speed control by way of controlling the pressure behind the plunger through either pneumatics or hydraulics. Through direct control, the flow rate can be calculated by the rate volume is displaced in the syringe. An example of this calculation would be if a 2" diameter plunger moved 3" into the material in 5 seconds, then the flow rate (Q) can be calculated using (2-1,2-2), where V is the volume of material displaced, h is the distance the plunger moved, r_s is the radius of the syringe, and t is the time elapsed.

$$V = h\pi r_s^2 = 3\pi \left(\frac{2}{2}\right)^2 = 3\pi \; in^3 \tag{2-1}$$

$$Q = \frac{V}{t} = \frac{3\pi}{5} \frac{in^3}{s} \tag{2-2}$$

Alternatively, the rate of displacement of the plunger can be controlled through pressure, and this would directly control the flow rate of the material. This, however, requires modeling the flow of a non-Newtonian fluid through a constricting tube. The flow rate can also be found empirically by exerting different pressures on the plunger and observing the flow rate of the material. The desired flow rate can be determined by using the translational speed of the syringe, the nozzle radius, and the layer height. If F is the linear speed of the syringe, h is the layer height, and r is the radius of the nozzle, then (2-3) calculates the required flow rate to deposit enough material. Equation (2-4) solves for the speed the lead screw must move the plunger.

$$Q = F\pi r^2 \tag{2-3}$$

$$\frac{h}{t} = \frac{Q}{\pi r^2} \tag{2-4}$$

Other factors complicate these calculations, such as the Barus effect (also known as die swell) where the extruded material expands beyond the nozzle diameter that interacts with adjacent

layers, intentionally over extruding to ensure enough contact with adjacent and subsequent layers, to diminish voids between layers, to compensate for material shrinkage during solidification. Other considerations are required to prevent self-buckling or yielding as layers are continuously stack on each other.

2.1.2 Stepper Motors

Hybrid synchronous stepper motors are the most common means 3D printers use to implement translational control due to their high positional accuracy without feedback control. In addition, these same stepper motors are used to drive filament through a hotend in an FFF process or drive a leadscrew for a DIW process. A stepper motor is a DC motor that is driven in discrete steps. An internal assembly of a hybrid stepper motor can be seen in figure 2.1. Here two sets of four electromagnetic coils of copper wire (phase A and phase B) with grooves called teeth, surround a permanent magnet rotor with a mismatched teeth pattern [69]. The rotor is magnetized along the axis, and the teeth on the rotor are slightly offset compared to those on the coils such that only a section of the rotor's teeth, on either side, line up with the teeth of two coils. The number of teeth and coils determine the step size of the hybrid motor, with 1.8° step size, or 200 steps per rotation, being a common variety. To generate motion, the phases are powered in an alternating sequence, and through electromagnetic induction a magnetic field is produced. Since the teeth are slightly misaligned the rotor will rotate to align the magnetic fields of the coil and rotor. Phases A and B are independently controlled through either a bipolar connection (each coil phase is controlled by only two wires) or unipolar connection (each coil is controlled by three wires) [70] as depicted in figure 2.2. Unipolar motors are easier to control since the center wire (center tap) can be routed to ground to prevent a more complicated control scheme. However, there are many motor controllers that can drive a bipolar stepper motor, and this configuration is more widely used. A unipolar connection can be converted to a bipolar connection by not connecting the center tap, or not connecting either end of the coil. The latter method decreases the overall torque of the motor, but it also decreases the amount of time it takes for the coils to saturate the magnetic field. This is particularly useful to drive stepper motors faster at the expense of less holding torque. Microstepping is a method to divide the full step of a stepper motor into smaller step size to give more positional precision. This is achieved by partially saturating both phases simultaneously. If both phases are generating an equal magnetic field, then the rotor will align partially to both coils, effectively doubling the number of steps per revolution or halving the step size. This is known as half-step microstepping. Some control boards can divide each step into 256 microsteps, however each microstep has only 0.61% holding torque compared to a full step [71] which can cause skipped steps due to the low holding torque.
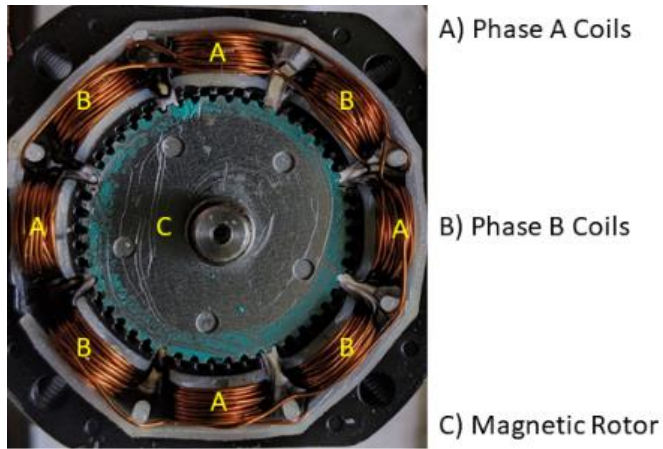
Figure 2.1: Internal assembly of a hybrid synchronous stepper motor
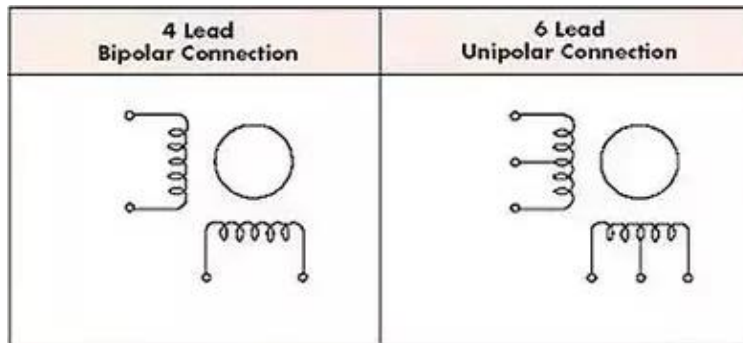
Figure 2.2: Stepper motor wire configuration
Source: [72]

2.1.3 Torque Consideration

Torque is defined by (2-5). Where τ is the torque, I is the system's moment of inertia, and α is the angular acceleration of the system.

$$\tau = I\alpha \qquad (2\text{-}5)$$

The first term that dictates the required torque is the moment of inertia of the system. This parameter is reasonably constant during a print, though it does vary as material is extruded through the system, especially if the feedstock material rotates with the assembly. This term can be calculated directly by measuring the system, or by calculating it from the BoM and design details. The second term is angular acceleration which depends on the parameters of the print. Figure 2.3 depicts the transition between two regions of differing constant rotational speeds at a constant linear speed throughout both regions. Equations (2-6,2-7) defines the angular acceleration and difference in rotational speed. Where ω is the rotational speed, V is the linear speed, L_T is the length of the transition region, r is the radius of the nozzle, and $Ratio_A, Ratio_B$ are the dimensionless rotational ratios for the respective regions

$$\alpha = \frac{V\Delta\omega}{L_T} \qquad (2\text{-}6)$$

$$\Delta\omega = \omega_B - \omega_A = \frac{V}{r}(Ratio_B - Ratio_A) \qquad (2\text{-}7)$$

The maximum angular acceleration (and thus maximum required torque) can be found when $V\Delta\omega$ is max, and L_T is minimum. Since r is constant throughout the print, V is the term that dictates the required angular acceleration strongest. The expected maximum difference in ratios is less than 10, while V in DIW prints can vary from 2 to 32 $\frac{mm}{s}$. L_T can be arbitrarily chosen, however significant small values (<0.1 mm) could quickly result in unachievable accelerations even at low speeds. Equations (2-5 – 2-7) help inform the design decisions. If high speeds and small transition regions are required, then the torque will have to be substantial, or I must be very small. The required torques inform which type of motors will be necessary or, for a given motor, what are is minimum distance for the transition region, and maximum speeds that can be done.

2.1.4 3D Printer's Control Boards

A 3D printer's control board needs to handle the position of the extruder, the mechanism of extrusion, and any peripherals that are necessary (fans, heaters, limit switches, etc.). This is accomplished through G-Code, a programming language used with CNC machines that has been repurposed for 3D printers. The 3D printer variants called "flavor" contain codes (One-line commands of the form G1 X100 Y100 F2000) that sequences all the actions the printer needs to take. These commands fall into two categories. The first category is commands that configures the system, such as setting the max speed, accelerations, current of a motor, or selecting which tool is active for a multitool system. The second category are commands that accomplish an action. The command G1 X10.25 Y-25.23 F2000 is a basic movement command that tells the system to move to the X position of 10.25 base units (these can be configured to be mm or inches), Y position to -25.23 base units at a speed of 2000 units per minute (called the feedrate).
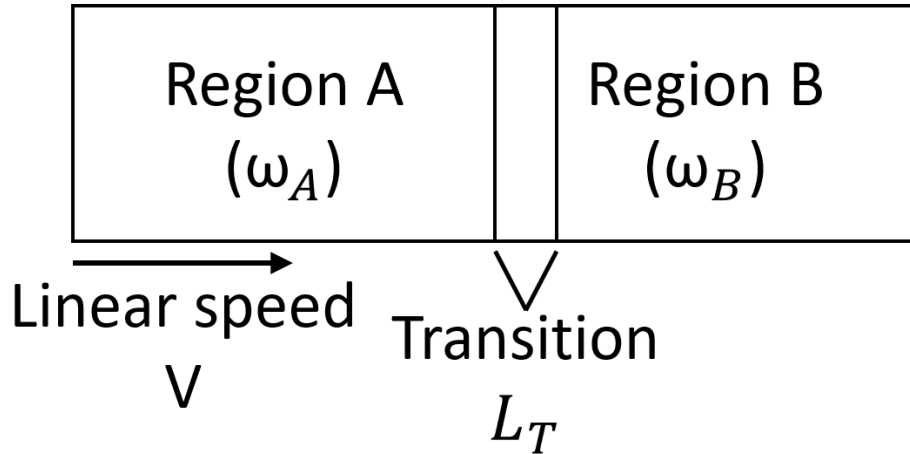
Figure 2.3: Transition between two regions of differing constant rotational velocity

However, there are several commands that can augment what this command means, such as changing from absolute coordinates to relative. This change would instead make the G1 command move in the X axis in the positive direction by 10.25 units, in the Y axis in the negative direction by 25.23 units, at a speed of 2000 units per minute. However, this interpretation might change in different "flavors" of G-code. One form might want the F parameter (the speed of movement or feedrate) to be in units per seconds or gives the option to swap between those two settings. There are many "flavors," and some are not open source, such as the type used for Ultimakers 3D printers. This confusion can cause problems if printing a file designed for a different printer, therefore most slicers—the programs that generate these commands—have several options of outputs to tailor to the specific printer at hand. This is especially important for printers of different constructions such as the delta printer or Scultpo Pro 2 3D printers. The following discussion will assume references made are to a cartesian-based 3D printer, since those are the easiest to describe. The control board receives these G-code commands either from portable memory like an SD card or a USB drive, or from another computer via a USB cable. These commands tell the system how far to move the motors, to set heaters' temperatures, fan speed, or other peripherals. The command used most regularly is the movement command, G1, as described earlier. Before printing or reliable movement can occur, the control board needs to know how many steps are necessary to move the axis 1 mm (this unit can be changed without loss of generality). This parameter is called steps/mm or x-step/y-steps/z-steps for the three-primary axis and e-steps for the extruder. If it takes 10 steps for the x axis to move 1mm, and the printer was tasked with moving the x axis 10mm, then the system would determine 100 steps are necessary to position the stepper motor in the desired position. The extruder's stepper motor dictates how much of the feedstock material should move, which is calculated based on the transition from the feedstock diameter, to nozzle diameter. The control of the stepper motors is accomplished using specific drivers. The control board signals the specific axis driver that 100 steps are necessary and signals the timing to effectively accomplish the desired feederate. The stepper driver then calculates the phase changes inside the coils of the stepper motors for the necessary motion. Microstepping of stepper motors is accomplished through pulse-width modulation (PWM) of the control voltage, and gives more positional accuracy to applications, though it does require more processing power to do successfully. In

addition, 3D printer control boards are also able to run fans at varying speeds using PWM, heaters for heated beds, and extruders also using PWM. However, since heating elements are relatively slow dynamic systems, bang-bang (fully on, then fully off) control is often utilized instead of a more sophisticated control system. Many of these control boards also have some general-purpose input/output (GPIO) pins for additional flexibility. However, these are digital or PWM controlled to imitate analog.

2.1.5 RDIW Existing Hardware

At the start of this work an existing RDIW extruder was already developed based on Raney, Compton et al. design. This extruder used a Shopbot Desktop CNC machine, pneumatics to control the pressure to the syringe controlled by the Shopbot (using G-Code), manual control to set the rotational speed of the extruder, and rotated the entire syringe containing the ink to print. Each of these components can be seen in figures 2.4-2.6. While this system was effective, it required significant set-up and calibration each time the print head was installed, or a new syringe was loaded. Additionally, the rotational control had to be done manually through a potentiometer dial. The means of rotation was accomplished by a DC motor and pulleys.

2.2 Design Considerations

A new design was desired to reduce the amount of calibration required for printing, and to automate the rotational control to incorporate G-Code handling for rotational ratio prescribed earlier. The next sections will walk through possible options to accomplish the RDIW extruder and the rationale for the design chosen.

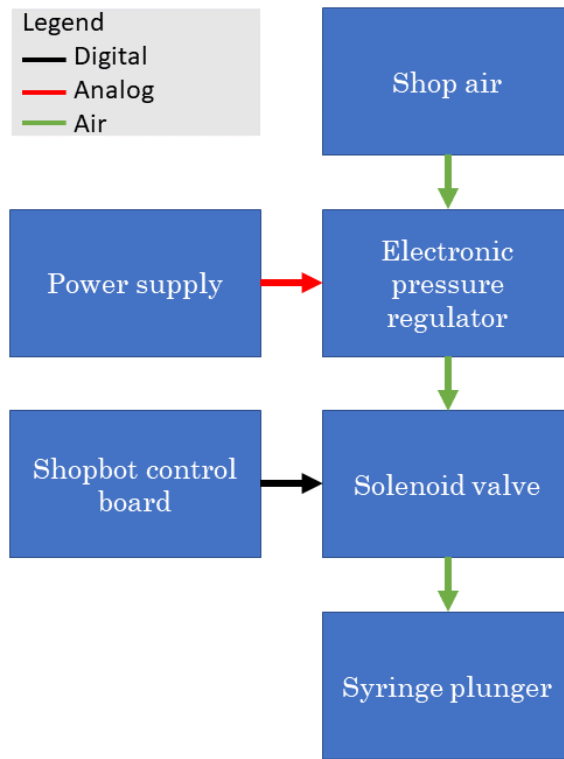*Figure 2.4:Shopbot's Desktop CNC Machine*
Source: [73]

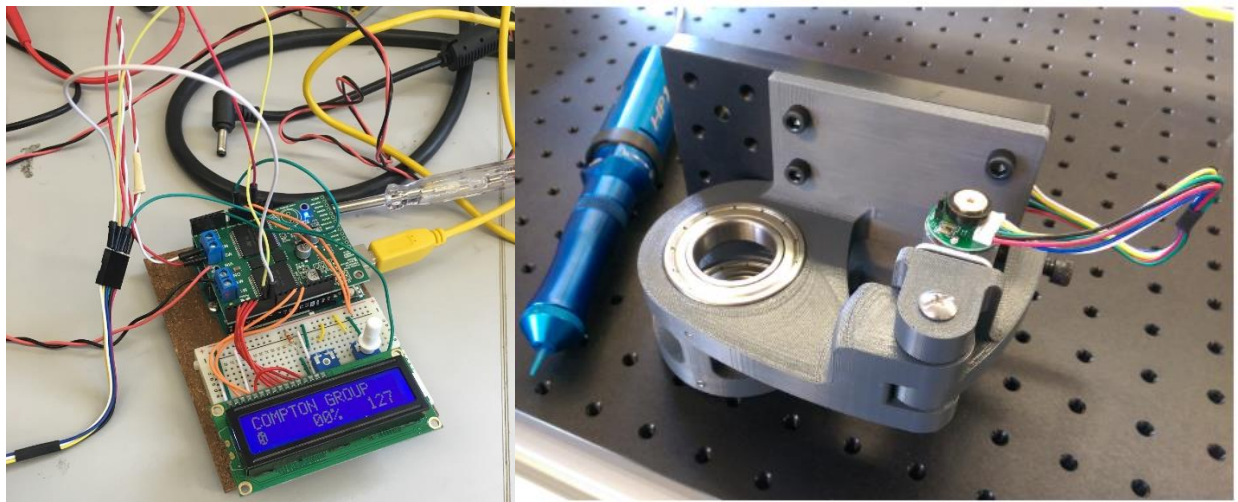*Figure 2.5: Pneumatics control diagram*

Figure 2.6: Existing RDIW rotational control board and fixture

The first part needed for this design is a fiber reinforced polymer feedstock material. There are several viable options for this composite. Raney, Compton et al. [28] chose to use two types of CF–epoxy composites, with fiber concentrations of 1.3% volume, 15.5% volume, and 18.5% volume. The first type, being a more brittle epoxy resin, consisted of dimethyl methylphosphonate, nanoclay (Nanocor I.34TCN), milled CF (Dialead K223HM; Mitsubishi Plastics), and epoxy resin (Momentive Epon 826), with Basionics VS03 as a curing agent. Their second composite consisted of fumed silica (CAB-O-SIL TS-530; Cabot), milled CF, and epoxy resin (Momentive Epon 8131), with Basionics VS03 as a curing agent. They used the flexible epoxy for both the 1.3% and 15.5% volume fiber concentration while using the more brittle epoxy resin for the 18.5% volume fiber concentration. This would be a reasonable composite to be able to print due to the widespread uses of CF-epoxy composites, therefore this type of composite forms the basis of the design of the new RDIW extruder.

With the characteristics of the composite known, parameters and constraints can start to develop. The milled fibers have an average diameter of 11 µm and lengths of 50 µm and 200 µm. To avoid clogging, the nozzle diameter should be greater than the longest anticipated length of CFs, and since a curing agent is used, the material might begin to harden before deposition—in that case a nozzle size of 400 µm should be great enough to prevent clogging. Therefore, the maximum nozzle gauge should be 22. To remove the need to clear such a small orifice as the material hardens, ensure maximum print time, and due to availability of parts, the nozzle should be disposable, which is a common practice in DIW. Three designs were considered to allow the nozzle to rotate, two of which are depicted in figure 2.7. First design is to add a rotary union inline between the feedstock material and the nozzle (this is the design Raney, Compton et al. chose). This design has the advantage that it requires a small number of additional parts, however it requires a specific rotary union to accomplish the speed and flow required. An alternative would be to rotate the feedstock material with the nozzle. This is simply taking the syringe with the nozzle attached and rotating it (this is the design the existing RDIW extruder utilizes). This design requires more torque since more components are rotating; however, it simplifies the design, since the rotary union is on the exterior of the syringe and thus doesn't need to be cleaned after use. This design is greatly complicated if a leadscrew is used to move the plunger, due to the complex interaction between a rotating syringe and a stationary leadscrew. The final alternative is to rotate a leadscrew system with the rotating syringe. This seems like an unlikely solution due to how much must rotate for the nozzle to rotate; this would require a significant motor to rotate quickly. The first option was chosen as the most reasonable solution to rotate the nozzle, and the best way to mitigate the necessary calibration for printing compared to the existing hardware.

In order to control the whole system, three possible control boards were considered. The platform that is intended to be used is a Shopbot Desktop CNC machine that is used for other DIW experiments and the previous assembly. This system has a three-axis gantry that can move the end effector in 3D space throughout the build volume of 610mm x 460mm x 140mm. The default control board has four stepper motor interfaces—three to control the gantry, an optional fourth stepper motor—five digital outputs that can be used to control peripherals such as solenoids valves for pressure control , and two additional interfaces for a spindle tool or router. This control board works very effectively; however, it uses a proprietary 'flavor' of G-code and custom software that prevents additional tasking on the controlling computer for safety concerns.
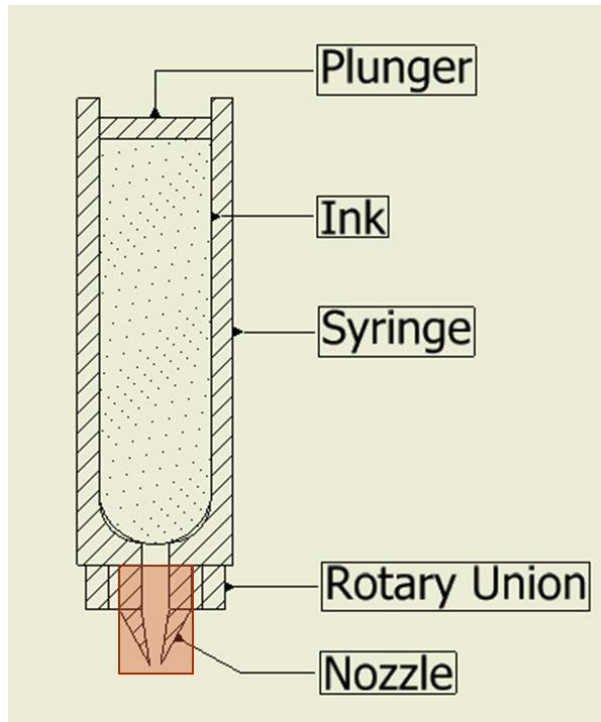
a) Rotary union inline between nozzle and feedstock material rotating only the nozzle. The orange box depicting the rotating portion
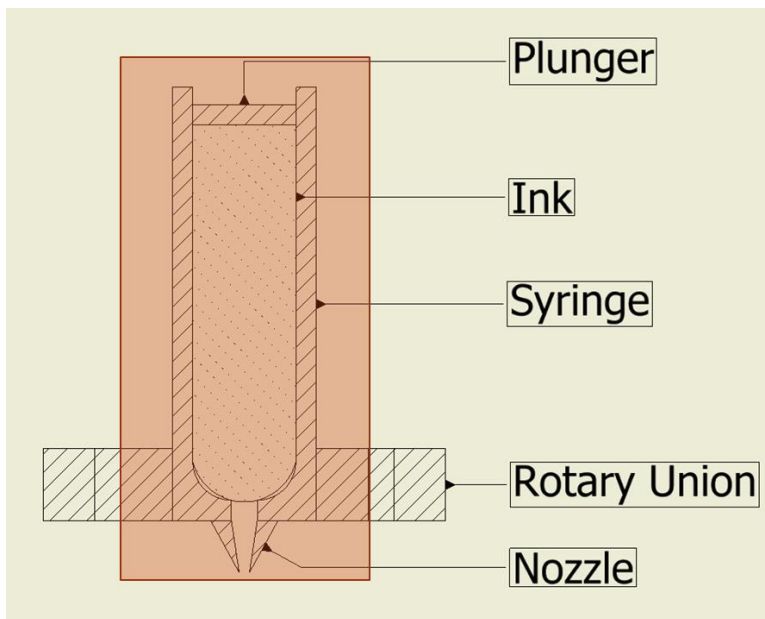
b) Rotary union inline rotating the entire syringe. The orange box depicting the rotating portion

Figure 2.7: Two methods of rotating a DIW nozzle

The second option considered is using an Arduino running a version of RepRap connected to a multi-axis stepper driver (i.e Leadshine MX4660, 4 axis stepper drive). This would allow the use of an open-source firmware such as Repiter-Firmware or Marlin. Pairing with a more significant stepper drive instead of a RAMPS board ensures the current drawn by the large three-axis gantry doesn't overwhelm the control board, though it comes at the cost of additional built-in functionality, such as fans or heaters that the RAMPs would have afforded. The last option considered was use of a single-board controller such as Smoothieboard or Duet 2. The advantage of this method is that the stepper motor drivers are designed to handle large motors, it uses an open-source firmware, and it still maintains room for additional functionality. These latter two options are comparable in price, while the first option has no additional cost since the hardware is already available. The last option was chosen to open more peripherals control for further development. The Duet 2 board was chosen for the additional feature such as SpreadCycle and Stallguard functions.

2.2.1 Motor Consideration

The existing extruder framework for 3D printers allow for stepper motors to be directly controlled inside the control loop handling the linear motion of the 3D printer. Accelerations are automatically matched so that the extruder keeps pace with the linear motion, extrusion speeds are dynamically set to ensure the material is fully extruded at the end of travel. While stepper motors have less torque at lower speeds than other type of motors, the ease of embedding them in the G-code makes stepper motors an attractive option for rotating the new RDIW extruder. The Duet 2 control board provided constraints for the stepper motors chosen. The system has a maximum of 24V supply, and the maximum current per phase is limited to 2A. Using the guidepost of 1000RPM from [28]. These parameters provided a rubric to select a stepper motor. The selected stepper motor had the maximum torque available within the constraints, from the available vendors. The torque curve can be seen in figure 2.8. The moment of inertia for each component can be estimated by using simple thin cylinders with all the mass accumulated at the greatest radius of the part, while the nozzle can be modeled as a hollow cone. Only a portion of the rotary union will rotate, which the stationary portion in turn will add friction to resist the rotating torque. In addition, as the head is primed with material this too will add to the moment of inertia. To simplified calculations the entire mass of the rotary union will be used to account for this frictional force and material loading. The equation for a thin-walled cylinder and cone are (2-8,2-9) respectively, where m is the mass of the component, and r is the largest radius.

$$I = mr^2 \qquad\qquad (2\text{-}8)$$
$$I = \frac{1}{2}mr^2 \qquad\qquad (2\text{-}9)$$

Table 2-1 tabulates the mass and radius of each component, and that part's contribution to the moment of inertia. The acceleration curves with different gearing configurations can be seen in figure 2.9 using the data from figure 2.8 and table 2-1. To determine the most suitable configuration, multiple parameters had to be varied (*Linear speed*, *nozzle size*, and *transition length*). Figures 2.10,2.11 depict the required angular acceleration and rotational rate, for a dimensionless ratio of 5, for various *nozzle sizes* (in mm), *linear speeds*, and four different transition length strategies. The first being setting L_T equal to nozzle's radius. These second strategy equal to the nozzle diameter. The third strategy equal to 0.5 mm. The last strategy equal

to 1 mm. This type of exploration is required to see what speeds are possible under which gearing situation, and to set proper transition lengths. If a parameter is first selected due to design criteria, this can set limits on the other parameters. High speed might be chosen to minimize processing time, while small nozzle size might be chosen for minimum feature size, or a small transition length might be chosen to allow for stark differences in fiber orientation. If speed is the utmost criteria, $32 \frac{mm}{s}$ is the fastest expected print speed for an DIW extruder. This selection would limit the nozzle's size to 0.8 - 1.0 mm as nozzles below 0.8 mm would require a rotational rate greater than the stepper motor with a 1-4 gearing ratio can achieve (as seen in figure 2.9). From figure 2.11 it can be observed that these parameters would require a transition length much greater than 1 mm since a transition length equal to 1 mm required $5000 \frac{rad}{s^2}$ and that is not achievable at the desired rotation rate under any of the gearing ratio. If small nozzle size is the utmost criteria, then selecting the 0.2 mm nozzle would limit linear speed to less than $7 \frac{mm}{s}$ due to the rotation rate approaching 3000 RPM. However, this would require a transition length greater than 0.5 mm. If minimizing the transition length was the utmost criteria, this would limit the print speed to less than $10 \frac{mm}{s}$ due to the high angular acceleration for smaller nozzles. These exercises point out that this stepper motor is only suitable for linear speeds less than $15 \frac{mm}{s}$, nozzle sizes greater than 0.6 mm, with a transition length greater than 0.5 mm. In this range the maximum rotational rate is 1500 RPM, and the maximum rotational acceleration is $5000 \frac{rad}{s^2}$, however no gearing ratio has both those parameters simultaneously therefore subsequent prints must weigh linear speed vs dimensionless rotational ratio to determine suitable gearing. Since all the equations used have had a linear dependence on the dimensionless rotational ratio; halving the desired ratio will halve the required rotational speed and angular acceleration allowing for greater linear speeds at smaller transition length, however fibers will be less rotated.

While these graphs focus on a stepper motor to accomplish the rotation, the same type of calculations could be used for a servo motor, or other DC motor. The stepper motor was chosen due to the ease it could be incorporated into the 3D printing extruder framework.

Table 2-1: Moment of Inertia calculations for the RDIW extruder

Component	Moment of Inertia [kgm^2]	Mass [g]	Radius [mm]
Rotary union	18.764 x 10^{-6}	153.7	11.049
3/8 to ¼ adapter	4.642 x 10^{-6}	32.7	11.915
¼ to Luer Lock adapter	3.732 x 10^{-6}	60.2	7.874
Pulley	35.585 x 10^{-6}	69.4	22.644
Chuck	4.839 x 10^{-6}	15.8	17.5
Nozzle	14.516 x 10^{-9}	0.25	7.62
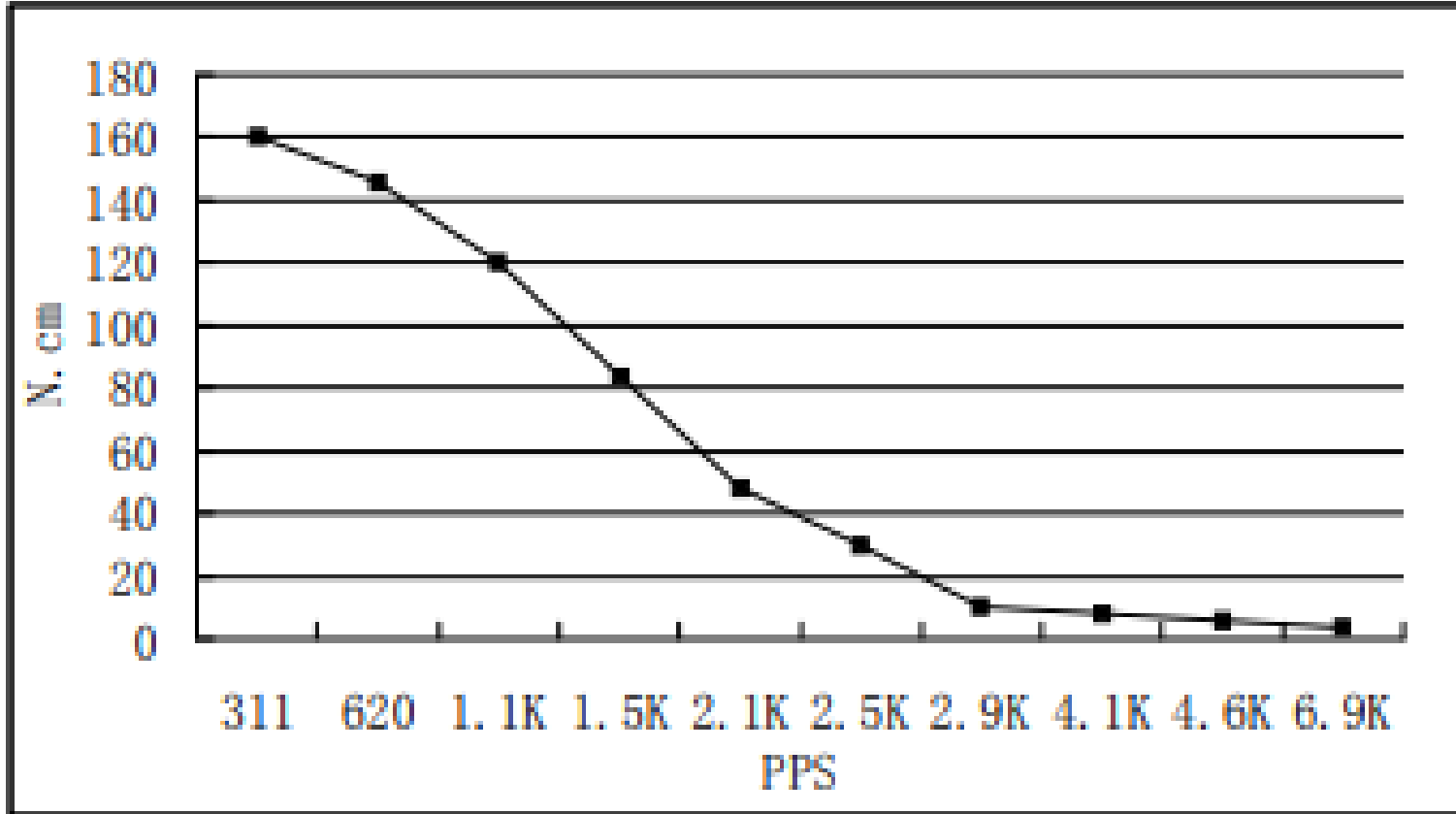
Figure 2.8: Pullout torque curve vs pulses per second (PPS) under half-stepping configuration
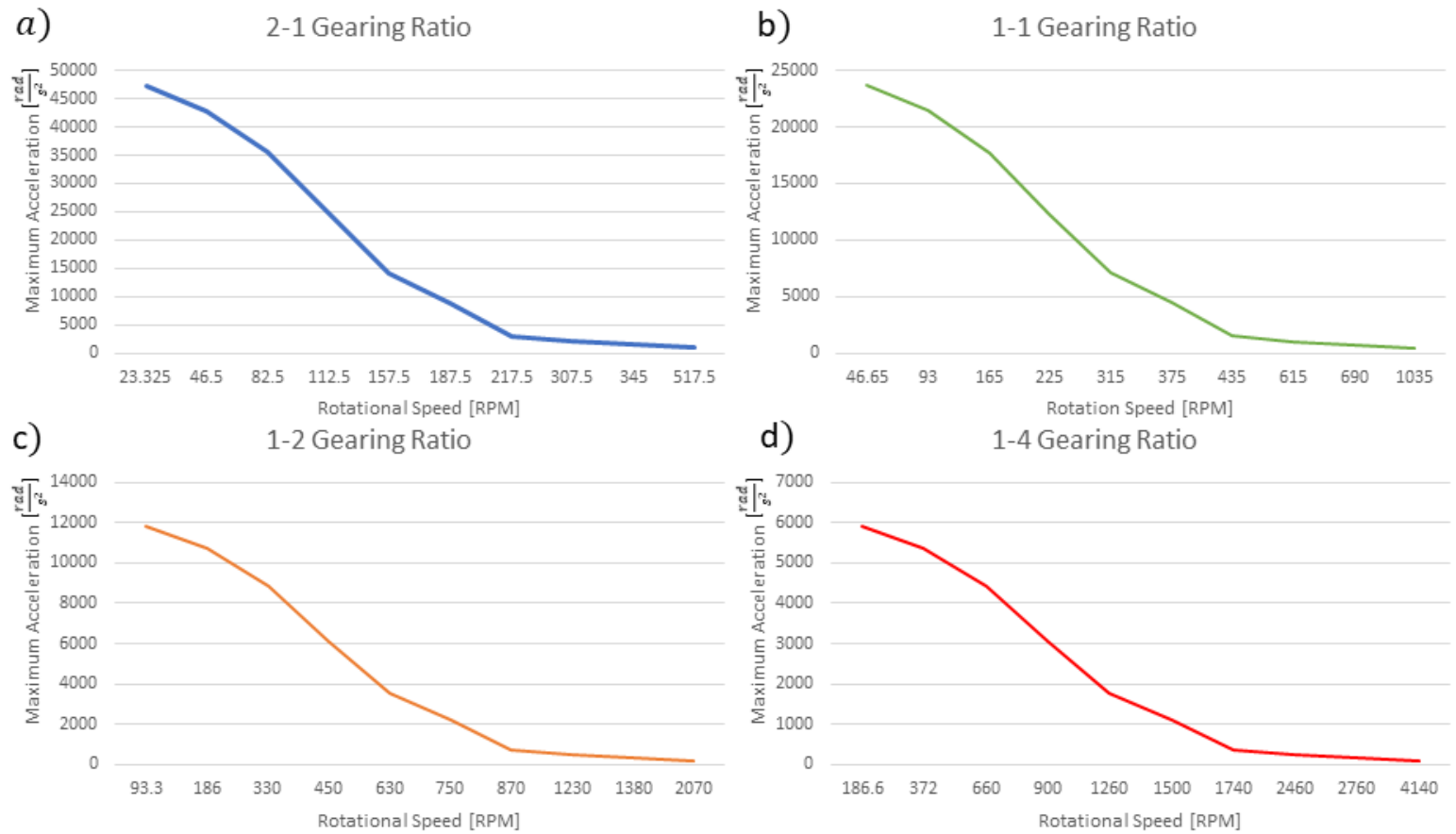
Figure 2.9: Maximum acceleration vs RPM at different gearing ratio. The ratios are in terms of print head vs stepper motor.
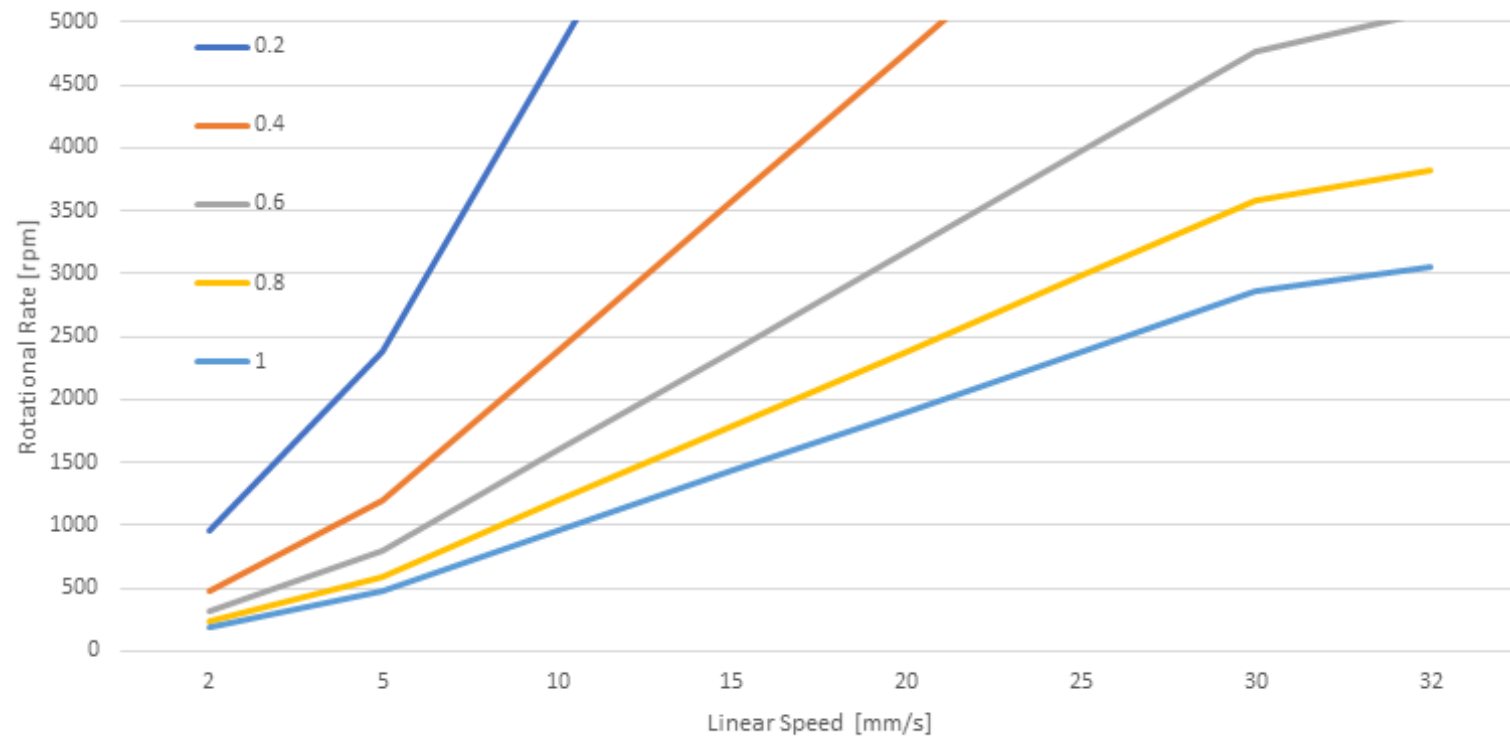
Figure 2.10: Maximum rotational rate vs linear speed for different nozzles sizes
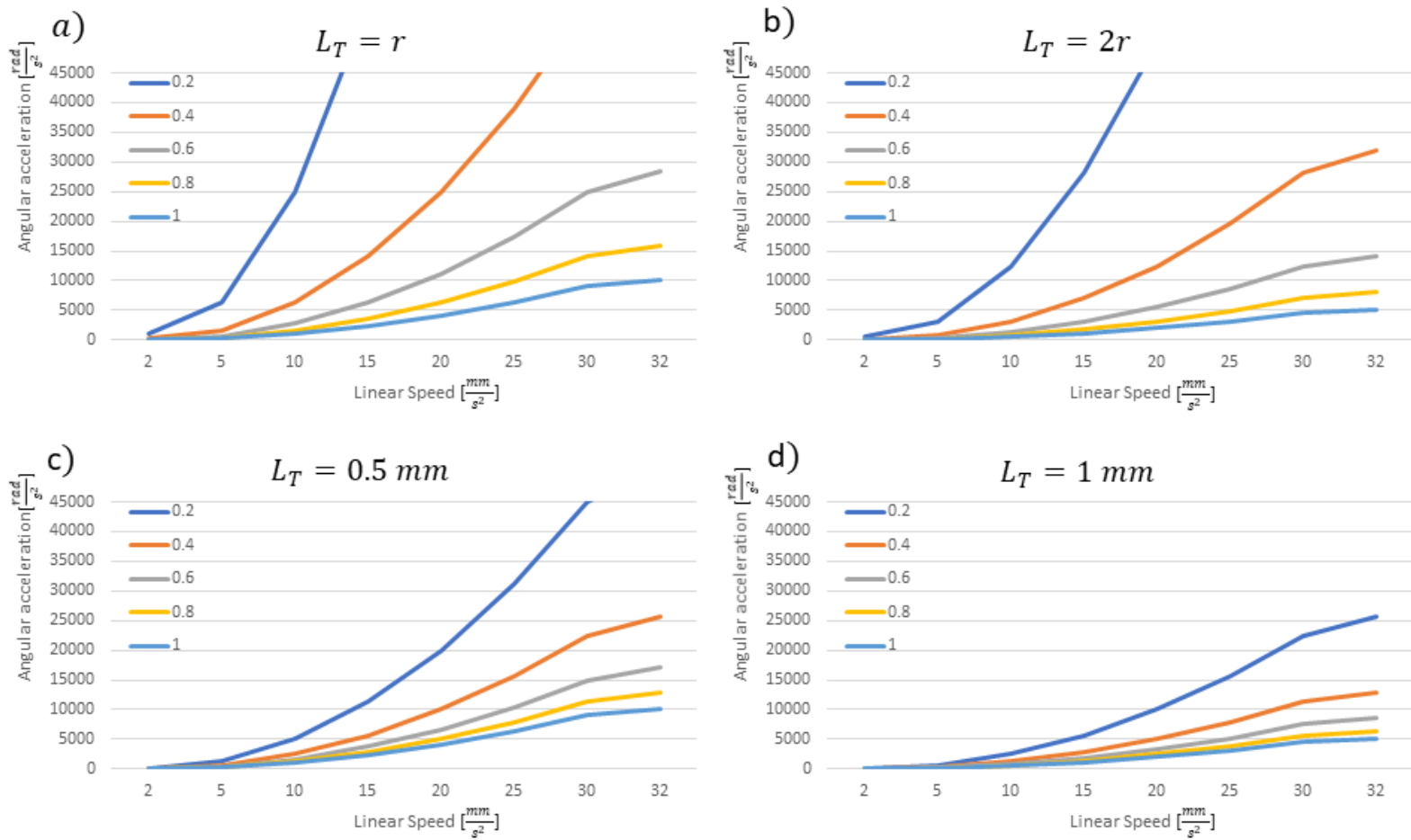
Figure 2.11: Maximum angular acceleration vs linear speeds for different nozzles sizes, at different transition length

2.3 Design Details

2.3.1 Ink Formation

The ink was formulated using a method like what was described by Raney, Compton et al for the brittle epoxy-resin with low fiber concentration in order to most easily see the effects the rotation has on fibers inside the PMC.
All mixing steps are performed under vacuum at 0.1 atm.
1.   Add 100g Epon 826 + 5g DICY
2.   Mix at 1800 rpm for 1 min.
3.   Scrape the sides of the container using a spatula and remix again at 1800 rpm for 1 min to help disperse the DICY powder more efficiently.
4.   Add the entire amount of Hex fibers (15g)
5.   Mix at 2000 rpm for a total of 12 min with 3 min increments and with 5 – 10 minutes breaks in between to let the mixer cool down (mixing at high rpm generates a lot of heat).
6.   Add half of the nanoclay amount (5g Garamite 7305).
7.   Mix at 2000 rpm for 3 minutes
8.   Wait for 5-10 minutes to help the mixer cools down.
9.   Scrape the sides of the container as the nanoclay is not dispersed fully after step 7.
10.   Add the other half of the nanoclay.
11.   Mix at 2000 rpm for 3 minutes
12.   Repeat steps 8+9.
13.   Mix again at 2000 rpm for 3 minutes.
14.   Rebate 8.
15.   Add 2g of Epodil diluent.
16.   Mix at 2000 rpm for 2 min.

2.3.2 RDIW

Figure 2.12 depicts the entire designed RDIW extruder in CAD. The nozzle chosen for the assembly is a Fisnar tapered dispensing tip, or blunt end dispensing tip (Figure 2.13). These tips are designed to extrude medium to high viscosity material and have Luer lock connections, making them a common choice for DIW.

The inline rotary union between the nozzle and feedstock material was chosen due to the simplicity of the design resulting with the least moment of inertia enabling use of a stepper motor for rotation. The two rotary unions considered were Qosina's Luer lock rotating connector (Figure 2.14, part number 20034) and Mosmatic's DGL rotary union (Figure 2.15, part number 31.051). While the inner diameter of the Qosina connector is more consistent with the diameter of tubing and nozzles typically used in DIW and it connects directly with the Fisnar nozzles, this connector is not rated for 1000RPM. Others' experiments showed that at this speed only smaller prints (<50 cm^3) were possible before the connector's seals would fuse and stop rotating.
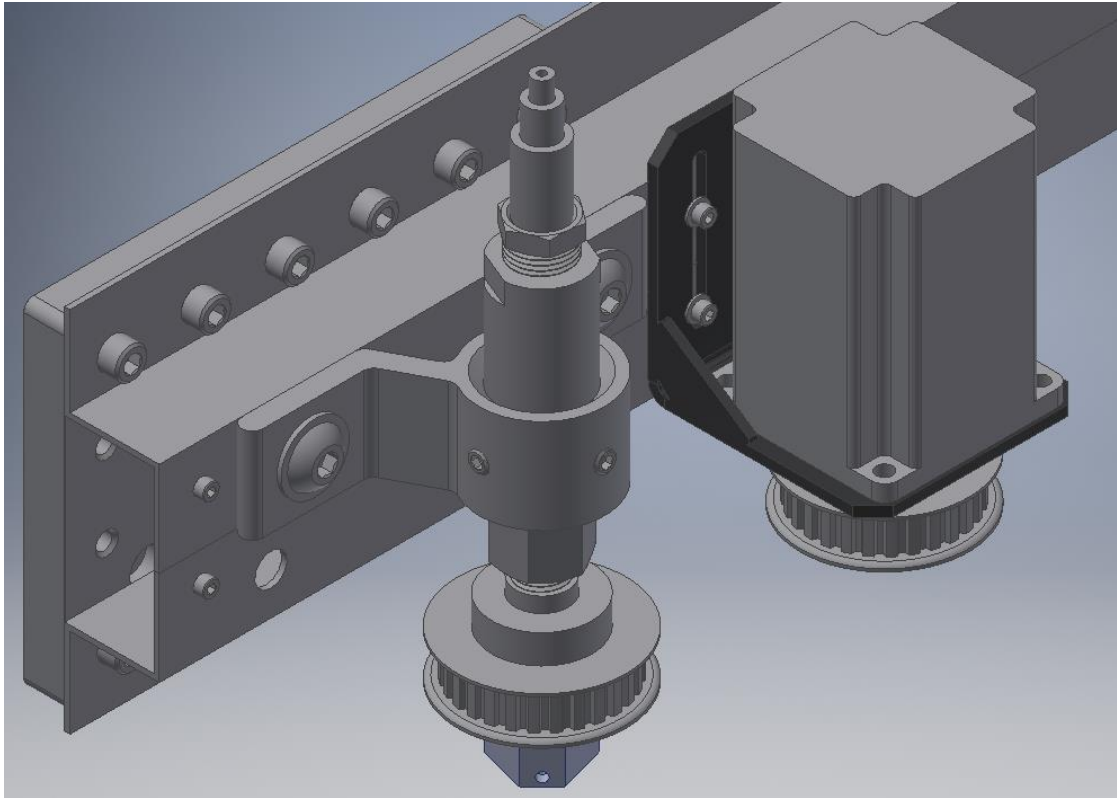
Figure 2.12: Isometric view of model of RDIW extruder

a) Luer lock tapered tip   b)1/2" Straight Cannula Blunt end tip

Figure 2.13: Finar's dispensing tips for medium to high viscosity materials
Source: [74]

Figure 2.14: Qosina rotating Luer lock connector.
 Source: [75]

Figure 2.15: Mosmatic DGL rotary union
 Source: [76]

The inner diameter of the DGL rotary union is ¼ inch, though large, the system could be primed before printing ensure steady flow through the deposition process. The DGL rotary union is rated for 1000RPM and has the option for EPDM seals to allow for acetone to be used to clean the rotary union. It does, however, has an overall length of 2.59 inches, which is approximately twice as large as the Qosina connector. The DGL has NPT threaded connectors so that two adapters would be required to connect to the nozzle and syringe. The DGL rotary union was chosen due to its sustainability and more rigid assembly. Unfortunately, during the sourcing process, only the 31.153 could be sourced, which has larger connections but still maintains a 1/4-inch inner diameter. The outside connections are 3/8 inch on either side; therefore, two additional adapters were necessary to convert these to 1/4 inch to connect to the syringe and nozzle. This assembly of changing adapters with the rotary union can be seen in figure 2.16. A pillow block bearing was chosen to give more flexibility in the design if additional components need to be rotated as well. With a slight bit of force, like tape, the upper portion of the rotary union can be kept stationary. An alternative mounting method would be to use a simple bracket

Syringe Attachment

Stationary Section

Rotary Union

Rotating Section

Nozzle

Figure 2.16: Mosomatic DGL 31.153 with necessary adapters and nozzle

A pressure-based system was chosen to drive the plunger due to existing hardware. The pressure is controlled through a solenoid and pressure regulator that is being supplied with shop air of 90 PSI. The solenoid valve is directly controlled by a digital output on the control board; however, the pressure regulator is not PWM-tolerant, which is required for many control boards to generate a voltage varying signal. Therefore, a separate voltage supply is manually controlled to set pressure going to the solenoid valve, while the solenoid valve passes pressure to the plunger only during printing and quickly removes the pressure when toggled off; this is accomplished by using a two-way valve, that during the printing process, connects the output of the pressure regulator to the syringe, else it is connected just to an open connection venting any pressure built up in the syringe.

A stepper motor was chosen to rotate the nozzle due to ease of programmability and incorporation into the printer control scheme. A DC motor could still be used if higher print speeds and rotational speeds were desired. A timing belt system is used to transfer rotational energy from the stepper motor to a pulley directly attached to the adapter attachment. This pulley had to be drilled out so it could be mated with desired adapter. A set screw and interference fit are used to ensure the shafts are sufficiently mated. It is expected that the stepper motor can handle the rotations called for, so the same pulley is used for the master and slave pulleys giving a 1-1 ratio on rotation and torque following the graphs of figures 2.8-2.11.

The entire assembly is attached to two Z-bars with an aluminum flat-bracket securing the bars together. The Z-bars affix to the baseplate of the Shopbot gantry system. An exploded view of all parts and a bill of material can be found in the appendix (Figure A.1 and table A-1).

Finally, a chuck-like assembly is used to guide the nozzle towards the center of rotation. This assembly can be seen in figure 2.17. The nozzle can be repositioned using the three screws pressing into the nozzle slightly. Through iterative testing using a marking tool, the eccentricity or wobble of the nozzle can be determined during rotation. At rest, the screws can be adjusted to push the marked side towards the unmark side, and then the process can repeat until the wobble of the nozzle is indiscernible. The entire assembly can be seen in figure 2.18.

2.3.3 Control Board

A single-board controller was selected to enable the most functionality in future work with this system. The control board chosen was the Duet 2 due to the Trinamic embedded in the control board. These drivers have SpreadCycle™ and CoolStep™ features that assist smoother positioning control, especially at higher speed, and that decrease the current stepper motors use down to the minimum holding torque required. This control board also offers up to five stepper motors and various digital output channels—some purely digital, some PWM. This allows for future iterations to directly control the pressure regulator voltage supply. In order to get the stepper motor to rotate as fast as

necessary it had to be configured as a bipolar motor using the center taps instead of either side of the coil. In addition, ¼ microstepping was used to allow for a smoother rotation, decreasing the detent torque and allowing the motor to spin faster. In addition, since the rotation is being controlled by a stepper motor that is configured to move in discrete steps, the number of rotations for the print move is necessary. Put another way, the control board dictates the desired position of the stepper motor, therefore, to set the speed of the motor, the total distance that motor should travel in the given time is necessary. Setting the E-steps of the motor to be 200 allows directly specifying how many rotations are necessary. Equation (2-10) determines the number of rotations based on the desired rotational ratio R, the radius of the nozzle r_s, and L the length traveled for the deposition.

$$\text{Rotations} = \frac{RL}{2\pi r_s} \qquad (2\text{-}10)$$

In order to maintain timing on extrusions, the control board will automatically match the extruder speed to the necessary speed to finish the extrusion at the same time. Meaning, if the amount to extrude doubles, then the speed would double to ensure the extruder doesn't lose timing with the rest of the system. This can be leverage since using (2-10) the rotations can be directly fed with the control board handling the necessary speed calculations. Some testing of coil mode and microstepping can be found in the appendix (Figure A.2)

Figure 2.17: Chuck-like assembly for guiding the nozzle center to compensate for any eccentricity
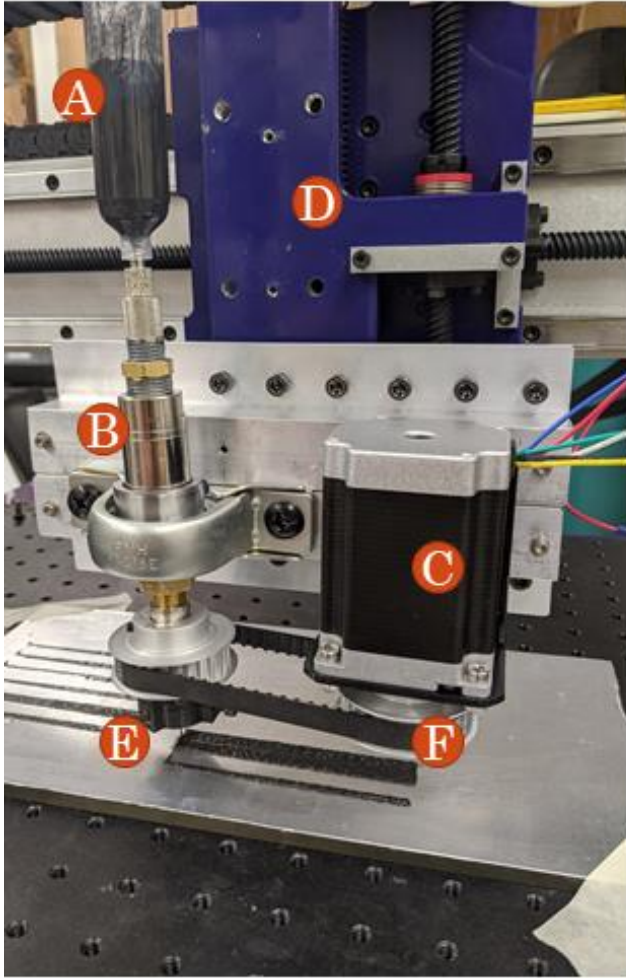
A) Syringe

B) Rotary Union

C) Stepper Motor

D) Gantry System

E) Chuck Assembly

F) Pulley System

Figure 2.18: Assembled RDIW extruder on the Shopbot gantry

2.4 Results

To demonstrate the locally programmable orientation of the fibers a simple rectangle was printed with 6 distinct sections sliced equally down the short side, as depicted in at a nozzle size of 0.979mm. The rectangular was printed at a consistent height of around 0.6mm. The speed and rotation rate of each section can be seen in table 2-2. Figures 2.19-2.21 show the sample, direction of the print path, and example G-Code how the print was design. Figures 2.22-2.24 are micrographs of a single layer sample. Additionally, a two-line sample to help mitigate effects of multiple lines interacting, these are shown in figure 2.25. Each region has a different rotational ratio as described in (1-1).

Table 2-2: Linear and angular speed of the extruder while printing the rectangular sample depicted in Figure 2.19

Section Number Rotational Ratio	Linear Speed [mm/s]	Rotation Rate [RPM]
0	5.0	0
1	5.0	97.54
2	5.0	195.08
3	5.0	292.62
4	5.0	390.17
5	5.0	487.71
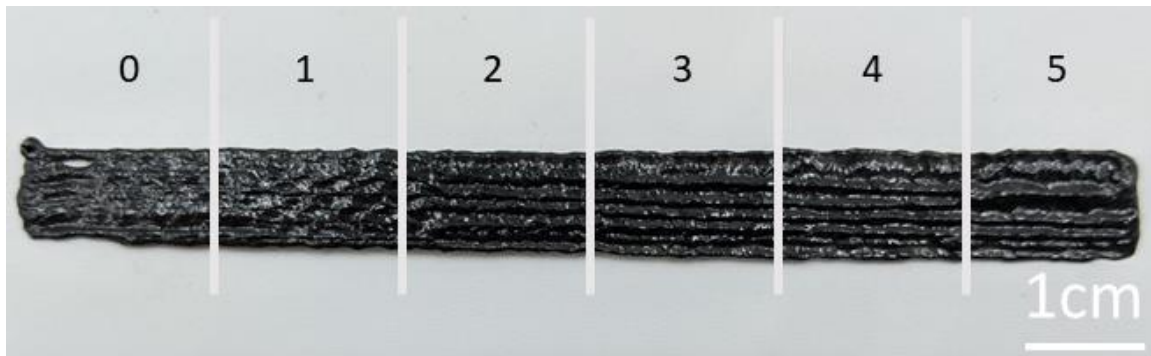
Figure 2.19: Printed rectangular sample with varying rotational ratios
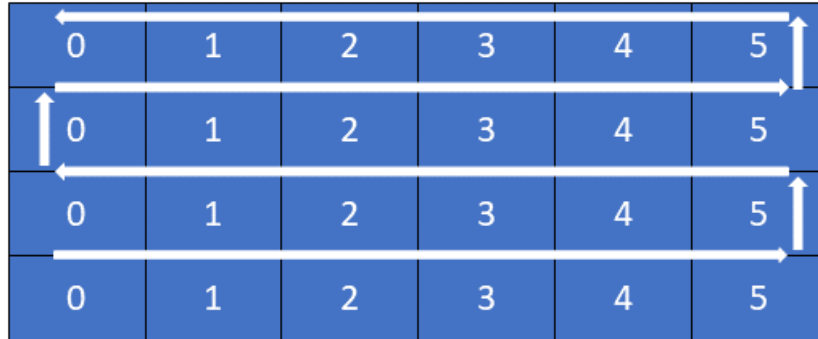
Figure 2.20: Print path configuration

```
G91                 - Relative positioning
M83                 - Relative extruder move
M906 E2000          - Sets motor currents
M92 E200            - Sets steps per mm
M350 E4             - Sets microstepping
G1 F300             - Sets linear speeds


G1 X15 E0           - Move 15 mm, rotate none
G1 X15 E4.877       - Move 15 mm, rotate 4.877 rotations
G1 X15 E9.754       - Move 15 mm, rotate 9.754 rotations
G1 X15 E14.631      - Move 15 mm, rotate 14.631 rotations
G1 X15 E19.508      - Move 15 mm, rotate 19.508 rotations
G1 X15 E24.385      - Move 15 mm, rotate 24.385 rotations
```

Figure 2.21: Example of a single bead pass for the rectangular sample with varying rotational ratios and rotational speeds.

42
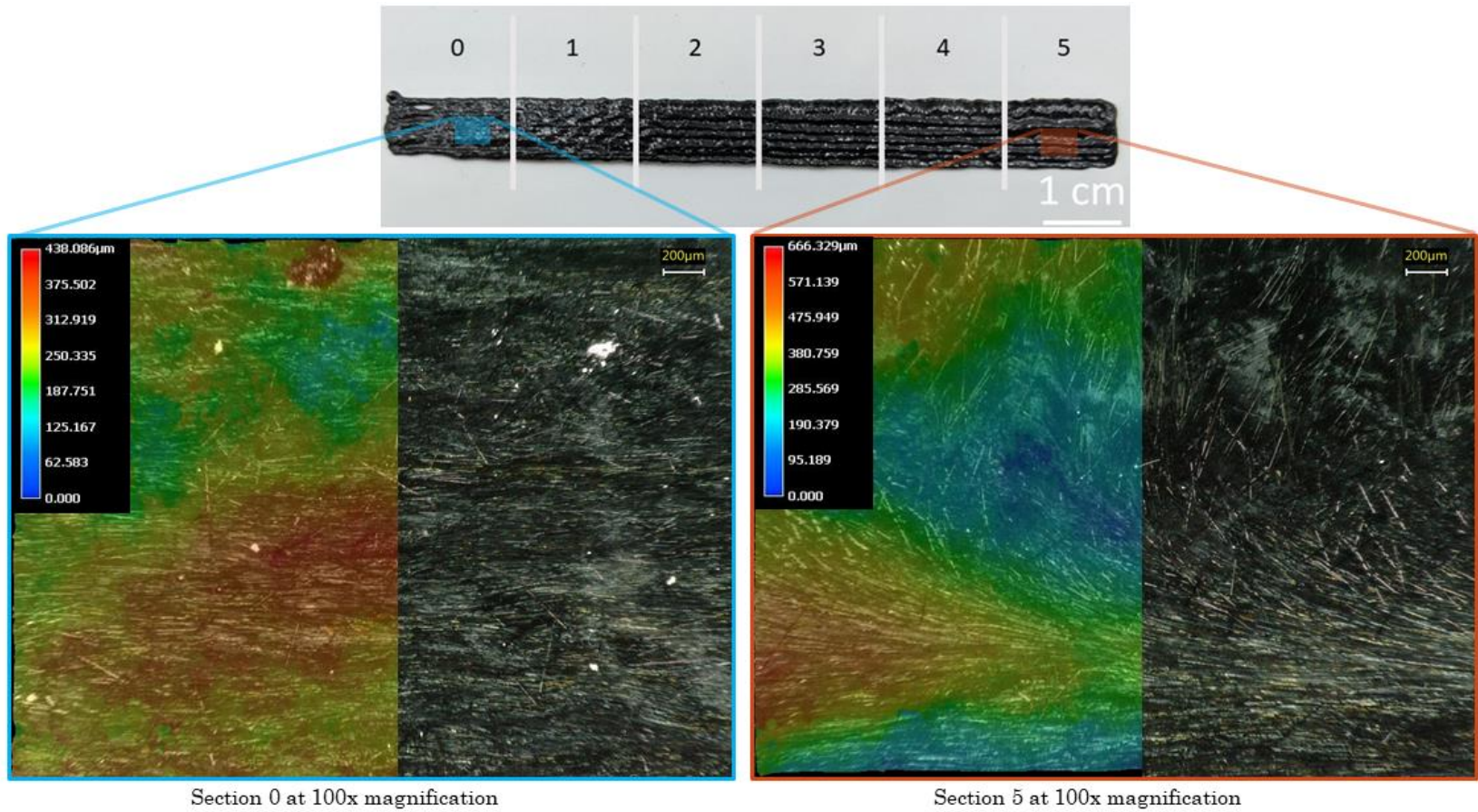
Figure 2.22: The two extreme regions of the single layer sample at 30x magnification.
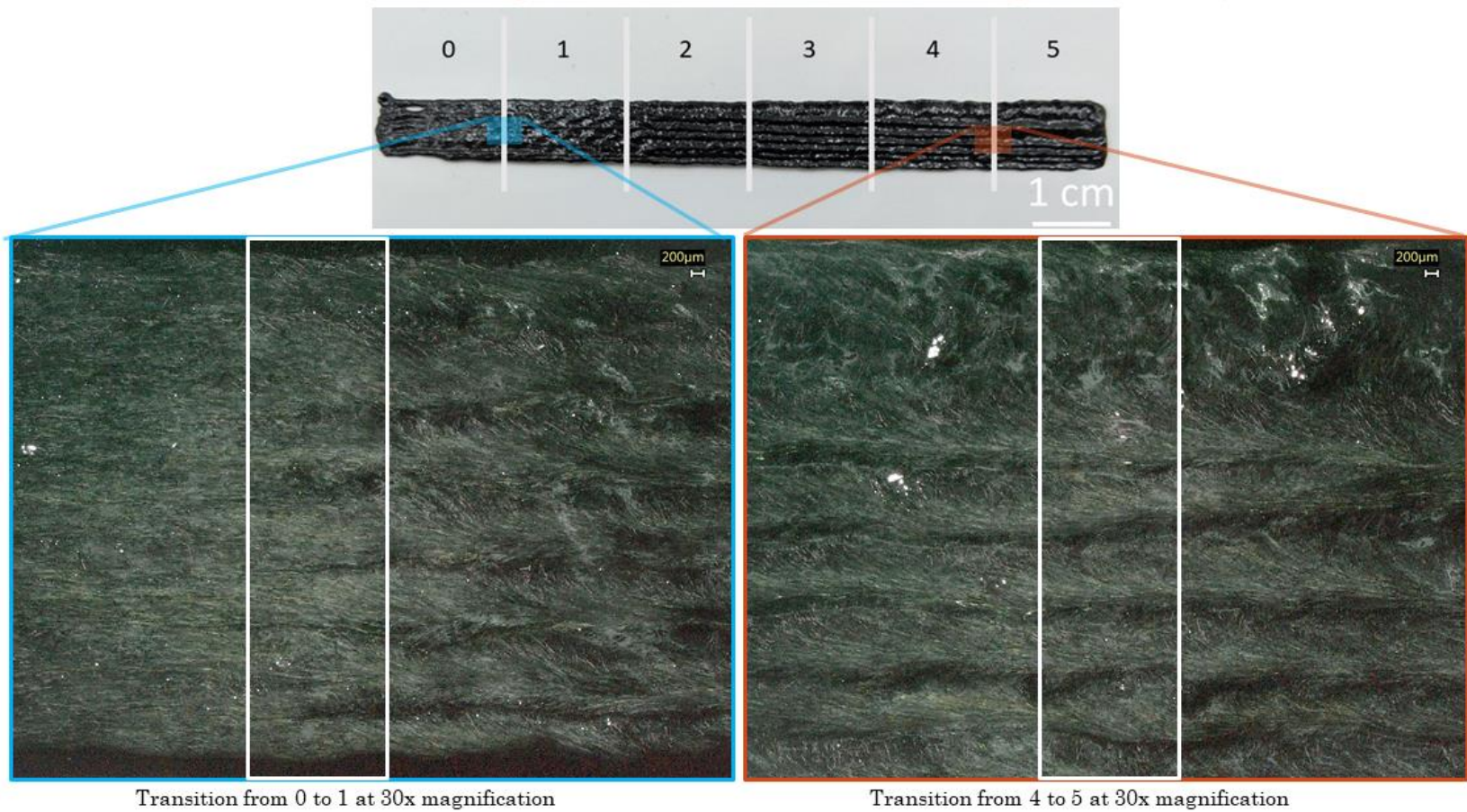
Figure 2.23: The two extreme transition regions of the single layer sample at 30x magnification. The white boxes signifies the estimated region of transition between the individual rotational regions
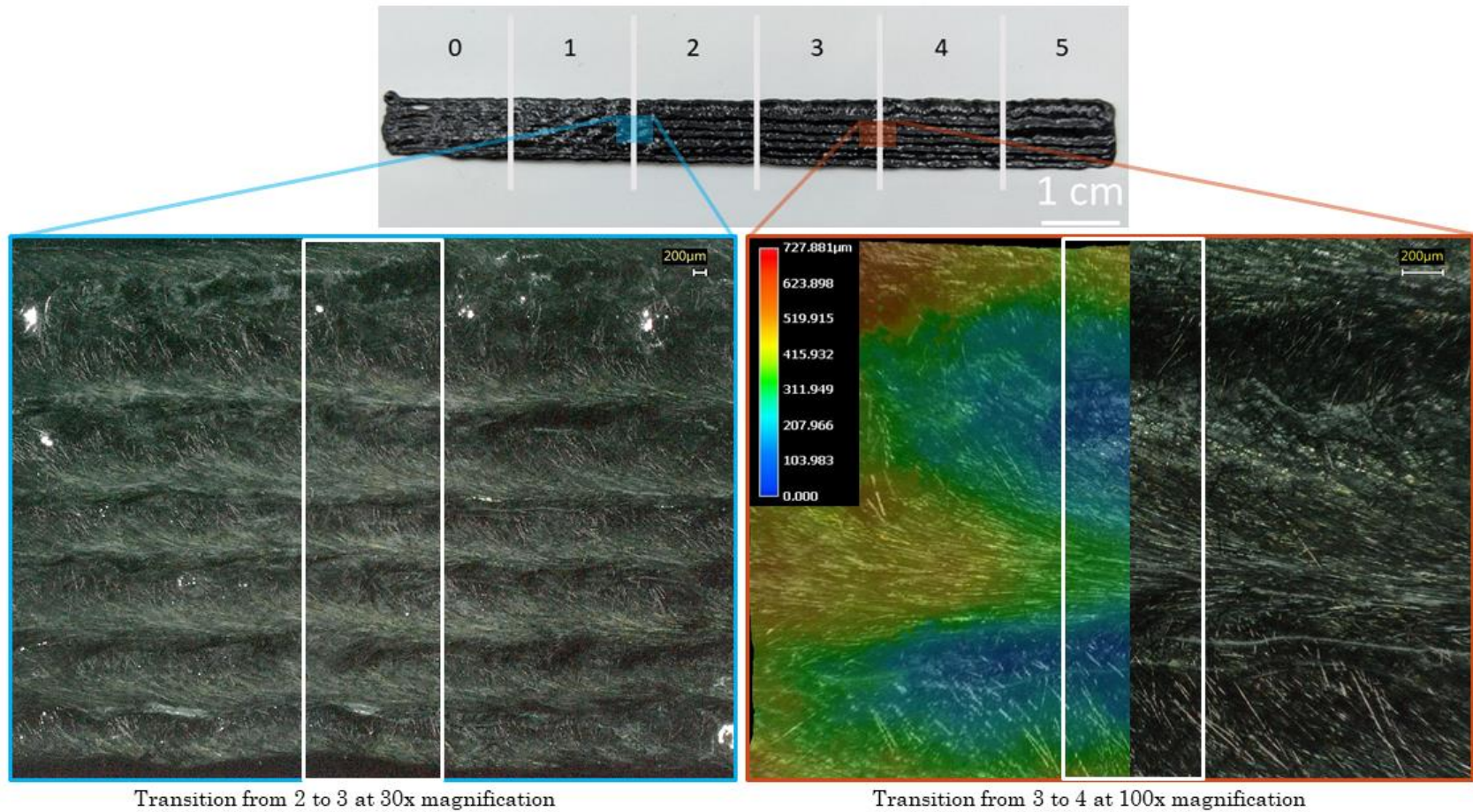
Figure 2.24: Two intermediate transition regions of the single layer sample at 30x and 100x magnification. The white boxes signifies the estimated region of transition between the individual rotational regions
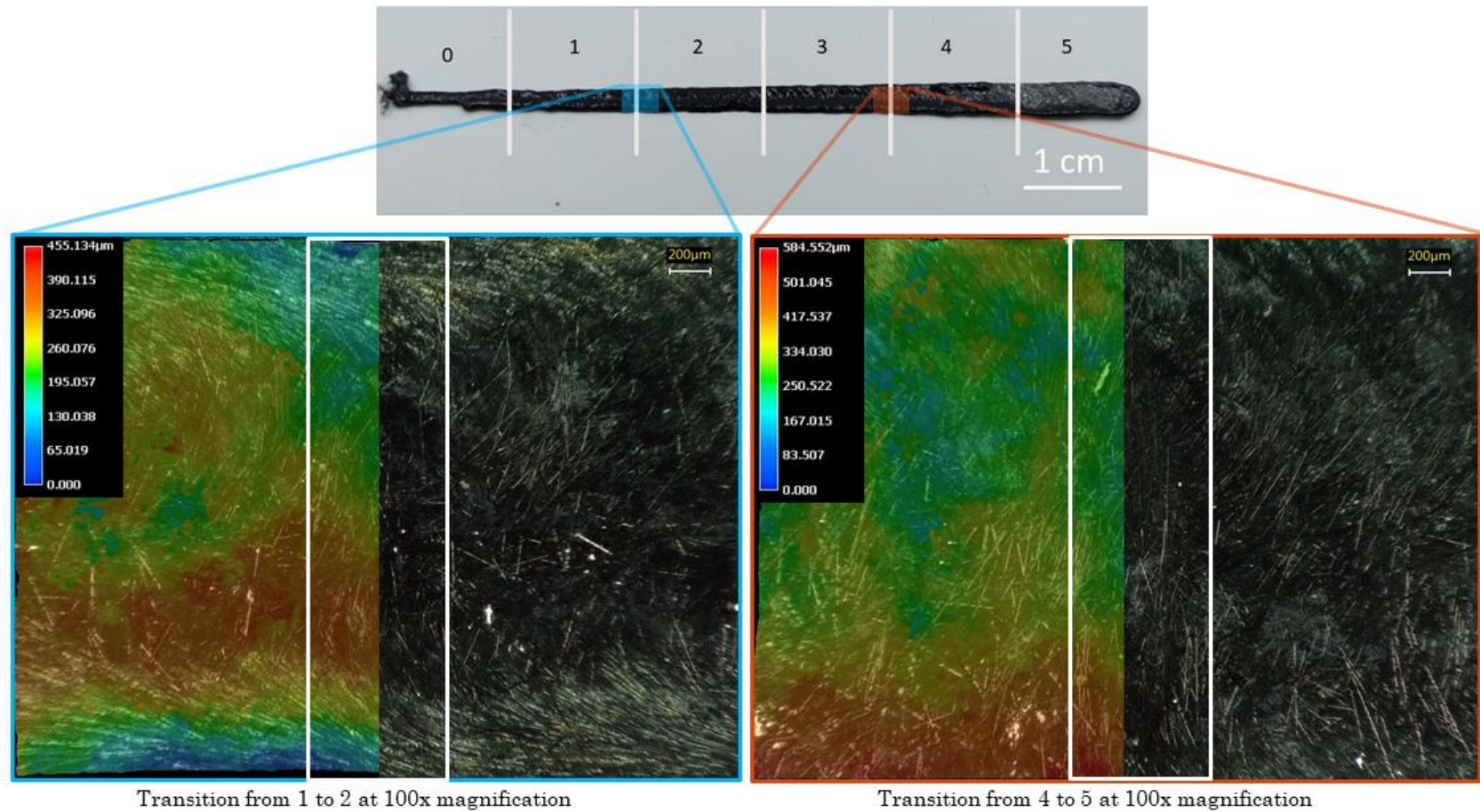
Figure 2.25: Two transition regions of a two-line sample at 100x magnification. The white boxes signifies the estimated region of transition between the individual rotational regions

2.5 Discussion

During the testing of the RDIW, the extruder was unable to print a more viscous mixture. At 12% volume of CFs, the rotary union component filled up partly, but even after considerable pressures (90 PSI), the feedstock material would not propagate out of the nozzle. It is believed that the various changes of diameter led to insufficient pressure to flow the material. An alternative mixture was made that had only 4% volume CFs, and this mixture was printable. The two samples printed using this mixture show that fibers are reoriented, and the degree by which they are reoriented is proportional to the rotational ratio, agreeing with the work done by Raney, Compton et al, with a rotational ratio of 5 resulting with fibers being reoriented perpendicular to the print path. The size of the transition between two rotational ratios seems to be on the order of 1 mm. And there is some interaction between the previous deposited lines that is causing material to raise along rows in the material. It is suspected that this is caused by the extruder depositing too close to previously deposited material. As the extruder drags material along it seems to align the fibers along that row as well, creating highly aligned rows that are raised higher than the surrounding material (Figure 2.25).

Considerations must be made on the effort it takes to clean an extruder like this. Due to the small diameter of several components, threads, or cavities, a lot of material can get stuck in hard to reach places, taking effort to clean. It would be worth considering some alternatives, such as rotating the syringe itself so that only the disposable nozzle and syringe itself is a cleaning concern. A noticeable wobble was observed during printing; however, the chuck-like assembly was able to correct for the eccentricity. During the testing process, the stepper motor was found to be incapable of consistently fast rotation over a longer print. As the prints got longer the stepper motor would eventually stall over several rotational sections. It is believed to be overheating since the system operates fine over several moves, and then it suddenly starts failing and maintains failing until the system can rest. Additionally, the stepper motor could only be rotated up to 1000RPM consistently. This limited the maximum print speed possible, slowing down print. Therefore, there are two recommended changes to the system. The first change is to rotate only the syringe and nozzle. This would prevent the pressure changes diminishing flow and reduce the amount that needs to be cleaned. The second change would be to use a more significant motor; while a large stepper could be a solution, it is believed that a DC motor could be just as effective when utilizing a PWM channel for fans on the Duet 2 or a daughterboard that can use feedback control to maintain a desired RPM fed to it from the Duet 2.

Chapter 3 Rotational Fused Filament Fabrication (RFFF) Extruder

3.1 Introduction

Following the procedure as with the RDIW extruder, the same four major components were identified as necessary. First was a short fiber reinforced thermoplastic composite. Second was an FFF extruder compatible with the chosen composite and with a nozzle that can be rotated. Third was a means to rotate the nozzle. The final need was a means to sync the rotation of the nozzle to the desired regions of alignment of deposition. The next few sections will cover some background information pertaining to these specific requirements not previously discussed.

3.1.1 FFF Extruder Design

A traditional FFF extruder can be broken up into two major regions. These two regions can be seen in figure 3.1Figure 3.1:. The first region that heats the filament past its glass transition temperature is commonly referred to as the hotend. The second region, which moves the filament into or out of the hotend, can be called the cold end, though it is more commonly referred to as the extruder. This can cause some confusion since the entire assembly can also share this name. Therefore, to avoid confusion, this thesis will refer to the region that moves the filament as the cold end and the entire assembly as the extruder. The hotend can be broken up into four major components: nozzle, heating block, heat break, and heat sink, depicted in figure 3.2 The nozzle shapes the larger filament size down to the nozzle diameter. In commercial small-scale additive manufacturing, the feedstock filament is typically 1.75mm or 3.00mm in diameter [77], while the nozzles range from 0.1mm up to 1mm. The heating block is the section that transfers heat to make the filament malleable. A heating element embedded in the heating block generates the required temperature, while a thermistor or another temperature probe close to the nozzle reports the temperature reading to the associated control board. The heat break and heat sink, equipped with a cooling fan, work in tandem to create a thermally isolated block between the heating block and the rest of the extruder. The heat break is typically a narrow shaft of metal that has low thermal conductivity. (i.e. titanium at 5.8-22.5 $\frac{W}{mK}$ vs. copper at 401 $\frac{W}{mK}$). Using titanium's strength, a narrow heat break can connect the heating block to the heat sink. Due to the low thermal conductivity and narrow passage, it takes a significant time for the temperature to pass through the heat break to the heat sink. With the fan actively blowing on the heat sink, the heat transferred by the heat break is cooled by the air, maintaining the ambient temperature or slightly higher. If this fan was disabled, the heat sink would warm considerably. Figure 3.3 depicts the temperature profiles of the FFF hotend depicted in figure 3.2 at different air speeds. This cooling serves not only to protect the components upstream, but also to cool any filament that is pushed back up the filament shaft—called back flow—creating a plunger of sorts to help push the filament out of the nozzle. The filament transitions from a stiff material into a flexible material as the filament is heated beyond its glass transition temperature and towards the melting temperature. Common thermoplastic materials used in FFF 3D printing can be seen in figure 1.4, along with some other classifications.
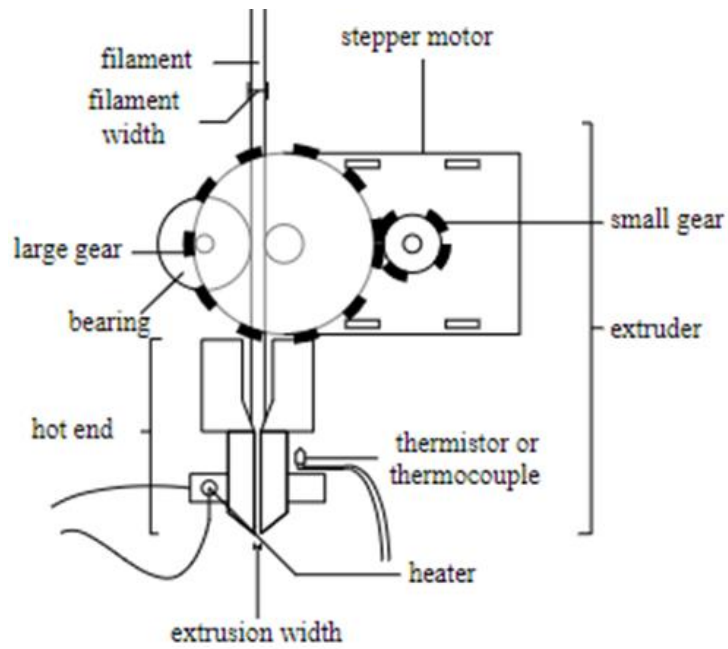
Figure 3.1: Generic FFF extruder
Source: [77]
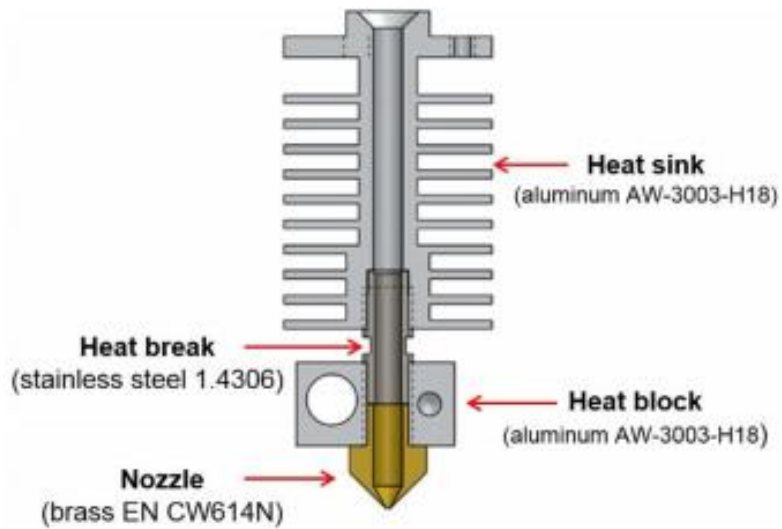
Figure 3.2: Cross section of an FFF hotend
Source: [78]
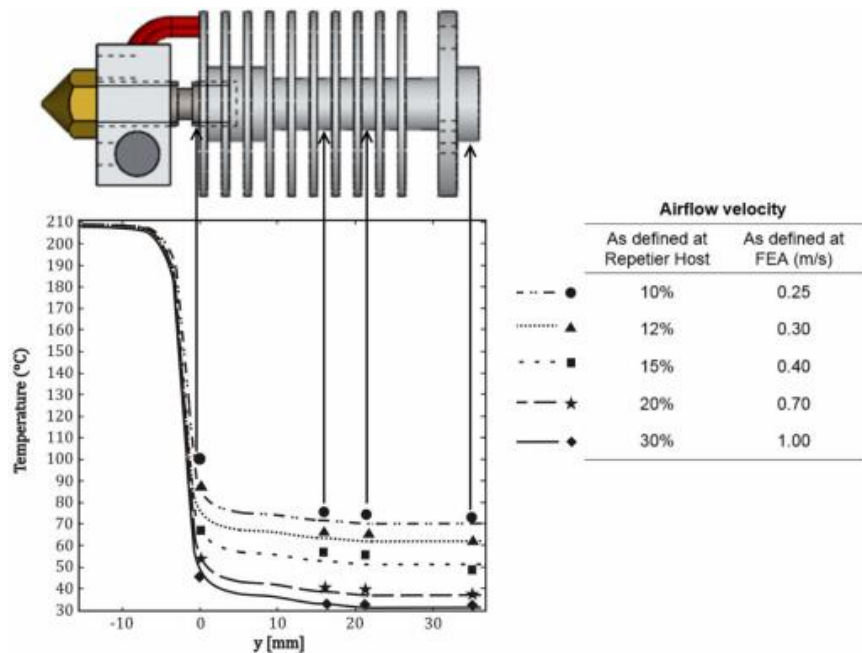
Figure 3.3: Temperature behavior of an FFF hotend under different forced air flows
Source: [78]

Some examples of the temperatures these extruders need to reach are as follows: PLA prints at temperature of 180-210°C [79], while PEEK prints at temperature of 250-343°C [80]. This demonstrates that extruders can handle a range of temperatures, with some extruders specifically designed for higher or lower temperatures.

The components in figure 3.1 that are not included in the hotend comprise the cold end. These components consist of a stepper motor with a gear that interfaces with the filament. This gear can be stepped up into a larger gear to give greater torque when moving the filament, however a single gear is just as common. On the opposite side of the filament from the gear is a tensioner bearing that can be moved closer to the filament, to allow the filament to be pinched harder by the interaction, or farther away. There is a range of acceptable pressure before the filament just jams the system or breaks, or before the gear doesn't grab hold of the filament at all. This can change from filament to filament. An alternative method is to use two stepper gears in tandem with gears on their output shaft to enable significant grip on the filament. This is less common for small-scale 3D printers. It is typically the cold end that attaches to the translation system, considering the temperatures the hotend reaches. Another configuration for an extruder is setting the motivating stepper motor completely off the translation system and just feeding the filament through a guide tube. This configuration is called a Bowden extruder, and it is being utilized in Ultimaker's 3D printers. While this reduces the mass that needs to be moved, this prevents using flexible filaments like Ninja-Flex. The

previous system, that has the stepper motor attached directly to the hotend, is referred to as direct-drive. However, one component not shown in this image is the part-blower fan. This fan is aimed directly at the print surface below the nozzle. This part can assist cooling the printed material quickly if necessary (such as for bridging gaps in material).

These two designs deal with FFF based extrusion, however there are alternative mechanisms closely related. One such mechanism is using Moineau-based pumps (also known as progressive cavity pumps) to melt and dispense pellets, even using a stepper motor to accomplish this [81]. This design uses an auger-like mechanism to transfer plastic pellets to a Moineau rotor to dispense the plastic. NASA has been researching this method for very large-scale 3D printing [7, 82]. Though these auger-based approaches have been done several times, these designs do not pick up much traction in the small-scale commercial markets. It is worth mentioning that Cosine does have a pellet feed extruder for the medium to large scale 3D printer.

3.2 Design Considerations

Unlike with the RDIW extruder, a rotating thermoplastic extruder has not been publicly attempted before, therefore commercially available components will serve as the basis of the design. There are several thermoplastic composite filaments available, however the selection process is limited compared to inks for DIW. These filaments are typically reinforced with CF or GF, with CF being the more common of those two, however, the fiber loading is predetermined in the 10% – 20% volume range [83]. Using PLA as the polymer matrix is a likely candidate due to the popularity of the material, the ease to print with, and the relatively low temperature required to print. An alternative would be to use pellets in an auger-drive extruder. These pellets could be augmented with additional fibers, or polymer to set the volume ratio between these two dynamically. Two large concerns with using CF or GF thermoplastics is the abrasiveness of the fibers, and the minimum size of the nozzle. Therefore, using a harden steel is preferred to a brass nozzle. Additionally, a minimum nozzle size of at least 0.4 mm is necessary to prevent clogging, like the RDIW extruder minimum nozzle size.

In order to rotate the nozzle, three possible configurations were considered, pulling much from the considerations with the RDIW extruder. The first two options augment the extruder by adding rotation just to parts of the hotend, while the last option considers rotating the entire extruder. The first option is to place the rotary union between nozzle and the heating block (Figure 3.4). This option is ideal since any material that passes the rotary union will transfer less torsional load from the rotating system twisting the filament, since this material should be the most malleable entering the nozzle. However, the rotary union would have to be able to pass significant heat energy to the nozzle while keeping a tight seal to prevent the material from leaking. This seal would have to handle temperatures of at least 185°C (the minimum printing temperature of PLA). In addition, whatever mechanism that generates rotation would have to directly interface with the nozzle or rotary union that will also be at elevated temperature. This
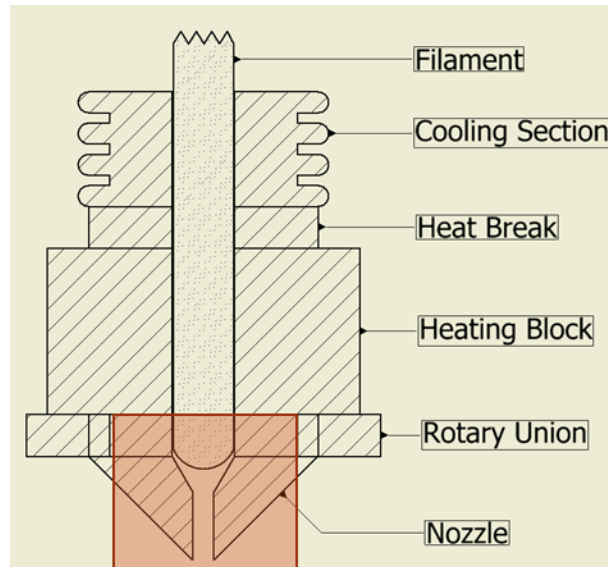
Figure 3.4: Inline rotation of just the nozzle of an FFF extruder. The orange box highlights the components that will be rotating.

would require significant augmentation to the current FFF extruder design, and specific requirements for the rotary union speed and temperature constraints.

The second option is to place a rotary union between the heat break and heating block (Figure 3.5). This would allow the heating block and nozzle interaction to remain constant, and the rotary union could assist the heat break functionality, preventing heating from flowing up the hotend, and reducing the temperature the rotary union sees. However, since filament passing the rotary union is still stiff, there are concerns that the rotation of the heat break will torsional load the filament causing the filament to break in a direct-drive or Bowden system. An auger drive would simplify this interaction since the feedstock material us not continuous, however flow becomes more dynamic with the interaction of two rotating systems.

The final option would be to rotate the entire extruder, by adding a rotary union connecting the extruder to some stationary structure (Figure 3.6). In order to avoid breaking the filament, two solutions are considered. The first solution is to carry the filament on the extruder. This would prevent any torsional load, though it could limit the amount able to be printed before reloading the extruder. The second solution is to redesign the heating block to allow for a significant amount of the filament to be malleable enough to prevent the torsional load from growing great enough to break the filament. The auger system sounds the most promising since it simplifies the redesign of the extruder, provided an acceptable rotary union could be sourced. However, following
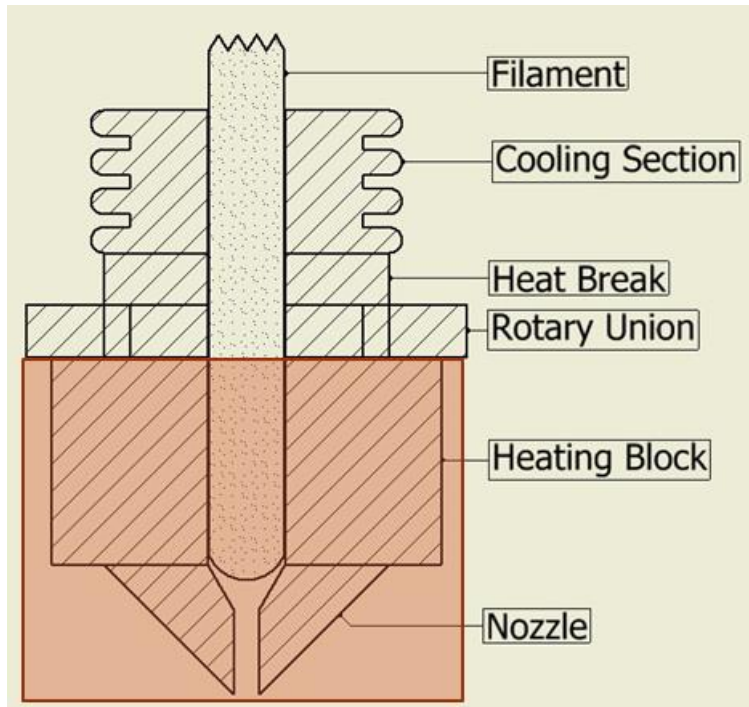
Figure 3.5: Inline rotation of the nozzle and heating block of an FFF extruder. The orange box highlights the components that will be rotating.
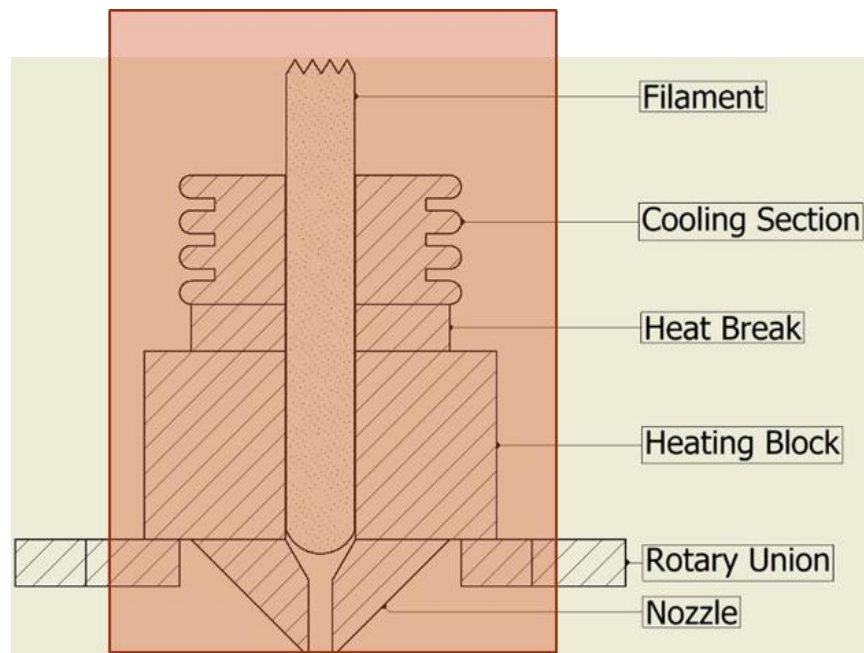

Figure 3.6: Assembly rotation. A rotary union is incorporated outside the hotend assembly of an FFF extruder. The orange box highlights the components that will be rotating.

the same steps in RDIW extruder design (first rotate the syringe, then add a rotary union to make a more sophisticated design), rotating the entire assembly was considered the most plausible, even with being the most audacious idea, this design requires little redesign of commercial equipment. The largest hurdles would come with balancing the rotation as is typically done with centrifuges, and generating the rotation using G-Code.

Again, stepper motors were the first desired means to rotate the extruder, however if the entire extruder is rotating, then the total inertia of the system would have to be very small for the stepper motor to handle the rotations. Therefore, a more significant DC motor is required, namely a spindle tool that can rotate 5,000 RPM and higher and supply significant torque. This would enable much faster prints compared to the RDIW extruder and larger moment of inertia. The rotational rate would be less controlled due to the open-loop control scheme, though additional sensors can be utilized if more precision is required then speed curve calibration.

Two possible options were considered for the means to sync up the rotation to extrusions. The first being to use a commercially available medium-large scale 3D printer. This would allow reusing existing extruders for their machine without the need to create unique mounts for extruders. The first of two such printers considered was the Hyrel 3D Hydra 16A (Figure 3.7Figure 3.7:), with several possible extruder assemblies, particularly the Mk2-250 dual stepper motor extruder (Figure 3.8Figure 3.8:). The second printer considered was the Cosine AM1 (Figure 3.9), specifically looking at the possibility of the pellet-feed extruder (Figure 3.10). Though that is not quite FFF, it would still demonstrate the reorientation of a reinforced thermoplastic composite. These two options give flexibility on the extruder being used and have a large workspace and head room for a taller assembly if need be. A third option is to repurpose another CNC machine to be a thermoplastic based system. This would require either making a new thermoplastic extruder all together or using existing hardware which follows the same train of thought the first two options considered. While other medium-scale 3D printers could also satisfy these requirements, the nature of the partnership of this project required the use of either of these systems. Due to the popularity of FFF systems, the Hyrel 3D system was chosen as the base to work from with the RFFF extruder.

3.3 Design Details

The designed extruder can be seen in figure 3.11. CarbonX PLA+CF filament was considered the starting filament since the fiber concentration by weight is similar to the work done by Raney, Compton et al, and PLA is a very common thermoplastic to print with. In order to rotate either just the nozzle, or the nozzle and heating block configurations a rotary union would have to satisfy four conditions. These conditions include an inner diameter <1/4" (and ideal an OD less than 1" in order to interface easily with a traditional FFF extruder), rotate at least 1000 RPM, handle at least 180-230°C temperatures, and pressure typical in FFF extruders (varies with material, however tends to be less than 100 PSI). Unfortunately, no such rotary union could be found. This resulted in the assembly rotation being the only viable option without a new rotary union.
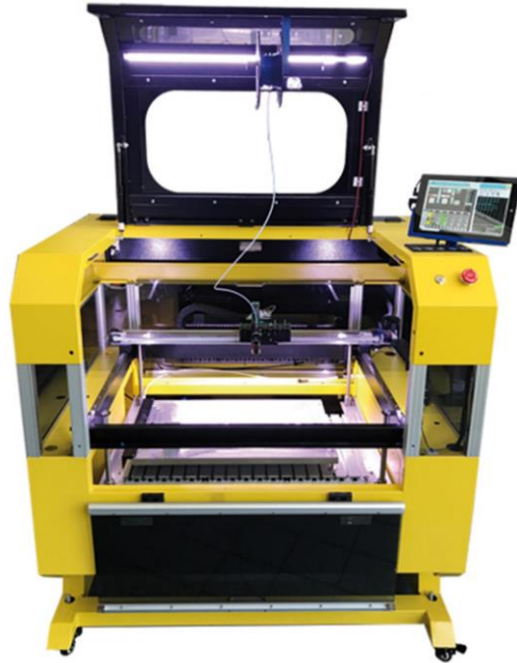
Figure 3.7: Hyrel Hydra 16A 3D printer
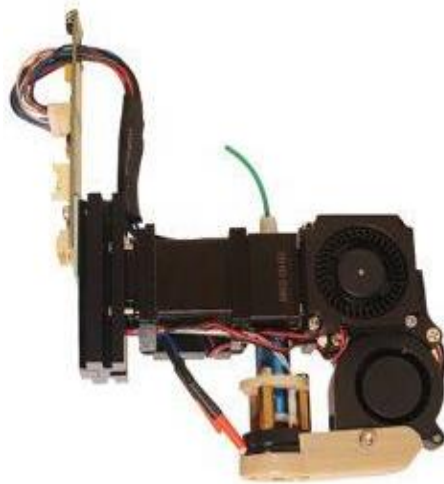Source: [84]

Figure 3.8: Mk2-250 hotend assembly
Source: [84]

Figure 3.9: Cosine AM1 3D printer
Source: [85]

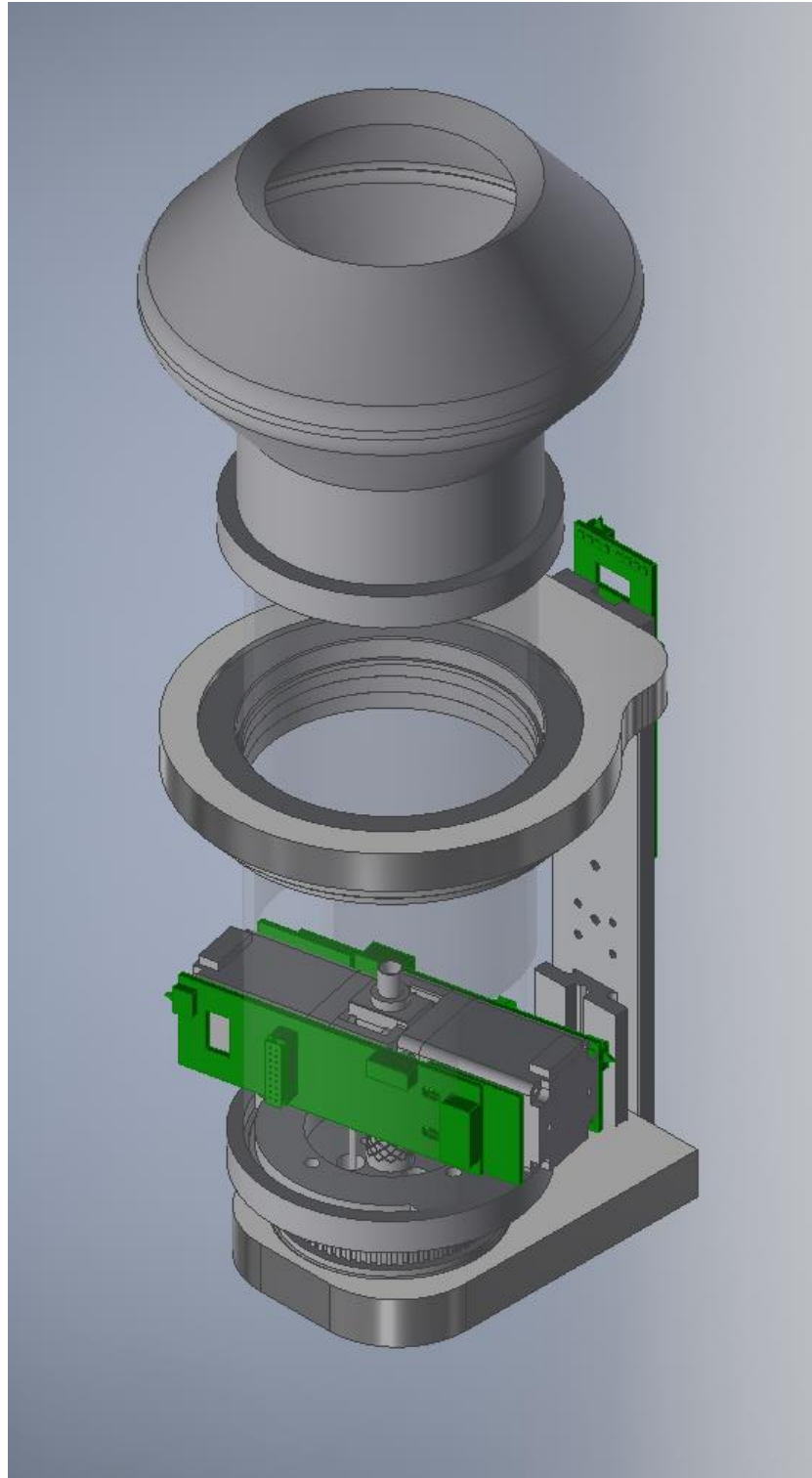*Figure 3.10: Cosine pellet fed extruder*
Source: [86]

Figure 3.11: Isometric view of model of RFFF extruder

Balancing the weight of such a rotation is crucial to avoid severe eccentricity of the nozzle. Here, the Hyrel Mk2-250, depicted in figure 3.8, was able to stand out from other extruders. Due to the dual stepper motors across the filament axis, any rotational effect of these weights would balance each other. The rest of the extruder is reasonably balanced if the part blower fan is removed. This removes the functionality of bridging; however, this feature is not required in this body of work. All components of the Mk1-250 can be seen in figure 3.12 and table 3-1. The Mk2 is simply the Mk1 with an additional stepper motors driving the filament instead of a tensional pulley. The Hyrel's extruders are controlled by a separate board that is physically attached to the extruder. This allows for unique programming for individual "heads" (the various type of extruders or devices Hyrel can equip in their 3D printers). In order to distinguish these two control boards—the main control board for the entire system and the control board for just a head—the main control board will be called the motherboard, while the control boards for the extruders will be called daughterboards. The daughterboard can be relocated, provided it can communicate with both the motherboard and the extruder itself. The means by which the daughterboard and motherboard interface is called the yoke. This is also the support structure for all the heads that can be equipped. Since the entire assembly is rotating, large bearings could be used since a sophisticated rotary union could be more cumbersome than necessary. Using pulleys link through a timing belt the entire system can be propelled, like the RDIW extruder. The interaction between the slave pulley, bearing, and the hotend can be seen in figure 3.13.

The greatest challenge with rotating the entire assembly is how to get power and signal to the daughterboard for the extruder. Four solutions were considered. The first was to remove the daughterboard from the rotating assembly, however this result with control signals must be passed through to the extruder, which recreates the original problem of how to pass signals and power. The second solution considered was using a slip ring at the top of the rotating assembly to pass signal and power. This is the common approach to these types of problems, as slip rings are quite effective at passing signal. However, they typically require signals passing through the center of the rotating axis; this could be problematic depending on the method of carrying the filament along with the rotating assembly. The third option considered was to use a cruder method to accomplish slip rings: if power could be passed to the daughterboard, then wireless communication could be utilized between the motherboard and daughterboard. Power could be transmitted through bearings, assuming they make enough contact throughout their rotation, like how slip rings accomplish the task with brushes. The final option considered was using a battery pack to power the system and wireless communication to control the system. This would limit the print time possible, however the filament carried along does such already. This method faces challenges with a strong battery typically being quite heavy, raising questions as to how this battery could be offset to avoid the wobble of the nozzle, and increasing the motor to compensate for the added weight. Using the bearings as slip rings was the chosen method, due to its simplicity and lack of

SECURE CABLES WITH
CABLE TIE (22) HERE

SEAL IN PLACE WITH RTV SILICONE (27)
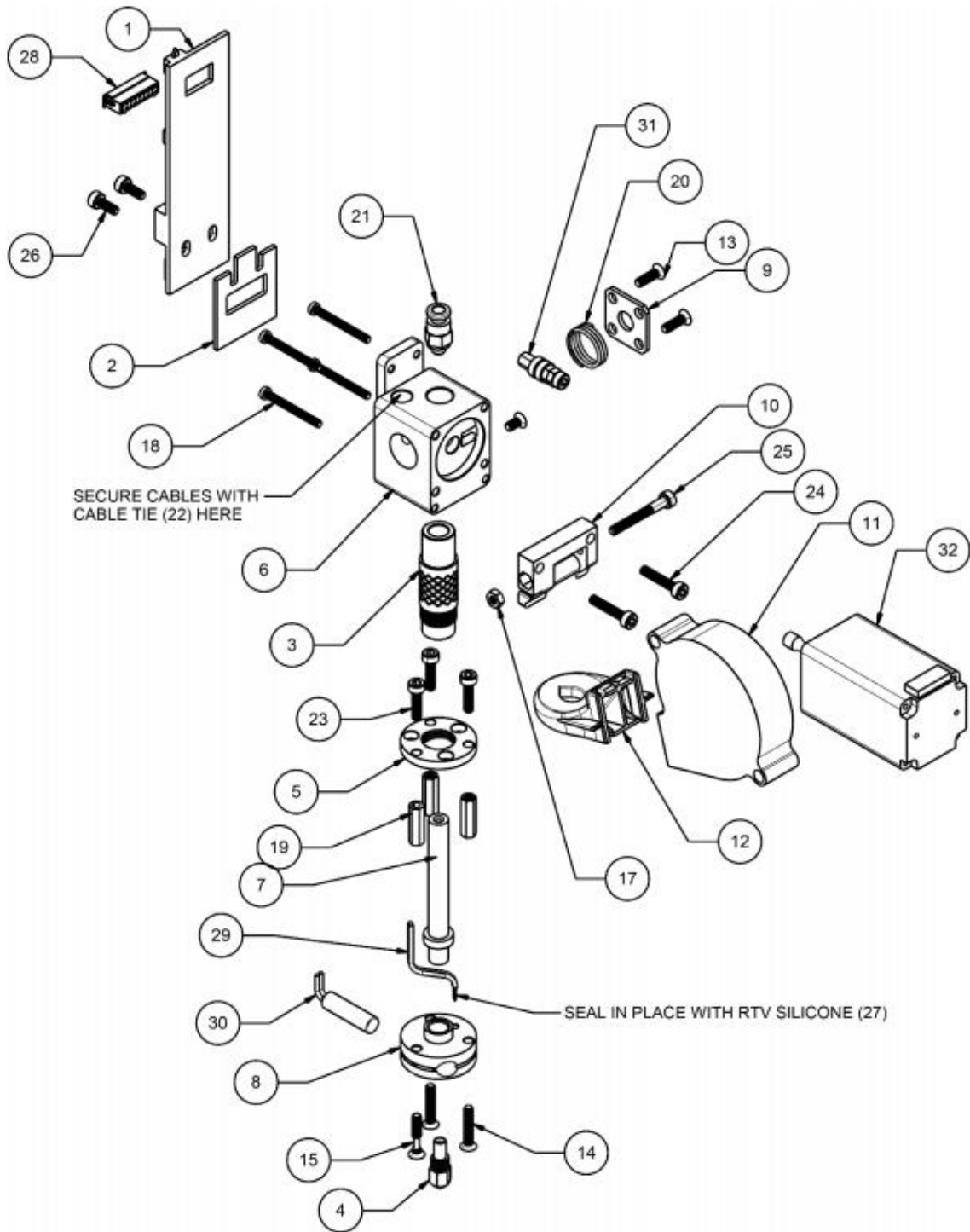
Figure 3.12: Mk1-250 exploded view.
Source: [84]

59

Table 3-1: Mk1-250 Bill of Materials
Source: [84]

ITEM	Qty.	Part No.	Part Name
1	1	102081	102081.ExtrusionHeadCircuitBoard
2	1	102508	102508.PCBSpacerStop.H3D
3	1	102511-6	102511-6 Knurled Aluminum Material Tube
4	1	102512-1.75	102512-1.75.HotTip.1.75mmFilament
5	1	102532	102532-2B.RoundPEEK
6	1	102533-5	102533-5.MK1-400 Body
7	1	102534	102534.PTFE.New
8	1	102535	102535.RoundHeatCartridge
9	1	102536-1	102536-1.Spring.Cover.MK1.H3D.v2
10	1	103109-1	103109-1_Mk1_Quiet_Storm_Attachment v8
11	1	103109-3	103109-3.QUIETSTORMBLOWER
12	1	103109-5	103109-5_MK1_PAN NOZZLE kjg new fan dimensions.V5.5
13	2	200086-10	200086-10.Screw,M3x10mm.FlatPhil
14	2	200086-16	200086-16.M3x16FlatHead.92010A126
15	1	200086-16-U	200086-16-U.Modified M3x16 Flat Head
16	1	200086-6	200086-6.Screw,M3x6mm,FlatPhil
17	1	200088	200088.Nut,Hex,M3
18	4	200092-25	200092-25.M2.5x25.Pan.92000A112
19	3	200101-15	200101-15.STANDOFF - M3X15, HEX, FF, BRASS
20	1	200127-.75	200127-.75.Spring.Compression.75x.48x.045
21	1	200140-4	200140-4.4MM Pneumatic Connector
22	1	200225	200225.Cable Tie, 0.075" x 3"
23	3	200303-12	200303-12.Screw,M3x12mm,SocketCap
24	2	200303-16	200303-16.M3x16.SocketCap
25	1	200303-25	200303-25.M3X25.SOCKETCAP
26	2	200303-8	200303-8.Screw,M3x8mm,SocketCap
27	0.3	200509-2.8	200509-2.8 Silicone RTV, 2.8oz
28	1	300015-18	300015-18.Conn, HOUSING PHD 2mm 18POS
29	1	301112	301112.Platinum RTD
30	1	301450	301450 Heating Element, 40W
31	1	402106-3	402106-3.bearingassem_mk1
32	1	420019-1	420019-1.MOTOR.STEPPING.0.8A.28X28X52MM

A) Nozzle

B) Lower Bearing

C) Slave Pulley

D) Heating Block

E) Access Hole

F) Standoffs

G) Tube Mount
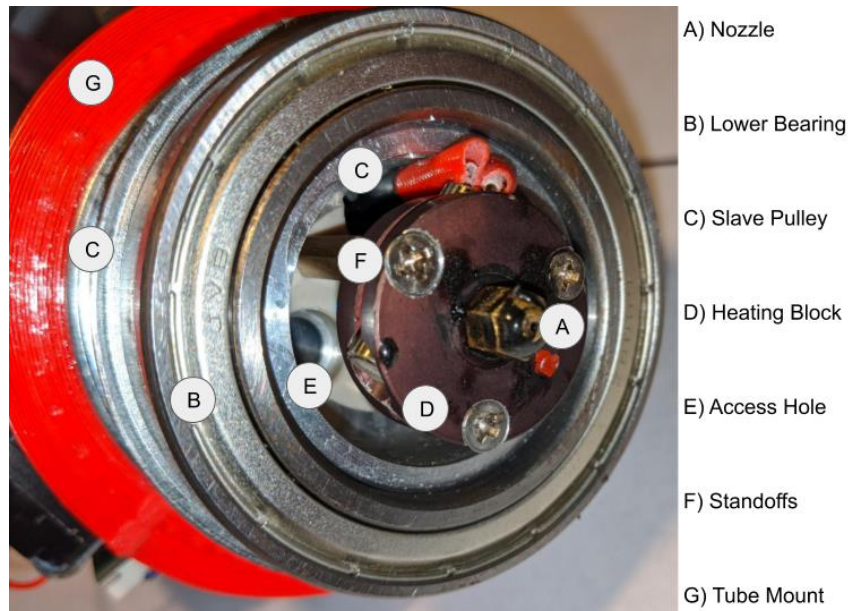
Figure 3.13: Interactions between Mk2-250 extruder, slave pulley, and bearing

interference with other components. An additional bearing was added to the top of the assembly to provide structural support as weight was added toward the top of the rotation. Between the top and bottom bearing, this allowed 12V and ground to be passed to the daughterboard. This required several parts to be made from plastic instead of metal to avoid shorting the rails. In addition, a 5V regulator must be used to step the 12V down to 5V since this is typically passed by the yoke, and only the 12V rail was passed through the bearings.

Once the daughterboard was powered, only the control signals were required to be passed. The HC-05 Bluetooth modules were chosen to transmit these signals. These modules act as a transparent serial link, meaning they pass on any information sent to them without responding or modifying the signal. This required special programming from the Hyrel team to ensure these transparent links do not add substantial delays that would trigger a shutdown of the system (a safety feature implemented to ensure heaters are shut down in case of loss of communication). Unfortunately, the typical method of communications from the motherboard is not serial. Therefore, a more complicated route was required. Figure 3.14 depicts this interaction graphically. A full wiring diagram can be found in the appendix (Figure A.4). Three daughterboards were required, the first daughterboard communicates directly with the yoke. This daughterboard then packages the necessary information and transmits it over the Bluetooth connection through a programming pinhead. On the rotating assembly side, another Bluetooth module is listening and takes the necessary information into the daughterboard. This daughterboard then takes the role of the motherboard to the remaining daughterboard directly. This
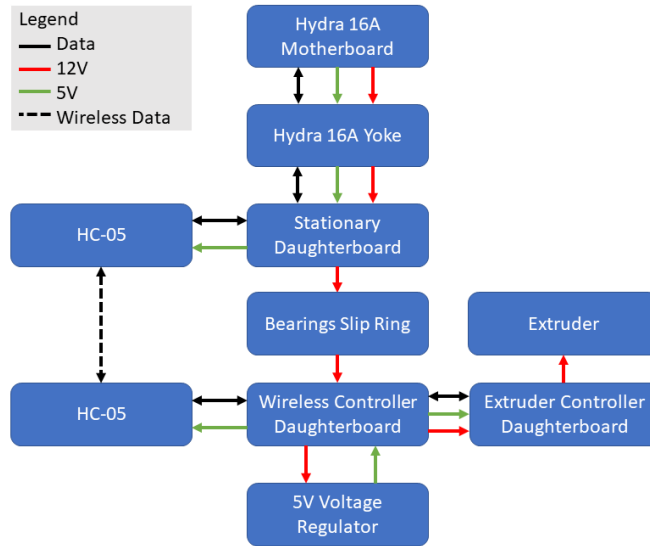
Figure 3.14: Simplified diagram of daughterboards' interactions with the motherboard and extruder

daughterboard then executes the command on the extruder and returns a successful or error message back through the chain to the motherboard. These two daughterboards on the rotating assembly are directly fixed on either side of the stepper motors as seen in figure 3.15. This balances the weight around the axis of rotation. A polycarbonate tube surrounds the assembly to prevent any wires or objects from interacting with the rotary union or vice versa. This tubing is directly attached to the slave pulley. Finally, the filament is stored with a donut-shaped hat that keeps the filament inside of it while printing. This filament is carefully coiled inside so that the stepper motors can pull filament out of it easily. The final assembly can be seen in figure 3.16.

3.4 Results

Two types of samples were printed with a 1 mm nozzle. The first sample is a single walled square, and the second sample is a simple bar with distinct sections of rotated and nonrotated sections. The speeds, rotational rate, and ratio is summarized in Table 3-2, while the samples can be seen in figures 3.17,3.18. Cross section micrographs can be seen in figures 3.19,3.20 depicting the internal structure of the printed samples. The exploded view of the RFFF extruder can be found in the appendix along with the BoM (Figure A.3 and table A-2)

A) Wireless Transceiver

B) Extruder Controller

C) Wireless Controller

D) MK2 Extruder Frame

E) Tube Mount
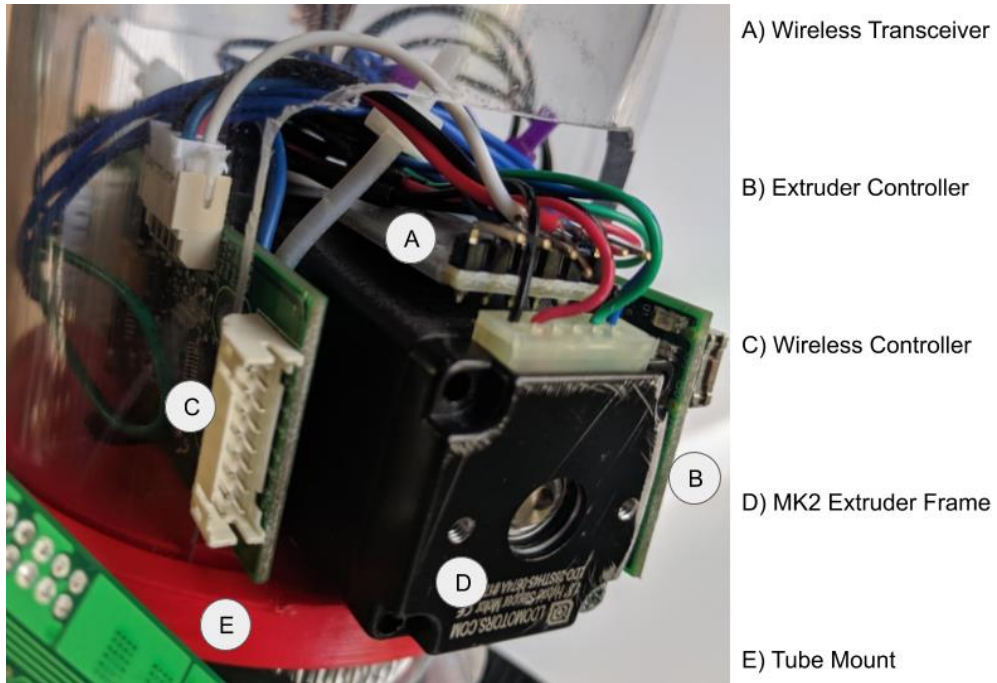
Figure 3.15: Mounting of daughterboards on the Mk2-250

A) Filament Housing

B) 12V Bearing

C) Spindle Tool

D) Yoke

E) MK2-250 Extruder

F) Pulley System

G) Ground bearing and mount
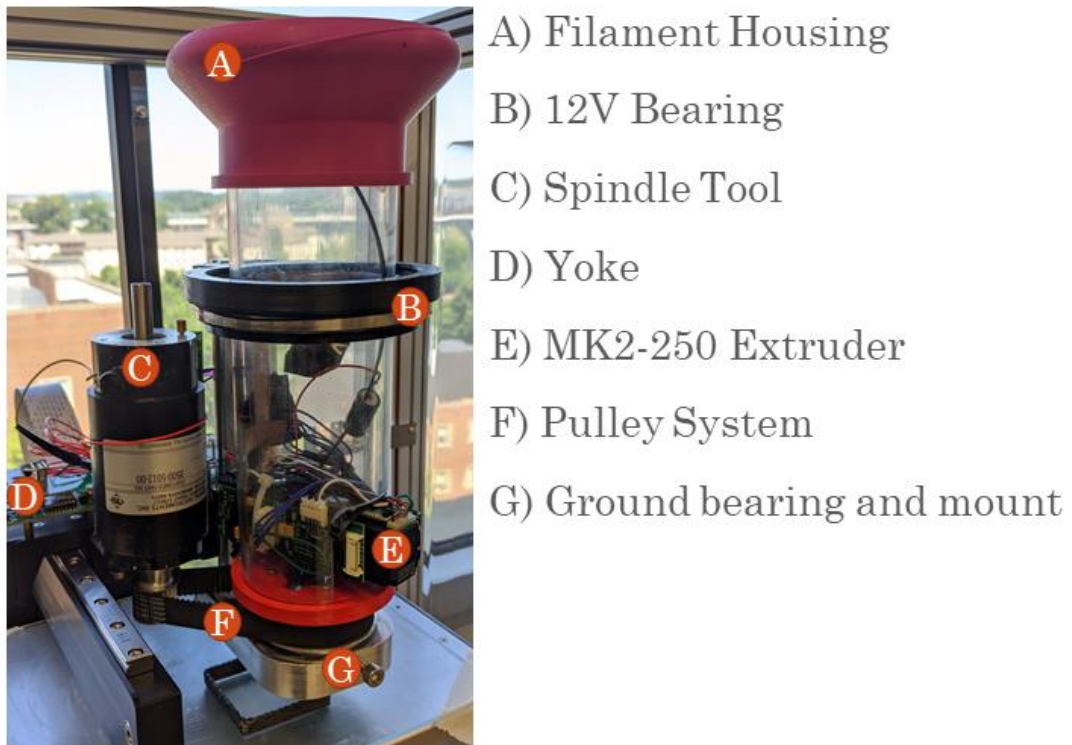
Figure 3.16: Installed RFFF extruder with DC motor in a Hyrel printer

63

Table 3-2: Linear and rotational speed of printed samples of the RFFF extruder

Sample Type	Linear Speed [mm/s]	Rotational Speed [RPM]	Calculated Rotational Ratio
Single wall square	10	300	3.14
Bar	20	500	1.31

Figure 3.17: Single walled sample with rotation constant throughout the printing process
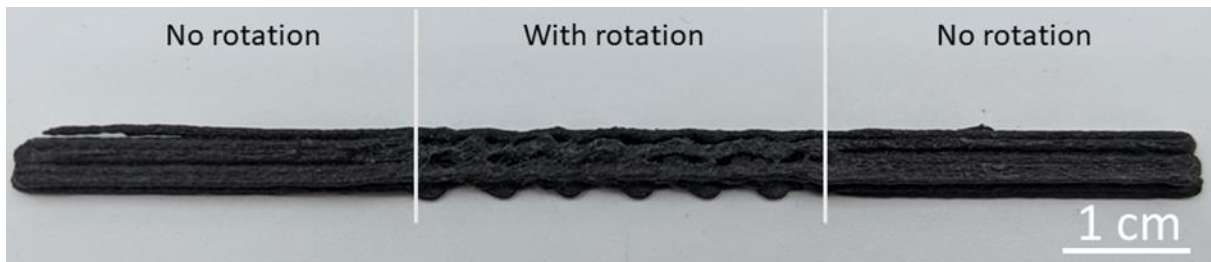
Figure 3.18: Bar sample with an intermediate section printed with rotation
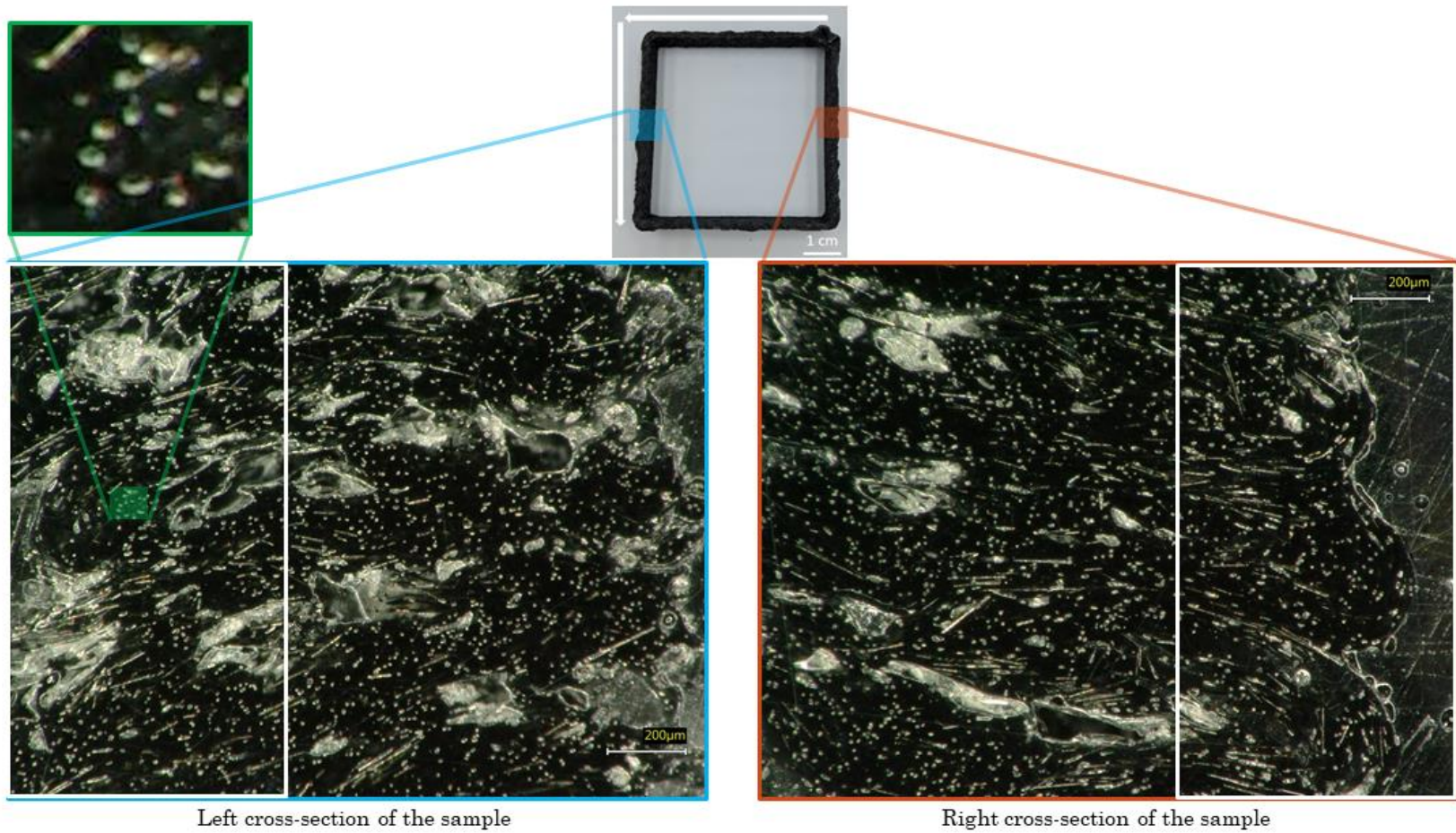
Figure 3.19: Cross section images of the highlighted sections of the single walled sample with constant rotation. The white box signifies the section where more horizontal fibers can be seen.

65
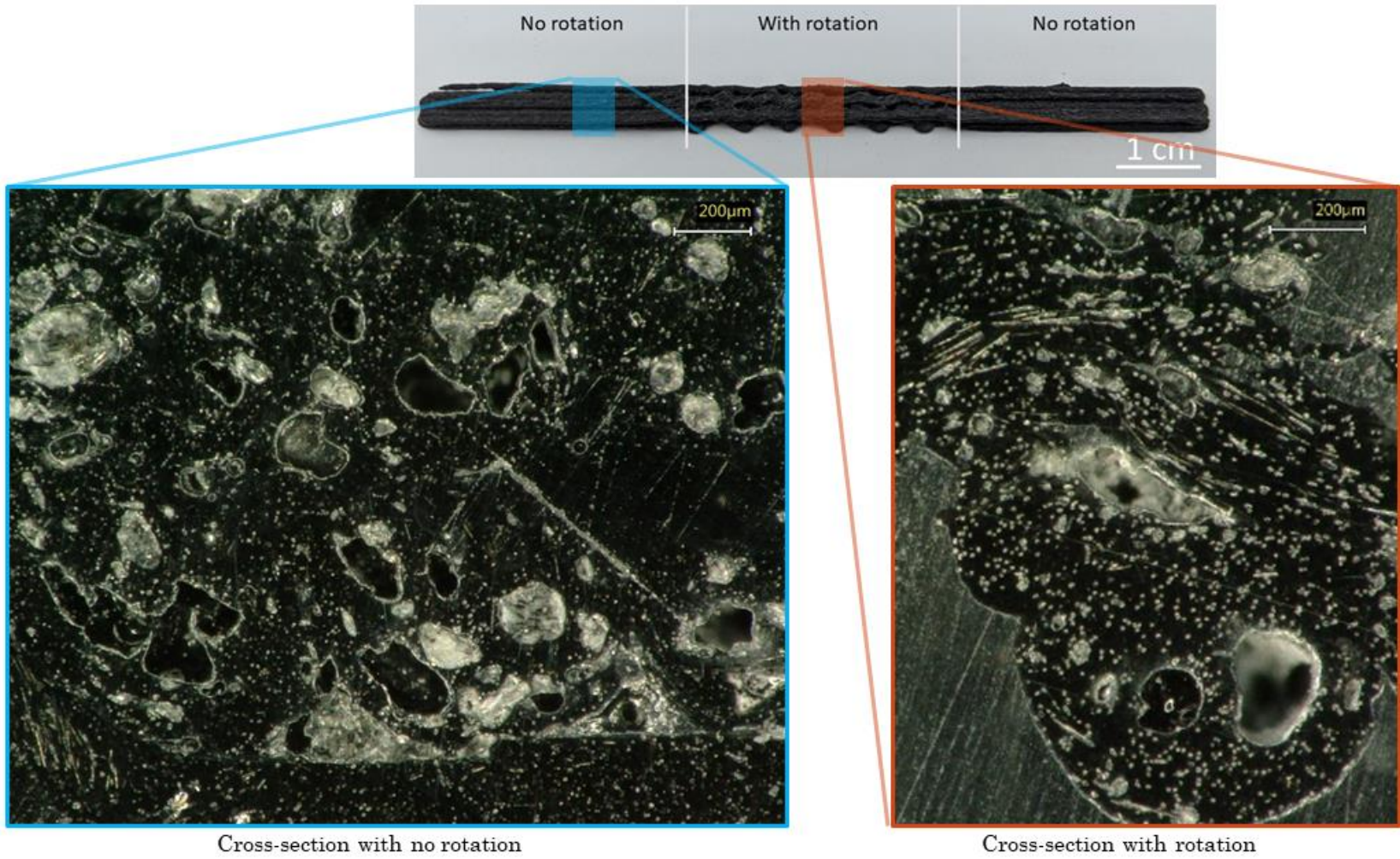
Figure 3.20: Cross section images of the highlighted sections of the variable rotation bar sample

3.5 Discussion

Even at a low rotational ratio, fibers can be seen to be reoriented. When examining the fibers in the single walled sample it is worth noting that more fibers on the outside of the sample are aligned orthogonally to the print path than the fibers on the inside of the shape. This suggests that the print velocity relative to direction of rotation has a part to play in determining the resulting fiber orientation. During the printing process the samples were porous, resulting in poor printed sample due to poor print parameters. The simple bar sample has significant voids. As seen in RDIW, the nozzle tends to wobble around. This is quite pronounced with the bar sample, since the lines are not able to fill in the gaps caused by the nozzle propagating around the axis of rotation. This type of error could be rectified using a chuck-system, like the one used with the RDIW, provided the temperatures can be withstood. The spindle tool speed was limited to 500 RPM. At higher speeds, the voltage passing through the bearings would drop below the necessary voltage for the voltage regulators on the control boards on the extruder. This could disconnect the rotating extruder from power. There are two recommended changes to this system. First, to change the bearing into actual slip rings, so that the rotations will not disconnect the extruder. The second change is to machine all the parts to allow for tighter tolerances, to reduce the amount of wobble the nozzle has. Additionally, adding a chuck would also assist in being able to nudge the extruder to the center of rotation. However, fibers can be seen to be influenced by this rotation, and wireless communication was utilized for an extruder, which hasn't been done prior.

Chapter 4 Conclusion and Recommendation

4.1 Conclusion

Though these systems still have some quirks to iron out, they show a lot of potential in allowing designers to have more control over their material specifications. If the anisotropy of the material can be controlled when the print path cannot be altered, this allows designers to reinforced stress concentrators, design how the parts will fail safely, and lay thermal or electrical conduit even perpendicular to the print direction. This is an incredibly effective tool to decouple the print path from fiber alignment in the plane.

The RDIW extruder was able to fullly reorient fibers perpendicular to the print direction and was able to quickly change the rotational rate via G-code to achieve different rotational ratio. The FFF extruder on the other hand, was only partially able to reorient fibers. This is due to issues with the construction limiting the rotational speed the extruder could travel.

These two methods are not really competing, as thermoplastics cannot be printed on a thermoset printer and vice versa. The primary driver would be scale. The RDIW is reasonably compact, allowing for small structures to be specifically reinforced or enhanced in a way. Alternatively, on the medium to very large-scale thermoset printing is still quite in its infancy. Thermoplastic, on the other hand, has made significant strides. RFFF would work more effectively, since as the nozzle size grows, the necessary rotation decreases (though more torque is then required to rotate more material). This scaling could also assist in finding a suitable rotary union.

4.2 Future Work

Though the fiber orientation can be controlled in the plane, there is still a great deal of reinforcement necessary between layers. If the part fails due to poor layer adhesion the overall strength of the individual layers means little. One avenue of further development is to take the lessons learned from reorienting through shear fields and applying that knowledge in all directions, truly decoupling the fiber orientation. One possible mechanism for how this could work is use of the Weissenberg effect to intermix layers to some degree. Another avenue is investigating auger/Moineau-based pumps to dynamically change fiber concentration during the print. This auger system could also be used to have inline-rotary union for rotational thermoplastic printing. Alternatively, a new hotend design could allow for the inline rotary union without twisting the filament. Another avenue is to revisit these two designs and make the modifications listed in the respective sections to better optimize the extruder. Finally, it is worth investigating what materials extrude best from these methods and what materials gain the most benefit from this level of control.

List of References

[1]   A. Alkhalidi and D. Hatuqay, "Energy efficient 3D printed buildings: Material and techniques selection," *Journal of Building Engineering,* vol. 30, 2020.

[2]   G. Yalcinkaya, "World's first 3D-printed steel bridge unveiled at Dutch Design Week," ed: de zeen, 2018.

[3]   M. Molitch-Hou, "Branch Technology Creates "Largest 3D-Printed Structure"," ed: Engineering.com, 2018.

[4]   L. Griffiths, "How 3D printing is shaping the future of aircraft maintenance, repair & overhaul," ed: tctMag, 2018.

[5]   B. Salmi, "The World's Largest 3D Metal Printer Is Churning Out Rockets," ed: IEEE Spectrum, 2019.

[6]   J. Stanfield, "NASA Marshall Advances 3-D Printed Rocket Engine Nozzle Technology," ed: NASA, 2018.

[7]   G. Anderson and Ridinger, "Top Five Teams Win a Share of $100,000 in Virtual Modeling Stage of NASA's 3D-Printed Habitat Competition," ed: NASA, 2018.

[8]   J. D., "Top 10 Applications of 3D Printing in Art," ed: 3D natives, 2017.

[9]   A. Cheng, "How Adidas Plans To Bring 3D Printing To The Masses," ed: Forbes, 2018.

[10]   V. Charbonneau, "3D Printing Complex Electronic Components Creates New Manufacturing Possibilities," ed: Engineering.com, 2019.

[11]   Z. Cohen, "How 3D Printing PCBs Aids Impedance Controlled Routing," ed: Nano Dimension, 2020.

[12]   S. Davies, "Bowman International manufactures bespoke Rollertrain bearing cages with Multi Jet Fusion," ed: tctMAG, 2018.

[13]   "Application Spotlight: 3D Printing for Heat Exchangers," ed: AMFG, 2019.

[14]   P. C. Liacouras, D. Sahajwalla, M. D. Beachler, T. Sleeman, V. B. Ho, and J. P. L. III, "Using computed tomography and 3D printing to construct custom prosthetics attachments and devices," *3D Printing in Medicine,* vol. 3, no. 8, 2017.

[15]   "3D-Printable Prosthetic Devices," ed: NIH.

[16]   F. Pati, D.-H. Ha, J. Jang, H. H. Han, J.-W. Rhie, and D.-W. Cho, "Biomimetic 3D tissue printing for soft tissue regeneration," *Biomaterials,* vol. 62, p. 164, 2015.

[17]   C. Mandrycky, Z. Wang, K. Kim, and D. Kim, "3D bioprinting for engineering complex tissues," *Biotechnology Advances,* vol. 34, no. 4, pp. 422-434, 2016, doi: 10.1016/j.biotechadv.2015.12.011.

[18]   O. Martikka, T. Kärki, and Q. Wu, "Mechanical Properties of 3D-Printed Wood-Plastic Composites," *Key Engineering Materials,* vol. 777, pp. 499-507, 2018, doi: 10.4028/www.scientific.net/KEM.777.499.

[19]   H. L. Tekinalp *et al.*, "Highly oriented carbon fiber–polymer composites via additive manufacturing," *Composites Science and Technology,* vol. 105, no. 5, pp. 144-150, 2014, doi: 10.1016/j.compscitech.2014.10.009.

[20]   A. Sdrobiş, R. N. Darie, M. Totolin, G. Cazacu, and C. Vasile, "Low density polyethylene composites containing cellulose pulp fibers," *Composites,* vol. 43, no. 4, pp. 1873-1880, 2012, doi: 10.1016/j.compositesb.2012.01.064.

[21]   Z. Wang and D. Smith, "Rheology Effects on Predicted Fiber Orientation and Elastic Properties in Large Scale Polymer Composite Additive Manufacturing," *Journal of Composites Science,* vol. 2, no. 1, 2018, doi: 10.3390/jcs2010010.

[22]   S. C. Tjong, *14 - Electrical and dielectric behavior of carbon nanotube-filled polymer composites*. Elsevier Ltd, 2010, pp. 495-528.

[23]   L. J. Love *et al.*, "The importance of carbon fiber to polymer additive manufacturing," *Journal of Materials Research,* vol. 29, no. 17, pp. 1893-1898, 2014.

[24]   J. Peng, T. L. Lin, and P. Calvert, "Orientation effects in freeformed short-fiber composites," *Composites Part A,* vol. 30, no. 2, pp. 133-138, 1999, doi: 10.1016/S1359-835X(98)00110-9.

[25]   S. Mortazavian and A. Fatemi, "Effects of fiber orientation and anisotropy on tensile strength and elastic modulus of short fiber reinforced polymer composites," *Composites Part B,* vol. 72, pp. 116-129, 2015, doi: 10.1016/j.compositesb.2014.11.041.

[26]   R. R. Collino, T. R. Ray, R. C. Fleming, J. D. Cornell, B. G. Compton, and M. R. Begley, "Deposition of ordered two-phase materials using microfluidic print nozzles with acoustic focusing.(Report)(Author abstract)," *Extreme Mechanics Letters,* vol. 8, p. 96, 2016, doi: 10.1016/j.eml.2016.04.003.

[27]   J. Martin, B. Fiore, and R. Erb, "Designing bioinspired composite reinforcement architectures via 3D magnetic printing," *Nature Communications,* vol. 6, no. 1, p. 8641, 2015, doi: 10.1038/ncomms9641.

[28]   J. R. Raney, B. G. Compton, J. Mueller, T. J. Ober, K. Shea, and J. A. Lewis, "Rotational 3D printing of damage-tolerant composites with programmable mechanics.(Report)," *Proceedings of the National Academy of Sciences of the United States,* vol. 115, no. 6, p. 1198, 2018, doi: 10.1073/pnas.1715157115.

[29]   *Standard Terminology for Additive Manufacturing*, A. International, West Conshohocken, PA, 2015. [Online]. Available: www.astm.org

[30]   H. Kodama, "Automatic method for fabricating a three-dimensional plastic model with photo-hardening polymer," *Review of Scientific Instruments,* vol. 52, no. 11, pp. 1770-1773, 1981, doi: 10.1063/1.1136492.

[31]   "Patent Application Titled "Apparatus and Method for Production of Three-Dimensional Objects" Published Online (USPTO 20170361529)," *Chemicals & Chemistry,* p. 7278, 2018.

[32]   J. Andrè, A. Mehautè, and O. Witte, "Dispositif pour rèalizer un modele de pièce industrielle," France Patent Appl. 2567668   1984.

[33]   B. Masters. "The Father Of 3D Printing – Bill Masters." https://billmasters3d.com/father-of-3d-printing/ (accessed June 15, 2020).

[34]   "4665492 Computer automated manufacturing process and system: William E Masters," *Robotics and Computer Integrated Manufacturing,* vol. 3, no. 4, pp. i-ii, 1987, doi: 10.1016/0736-5845(87)90060-3.

[35]   S. Crump, "Apparatus and method for creating three-dimensional objects," United States Patent Appl. 5121329, 1992.

[36]   J. Cesarano III, "Freeforming objects with low-binder slurry," United States Patent Appl. 6027326, 2000.

[37]   R. Jones *et al.*, "RepRap – the replicating rapid prototyper," *Robotica,* vol. 29, no. 1, pp. 177-191, 2011, doi: https://doi.org/10.1017/S026357471000069X.

[38]   E. J. De Bruijn, "On the viability of the open source development model for the design of physical objects Lessons learned from the RepRap project," Master of Science, Information Management, University of Tilburg, 2010.

[39]   L. Columbus. "The State of 3D Printing, 2018." Forbes. https://www.forbes.com/sites/louiscolumbus/2018/05/30/the-state-of-3d-printing-2018/#678d8fe07b0a (accessed June 15, 2020).

[40]   B. Redwood, F. Schoffer, and B. Garret, *The 3D Printing Handbook*. 3D Hubs, 2017.

[41]   E. Sirjani, P. J. Cragg, and M. K. Dymond, "Glass transition temperatures, melting temperatures, water contact angles and dimensional precision of simple fused deposition model 3D prints and 3D printed channels constructed from a range of commercially available filaments," *Chemical Data Collections,* vol. 22, 2019, doi: 10.1016/j.cdc.2019.100244.

[42]   A. Buhot, "Viscosity and Renewal Time of Polymer Reptation Models," *Macromolecules,* vol. 43, no. 21, pp. 9155-9159, 2010, doi: 10.1021/ma1015402.

[43]   C. McIlroy and P. D. Olmsted, "Disentanglement effects on welding behaviour of polymer melts during the fused-filament-fabrication method for additive manufacturing.(Report)," *Polymer,* vol. 123, no. C, p. 376, 2017, doi: 10.1016/j.polymer.2017.06.051.

[44]   S. A. Khan and I. Lazoglu, "Development of additively manufacturable and electrically conductive graphite–polymer composites," *<i data-test="journal-title" style="box-sizing: inherit;">Progress in Additive Manufacturing,* vol. 5, pp. 153-162, 2020, doi: https://doi.org/10.1007/s40964-019-00102-9.

[45]   B. N. Turner, R. Strong, and S. A. Gold, "A review of melt extrusion additive manufacturing processes: I. Process design and modeling," *Rapid Prototyping Journal,* vol. 20, no. 3, pp. 192-204, 2014, doi: 10.1108/RPJ-01-2013-0012.

[46]   "FLOW PROPERTIES OF POLYMER   TIME-INDEPENDENT FLUIDS." Polymer Properties Database. https://polymerdatabase.com/polymer%20physics/Viscosity2.html (accessed.

[47]   B. Xie, R. L. Parkhill, W. L. Warren, and J. E. Smay, "Direct Writing of Three-Dimensional Polymer Scaffolds Using Colloidal Gels," *Advanced Functional Materials,* vol. 16, no. 13, pp. 1685-1693, 2006, doi: 10.1002/adfm.200500666.

[48]   G. Franchin *et al.*, "Direct ink writing of geopolymeric inks," *Journal of the European Ceramic Society,* vol. 37, no. 6, pp. 2481-2489, 2017, doi: 10.1016/j.jeurceramsoc.2017.01.030.

[49]   B. G. Compton and J. A. Lewis, "3D-Printing of Lightweight Cellular Composites," *Advanced Materials,* vol. 26, no. 34, pp. 5930-5935, 2014, doi: 10.1002/adma.201401804.

[50]   "Reports from University of Nottingham Add New Data to Findings in Paracetamol Therapy (Extrusion 3d Printing of Paracetamol Tablets From a

Single Formulation With Tunable Release Profiles Through Control of Tablet Geometry)," *Obesity, Fitness & Wellness Week,* p. 5073, 2019.

[51] M. Vatani and J.-W. Choi, "Direct-print photopolymerization for 3D printing," *Rapid Prototyping Journal,* vol. 23, no. 2, pp. 337-343, 2017, doi: 10.1108/RPJ-11-2015-0172.

[52] T. Wu *et al.*, "Additively manufacturing high-performance bismaleimide architectures with ultraviolet-assisted direct ink writing," *Materials & Design,* vol. 180, 2019, doi: 10.1016/j.matdes.2019.107947.

[53] K. A. H. Dubey, P.A. Bhardwaj. Y.K. Author links open overlay panel, K. A. Dubey, P. A. Hassan, and B. Y.K., "High Performance Polymer Nanocomposites for Structural Applications," in *Materials Under Extreme Conditions*, A. K. Tyagi and S. Banerjee Eds.: Elsevier, 2017, ch. 5, pp. 159-194.

[54] J. Gonzalez-Gutierrez, S. Cano, S. Schuschnigg, C. Kukla, J. Sapkota, and C. Holzer, "Additive Manufacturing of Metallic and Ceramic Components by the Material Extrusion of Highly-Filled Polymers: A Review and Future Perspectives," *Materials,* vol. 11, no. 5, p. 840, 2018, doi: 10.3390/ma11050840.

[55] "The all new Scultpo Pro 2." Sculpto. https://sculpto.eu/sculpto-pro2/ (accessed June 15, 2020).

[56] "HE3D K200 Auto leveling Delta 3D Printer Kit." 3DPrinterBay. https://www.3dprintersbay.com/he3d-k200-delta-3d-printer-kit (accessed June 15, 2020).

[57] R. Zhang, Y. Zhang, Q. Zhang, H. Xie, W. Qian, and F. Wei, "Growth of Half-Meter Long Carbon Nanotubes Based on Schulz–Flory Distribution," *ACS Nano,* vol. 7, no. 7, pp. 6156-6161, 2013, doi: 10.1021/nn401995z.

[58] M. Piggott, "Load Bearing Fibre Composites," 2002, doi: 10.1007/b118150.

[59] S. Rana, *Fibrous and Textile Materials for Composite Applications* (Textile Science and Clothing Technology). Singapore: Springer Singapore, 2016.

[60] K. Ho and S. Erden, "Fiber reinforced composites," in *Fiber Technology for Fiber-Reinforced Composites*, M. Misra, M. O. Seydibeyoglu, and A. K. Mohanty Eds., 1st ed. Amsterdam: Elsevier Science, 2016, pp. 51-79.

[61] S. R. Song, W. Hwang, H. C. Park, and K. S. Han, "Optimum stacking sequence of composite laminates for maximum strength," *Mechanics of composite materials,* vol. 31, no. 3, pp. 290-300, 1995, doi: 10.1007/BF00615644.

[62] K. Álvarez, R. F. Lagos, and M. Aizpun, "Investigating the influence of infill percentage on the mechanical properties of fused deposition modelled ABS parts," *Ingeniería e investigación,* vol. 36, no. 3, pp. 110-116, 2016, doi: 10.15446/ing.investig.v36n3.56610.

[63] L. Baich, "Impact of Infill Design on Mechanical Strength and Production Cost in Material Extrusion Based Additive Manufacturing," Master of Science in Engineering, Industrial and Systems Engineering, YOUNGSTOWN STATE UNIVERSITY, 2016.

[64] L. Jin, C. Bower, and O. Zhou, "Alignment of carbon nanotubes in a polymer matrix by mechanical stretching," *Applied Physics Letters,* vol. 73, no. 9, pp. 1197-1199, 1998.

[65]   M. J. Lance, C.-H. Hsueh, I. N. Ivanov, and D. B. Geohegan, "Reorientation of Carbon Nanotubes in Polymer Matrix Composites using Compressive Loading," *Journal of Materials Research,* vol. 20, no. 4, 2005, doi: 10.1557/JMR.2005.0139.

[66]   C. Park and R. Robertson, "Aligned microstructure of some particulate polymer composites obtained with an electric field," *Journal of Materials Science,* vol. 33, no. 14, pp. 3541-3553, 1998, doi: 10.1023/A:1004638825477.

[67]   D. Kokkinis, M. Schaffner, and A. Studart, "Multimaterial magnetically assisted 3D printing of composite materials," *Nature Communications,* vol. 6, 2015, doi: 10.1038/ncomms9643.

[68]   R. R. Collino, T. R. Ray, R. C. Fleming, C. H. Sasaki, H. Haj-Hariri, and M. R. Begley, "Acoustic field controlled patterning and assembly of anisotropic particles," *Extreme Mechanics Letters,* vol. 5, p. 37, 2015, doi: 10.1016/j.eml.2015.09.003.

[69]   N. Johantgen and C. Ludwick, "How many phases are enough? Two and five-phase stepmotors share several commonalities; however, the former corrects phase imbalances quicker, while the latter produces much less vibration. So which is better?(Multiphase steppers)," *Motion System Design,* vol. 48, no. 2, p. 15, 2006.

[70]   T. Emanoil, "Some Aspects Regarding the Use of Digital Signal Controllers in Electrical Drivers for Stepper Motors," *Analele Universităţii "Eftimie Murgu" Reşiţa: Fascicola I, Inginerie,* vol. XXI, no. 2, pp. 346-356, 2014.

[71]   "Stepper Motor Technical Note: Microstepping Myths and Realities." Faulhaber. https://www.faulhaber.com/en/support/technical-support/motors/tutorials/stepper-motor-tutorial-microstepping/ (accessed June 15, 2020).

[72]   "Unipolar vs Bipolar Stepper Motor." Osmtec. https://www.osmtec.com/unipolar_vs_bipolar.htm (accessed June 15, 2020).

[73]   "ShopBot Desktop." Shopbot. https://www.shopbottools.com/products/desktop (accessed June 15, 2020).

[74]   "Dispensing Tips." Fisnar. https://www.fisnar.com/products/dispensing-accessories/dispensing-tips/blunt-end-dispensing-tips/ (accessed June 15, 2020).

[75]   Qosina. https://www.qosina.com/male-to-male-rotating-connector-high-pressure-20034 (accessed June 15, 2020).

[76]   "Rotary Union Catalog." Mosomatic. https://www.mosmatic.com/us/products/rotary-unions/?__cf_chl_jschl_tk__=3796e08cf5a4990592258c541bc0fec7b9423131-1592284392-0-AZDDIDVteyecxXDyzhVnBAp47GB8gesxoAn45eRZuZg5NXJT63acinZL_J6H zRqJwxnncUIMra6qK8PyWvE5rVqY02U5bLiaqD8zgO2T22YzeeukI0QmKpM 7bKTh3zq5zBt5EOHHzujrU_5BiuUUsATc4b2_5HQEH2QQQd9ePti1ua0BwwE xf6JxTcYIZGbynygGyQHUU7i7clin9LXTVRK4viYOTwJ9OseZCNzNz7arEDz vjJufTgxOKBNl05F7hFXbBwxHBC--8-G2uI5sgKg7YhPpLa0rGH2KzzJKvZuAR99L08lW3BbcTmle-DPfug (accessed June 15, 2020).

[77] "Extruders." RepRap. https://reprap.org/wiki/Category:Extruders (accessed June 15, 2020).

[78] A. Ouballouch, R. Elalaiji, I. Ouahmane, L. Lasri, and M. Sallaou, "Finite Element Analysis of a FDM 3D Printer Liquefier," *Key Engineering Materials,* vol. 820, pp. 173-178, 2019, doi: 10.4028/www.scientific.net/KEM.820.173.

[79] Z. Hay. "Best 3D Printing Temperatures for PLA, PETG, Nylon, TPU." All3DP. https://all3dp.com/2/the-best-printing-temperature-for-different-filaments/ (accessed June 15, 2020).

[80] "Material Overview PEEK." Fluorcarbon. http://www.fluorocarbon.co.uk/products/material-overview/peek (accessed June 15, 2020).

[81] E. Canessa, M. Baruzzo, and C. Fonda, "Study of Moineau-based pumps for the volumetric extrusion of pellets," *Additive Manufacturing,* vol. 17, pp. 143-150, 2017, doi: 10.1016/j.addma.2017.08.015.

[82] R. P. Mueller *et al.*, "Zero Launch Mass Three Dimensional Print Head," 2018. [Online]. Available: https://ntrs.nasa.gov/search.jsp?R=20180002949

[83] *CarbonX™ Carbon Fiber PLA Safety Data Sheet*,

[84] "THE HYDRA 16A – The Freestanding (Floor) Model " Hyrel 3D. http://www.hyrel3d.com/portfolio/hyrda16a/ (accessed June 15, 2020).

[85] "Consine Printer Catalog." https://www.cosineadditive.com/ (accessed June 15, 2020).

[86] "Cosine Printer Catalog." https://www.cosineadditive.com/ (accessed June 15, 2020).

Appendix

Figure A.1: Exploded view of RDIW extruder CAD model

BOM Level	Part Number	Part Name	Description
1	7062T16	Z-Bar	Multipurpose 6061 Aluminum Z-Bar 1/16" Wall Thickness, 1-1/8" High, 1 1/8" Outside Width
2	1394A23	Flat bracket	Flat-Surface Bracket Zinc-Plated Steel, 1-1/2" x 1/2"
3	1277N53	Timing belt pulley	28 teeth XL timing belt pulley
4	6484K223	Timing belt	13" ID XL timing belt
5	2183-1475-ND	Stepper motor	2A NEMA 23 Stepper motor
6	2258	L-Bracket	Steel L-Bracket for NEMA 23 Stepper Motors
7	5913K64	Pillow block bearing	Low-Profile Mounted Sealed Steel Ball Bearing for 1" Shaft Diameter
8	8001087	Nozzle	1/2″ Straight Cannula Blunt End Dispensing Tip
9	Custom	Chuck assembly	Collet to align nozzle with center of rotation
10	51465K31	Nozzle quick turn coupler	Brass Quick-Turn Tube Coupling for Air Plug, 1/4 NPT Female
11	50785K28	Reducing adapter	High-Pressure Brass Pipe Fitting Reducing Adapter, 3/8 NPT Female x ¼ NPT Male
12	31.153	Rotary union	DGL Rotary union
13	4429K412	Increasing adapter	Low-Pressure Brass Threaded Pipe Fitting Bushing Adapter with Hex Body, 3/8 Male x 1/4 Female NPT
14	51465K35	Syringe quick turn coupler	Brass Quick-Turn Tube Coupling for Air Socket, 1/4 NPT Male
15	MB4	Baseplate	MB4 - Aluminum Breadboard 4" x 6" x 1/2", 1/4"-20 Taps

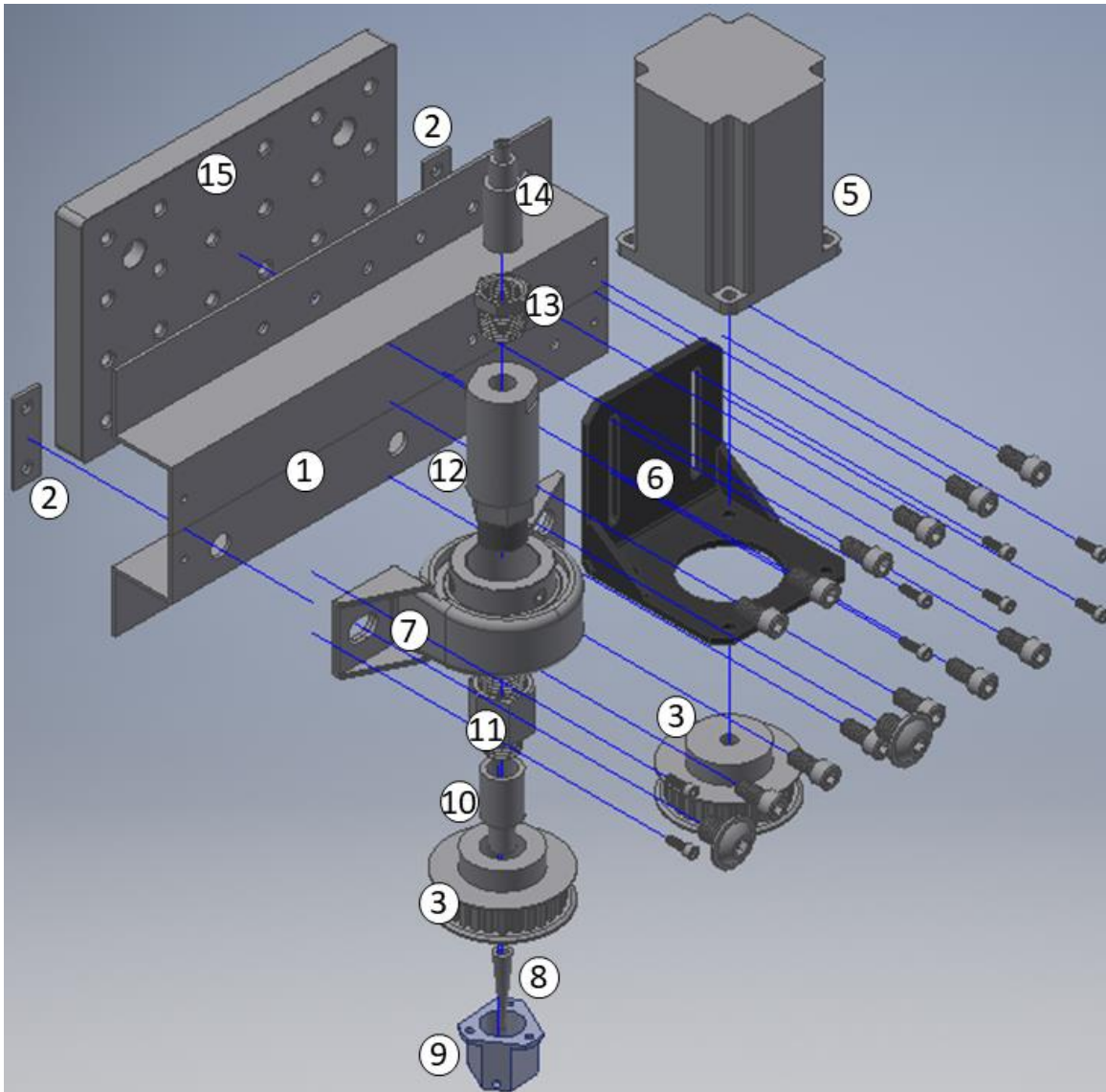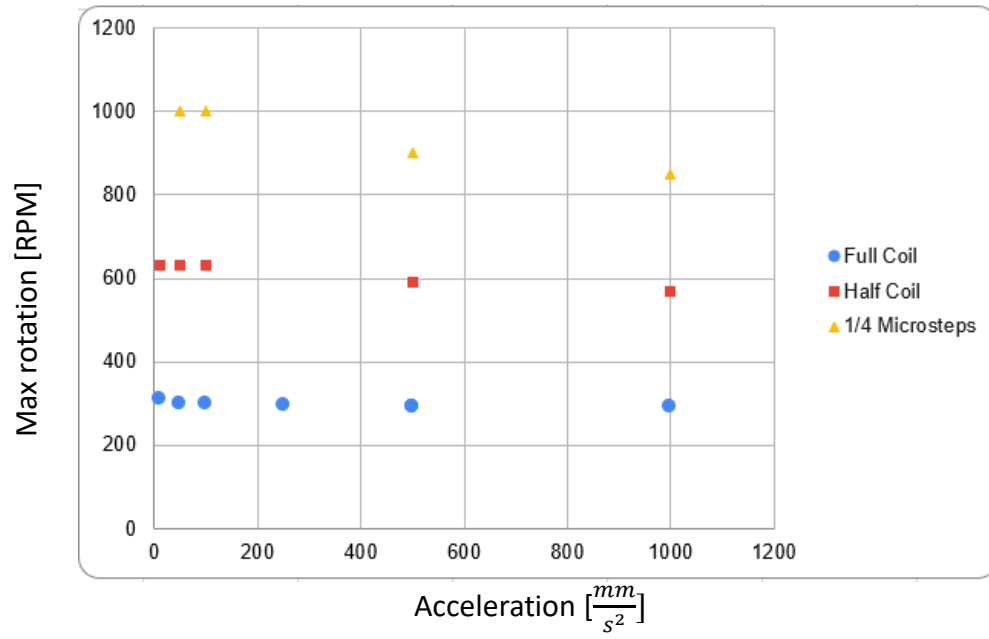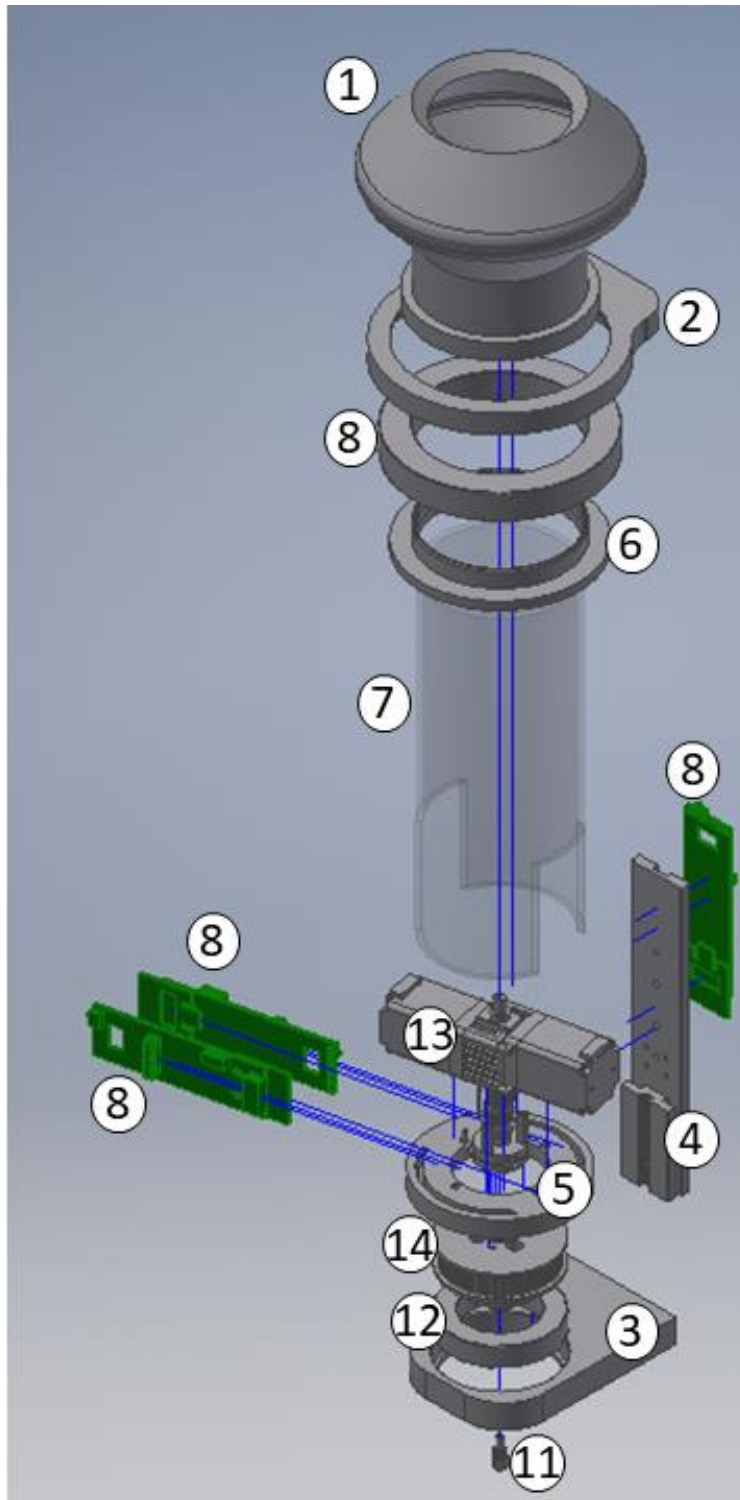*Figure A.2: Maximum federate for different acceleration and microstepping*

Figure A.3: Exploded view of RFFF extruder CAD model

Table A-2: Bill of Material for RFFF Extruder

| BOM Level	Part Number	Part Name	Description
1	Custom	Filament housing	Storage container for carried filament
2	Custom	Upper mounting bracket	Bracket to secure upper bearing and tube to gib
3	Custom	Lower mounting bracket	Bracket to secure lower bearing and tube to gib
4	Custom	Gib	Mounting interface to yoke and extruder
5	Custom	Tube mount	Interface between tube and slave pulley
6	Custom	Bearing mount	Clasp onto the tube ensure the bearing doesn't move down.
7	8486K471	Clear cast acrylic tube	Transparent tube to ensure rotating components do not get ejected
8	6216 2RS JEM	Upper Bearing	Bearing that secures the tube to the upper mounting bracket
9	Smart controller	Control board	Modular control board for Hyrel's heads
10	ST-1	Router	5000 RPM spindle motor
11	Nozzle	Nozzle	1mm brass nozzle
12	63206LLBC3/L627	Lower bearing	Bearing that secures the tube to the lower mounting bracket
13	Mk2-250	Modular head	Thermoplastic extruder with two stepper motors
14	60XLB037-6WA	Timing-belt pulley	60 teeth XL timing-belt pulley
15	16XLB037-6FA	Timing-belt pulley	16 teeth XL timing-belt pulley
16	170XL037	Timing-belt	85 teeth XL timing belt
17	ADP7142AUJZ-5.0-R7	Voltage regulator	LDO Voltage Regulators 40V 200mA LDO 5.0Vo
18	ARNEW-10PACK-84M5160	Capacitor	Aluminum Electrolytic Capacitors - Axial Leaded 470uF 25V 20% Axial
19	HC-05	Bluetooth module	Bluetooth serial transmission module
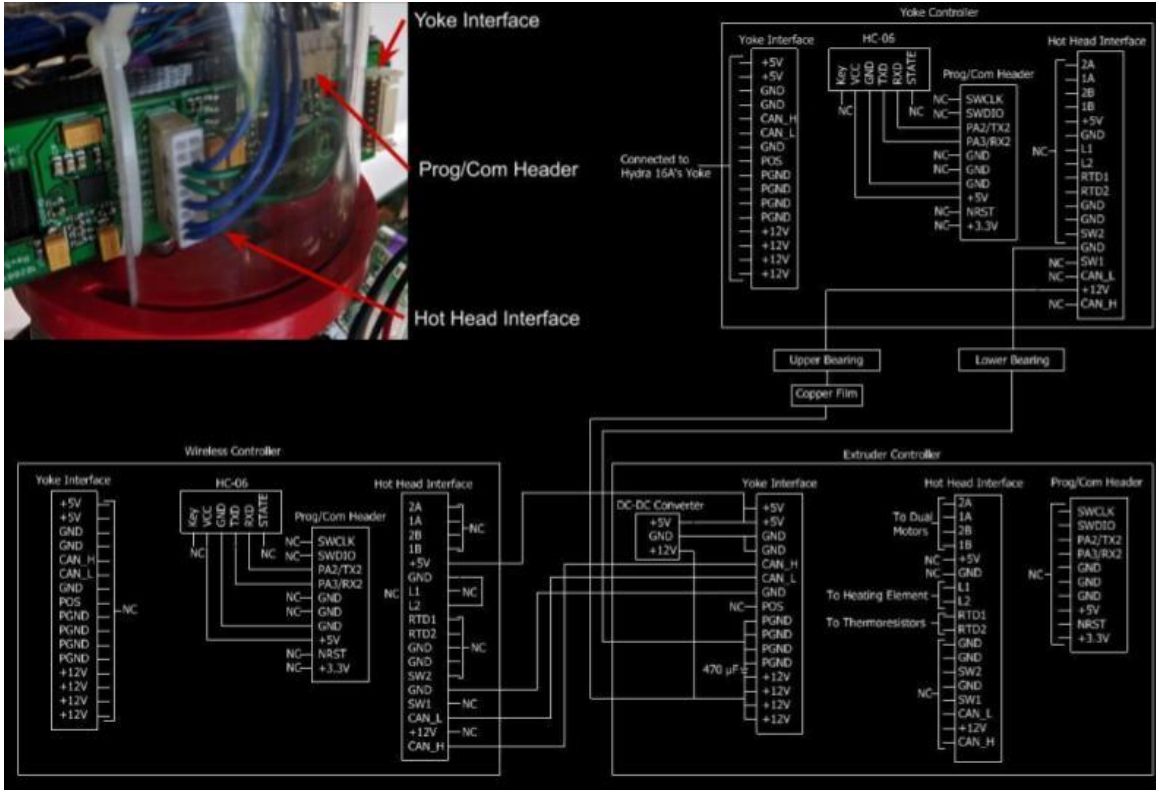
Figure A.4: Wiring diagram of the control boards attached to the rotating thermoplastic extruder

Vita

Michael Roberts was born in Mission Viejo, California. He moved to Cookeville, Tennessee in 1997. He attended Tennessee Technological University pursuing dual majors in Electrical Engineering and Computer Engineering in addition to a minor in applied mathematics. Michael graduated with two Bachelor of Science degrees in 2017. He then attended the University of Tennessee pursing a master's degree in Mechanical engineering. He graduated in August 2020 with a Master of Science degree.